Understanding Exportin-1 as an Anti-Cancer Target

By

Russell T. Burke

B.S., Oregon State University, 2010

A thesis submitted to the Faculty
of the Graduate School in partial
fulfillment of the requirements
for the degree of Doctor of Philosophy

Department of Molecular, Cellular, and Developmental Biology
2018

This thesis entitled:

Understanding Exportin-1 as an Anti-Cancer Target
Written by Russell T. Burke

Has been approved for the Department of Molecular, Cellular, and Developmental Biology

_____

James D. Orth, Ph.D., Advisor

_____

Rui Yi, Ph.D., Committee Chair

Date_____

The final copy of this thesis has been examined by the signatories, and we find that both the content and the form meet acceptable presentation standards of scholarly work in the above mentioned discipline.

Abstract

Burke, Russell T. (Ph.D. Molecular Cellular, and Developmental Biology)

Understanding Exportin-1 as an Anti-Cancer Target

Thesis Directed by Assistant Professor James D. Orth

Exportin-1 is a promising new anti-cancer target for selective inhibitors of nuclear export (SINE) molecules. Selinexor is a first-in-class SINE molecule in clinical trials for a variety of different cancers. Selinexor and other SINE molecules covalently bind exportin-1 and prevent nuclear export of cargo proteins. Over 200 Exportin-1 protein cargoes have been identified, including p53, pRB, IκB, and BRCA1. While early clinical success with inhibitors of Exportin-1 has been observed, the molecular mechanisms of response are still being examined. Previous studies have shown a variety of cell cycle effects and cell death. Here we show that inhibition of Exportin-1 causes DNA damage concurrent with nucleolar dysfunction. DNA damage occurs in about 35-45% of fibrosacrcoma derived cells, and to varying extent in other cancer derived cell lines. DNA damage occurs in G1-phase in 74% of the cells that acquire damage and 26% in S/G2-phase. In addition, more death is observed in cells that acquire DNA damage in G1-phase versus S/G2-phase. DNA damage occurs in large distinct foci, and are believed to be composed of clusters of double strand break sites. The proximity of DNA damage to nucleoli led to the investigation of nucleolar function. When Exportin-1 is inhibited, transcription of ribosomal RNA is reduced and proteins associated with ribosome biogenesis are redistributed within the nucleolus. Both these effects are indicative of nucleolar stress. When RNA polymerase I is acutely inhibited in combination with selinexor, DNA damage formation is no longer increased

over control treated cells. In addition, DNA damage formation is blocked when cell cycle progression is inhibited. These data suggest that DNA damage is dependent both on nucleolar function and cell cycle progression. DNA damage formation is enhanced both in cells that have a loss of function for p53 or overexpression of the RNA polymerase I transcription factor, UBF, indicating potential sensitivity in cancer where these two processes are often disrupted. In all, this thesis explores a variety of different pathways in the complex response to Exportin-1 inhibition. It presents a novel anti-cancer mechanism of selinexor, leading to a more complete understanding for therapeutically targeting Exportin-1.

Dedication

I would like to dedicate this thesis to the loving support of my family and friends. My wife, Kimberlie, picked up and moved to Colorado with me, and has supported and encouraged me throughout this endeavor. My son, Larson, will have turned one year old when this thesis is defended, and has been a constant motivation to progress as a scientist and a father. My parents and brother have provided ample support from afar. Finally, to the friends and family both within Colorado and beyond, I am ever grateful for your love and support.

Acknowledgments

First and foremost, I acknowledge James Orth for the constant support and feedback he has provided as an advisor. James provided a unique laboratory environment and the resources in order to follow my project to the completion of this thesis. Throughout my graduate career, James has driven me to ask better questions and pursue stronger science. I acknowledge Joshua Marcus who was a huge support when I entered the lab, and also created some of the cell lines used throughout this thesis. In addition, I would like to acknowledge everyone in the Orth lab, both past and present, who have contributed to the work contained here: Sarah Seto, Philip Martinez, Adrian Ramirez, George Polovin, and Dongjoo Park.

I would like to acknowledge my thesis committee: Drs. Rui Yi, Tin Tin Su, Ding Xue and Sabrina Spencer. They have contributed valuable feedback and critique throughout my graduate work that has resulted in a stronger and more in-depth body of work. They have also provided support as I transition to a postdoctoral position after graduation.

I acknowledge the Signaling and Cellular Regulation training grant (T32 GM08759) for its support and the opportunity to present my work to a wider audience. I would also like to acknowledge Dr. Natalie Ahn who directs the SCR training grant and has provided ample feedback throughout this project.

I would also like to acknowledge the University of Colorado Light Microscopy Core Facility for its instrumentation. I acknowledge Dr. Yossef Landesman and Karyopharm Therapeutics, Inc. for the SINE compounds and their generous gift of support to the University of Colorado Boulder to promote the study of cancer biology.

Table of Contents

List of Figures

Chapter 1 : Introduction

1.1: Exportin-1 Is a Mediator of Nuclear Export of Proteins

Karyopherins are a family of proteins that are mediators of molecular transport into and out of the nucleus; importins and exportins, respectively. Cargos of the karyopherin family include proteins, transfer RNA (tRNA) and double stranded RNA. Transport of the karyopherin-cargo complex is dependent on a Ran-GTP/-GDP gradient maintained at the nuclear envelope. In the cytoplasm, the Ran-GTPase activating protein (RanGAP) activates the hydrolytic activity of Ran to cycle from RanGTP to RanGDP. Within the nucleus, the Ran-guanine nucleotide exchange factor (RanGEF) replaces the GDP for GTP. Exportins bind RanGTP in the nucleus and transport to the cytoplasm through the nuclear port where RanGTP is hydrolyzed to RanGDP and the cargo is released. Importins transport into the nucleus where they bind RanGTP and the cargo is released (reviewed in (Mosammaparast and Pemberton, 2004)). The system of import and export through the karyopherin family allows for a robust transport of larger molecules through the nuclear pore with a defined directionality.

Exportin-1 (XPO1), also knowns as chromosome region maintenance 1 (CRM1), is one of seven identified exportins in mammalian cells. XPO1 binds and regulates the transport of over 200 identified cargo proteins from the nucleus to the cytoplasm (Xu et al., 2012). Cargoes of XPO1 each contain a nuclear export signal (NES) that consists of a variable, leucine-rich consensus sequence of $LX_{(1-3)}LX_{(2-3)}LXL$ (Bogerd et al., 1996). The hydrophobic NES binding pocket of XPO1 is accessible after binding of RanGTP in the nucleus, wherein the entire complex is shuttled out of the nucleus into the cytoplasm (Figure 1.1). Cargo binding may be regulated through a variety of means including phosphorylation of residues within the NES to

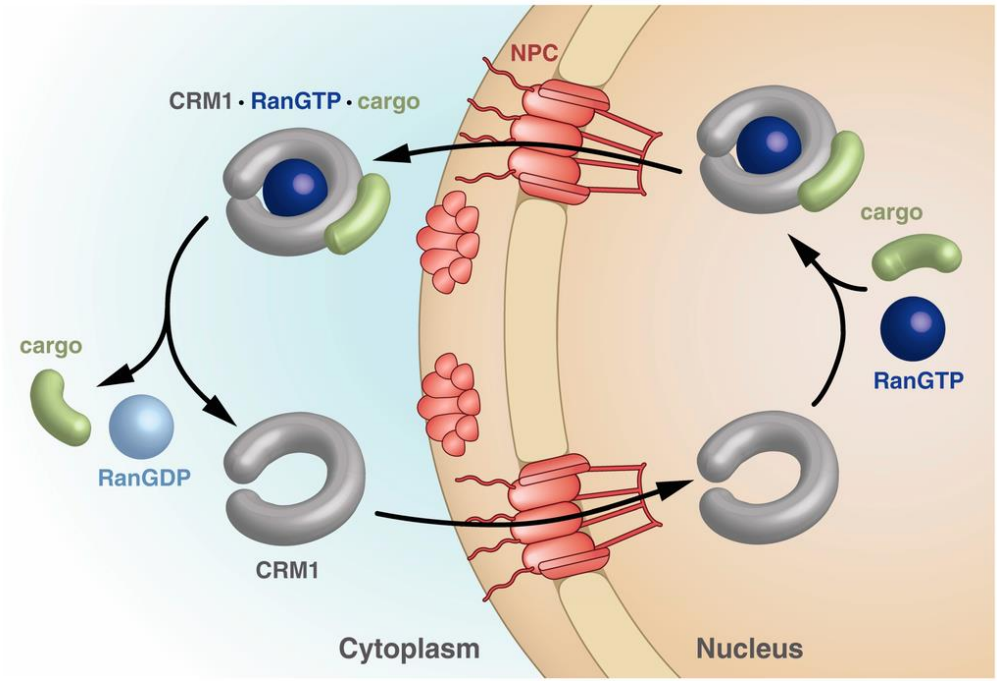

Figure 1.1: An overview of nuclear export of cargo proteins mediated by XPO1. Within the nucleus, XPO1 (CRM1, grey) binds RanGTP (dark blue) which then allows cargo to bind with a NES (green). The complex then diffuses to the cytoplasm through the nuclear pore (NPC) where upon RanGTP is hydrolyzed to RanGDP and the cargo is released. XPO1 is then imported back into the nucleus by another karyopherin family member. Figure adapted from Dickmanns et al., 2015.

add selectivity to XPO1 function (Domínguez et al., 2003; Zhang and Xiong, 2001). XPO1 may also function during mitotic spindle attachment during mitosis, although its role is not well understood (Funabiki et al., 1993; Knauer et al., 2006).

1.2: Exportin-I and Cancer

While the amount of XPO1 protein does not change as cells progress through different stages of the cell cycle (Kudo et al., 1997), it has been noted that XPO1 expression is increased in a variety of solid turmor, including pancreatic, ovarian, cervical and glioma cancers (Huang et al., 2009; Noske et al., 2008; Shen et al., 2009; van der Watt et al., 2009; Yao et al., 2009). In addition, increased expression of XPO1 in these malignancies correlated with more aggressive disease progression and poorer survival of patients (Huang et al., 2009; Shen et al., 2009; Yao et al., 2009). These findings suggest that XPO1 may have an important role in cancer development and progression.

Many XPO1 cargoes have been identified as having impacts on cancer progression in humans. These cargoes include p53, $p21^{Cip1}$, pRB, topoisomerase IIα and BRCA1 (Xu et al., 2012). The functions of these cargos dependent on cellular localization. Many XPO1 cargos exert their effects in the nucleus; including transcription factors such as p53 and pRB as well as DNA damage response (BRCA1) and cell cycle regulation ($p21^{Cip1}$ and Cyclin D1). While direct studies have not addressed the effects of overexpression of XPO1 on cancer cells, it is believed that higher levels of XPO1 leads to increased nuclear export of cargo proteins perhaps aiding in growth dysregulation. Given the importance of XPO1 cargoes on cancer progression and the

evidence of XPO1 overexpression having an effect on clinical outcome, recent efforts have focused on creating anti-cancer therapeutics that selectively target XPO1.

1.3: Selective Inhibitors of Nuclear Export

A class of molecules that specifically target XPO1, deemed selective inhibitors of nuclear export (SINE), are currently progressing through clinical trials. SINE molecules inhibit XPO1 by creating a slowly-reversible covalent bond to the sulfhydryl group of cysteine 528 in the cargo binding pocket. Binding of the SINE molecule prevents binding of the NES on cargo proteins, leading to nuclear accumulation of XPO1 cargoes. Early efforts to develop an inhibitor to XPO1 include the identification of the molecule leptomycin B produced by *Streptomyces sp.* (Hamamoto et al., 1983).While the activity of leptomycin B against cancer cells was promising both *in vitro* and in mouse models (Aloisi et al., 2006; Roberts et al., 1986), leptomycin B had significant toxicity in human patients (Newlands et al., 1996). Selinexor (KPT-330) is one SINE molecule that has demonstrated early success in clinical trials with both hematological malignancies and solid tumors. Similar to other therapeutics that form covalent bonds with their respective targets (reviewed in (Bauer, 2015)), clinical application is dependent on optimizing the binding kinetics of the SINE with XPO1.

Early studies with selinexor have revealed a wide range of anti-cancer effects from cell death and apoptosis to cell cycle arrest (Azmi et al., 2013; Lapalombella et al., 2012; Marcus et al., 2015). XPO1 cargo sequestration is observed within hours after selinexor treatment of cancer cell lines (Figure 1.2) (Marcus et al., 2015). Large scale proteomic changes are present after 18-

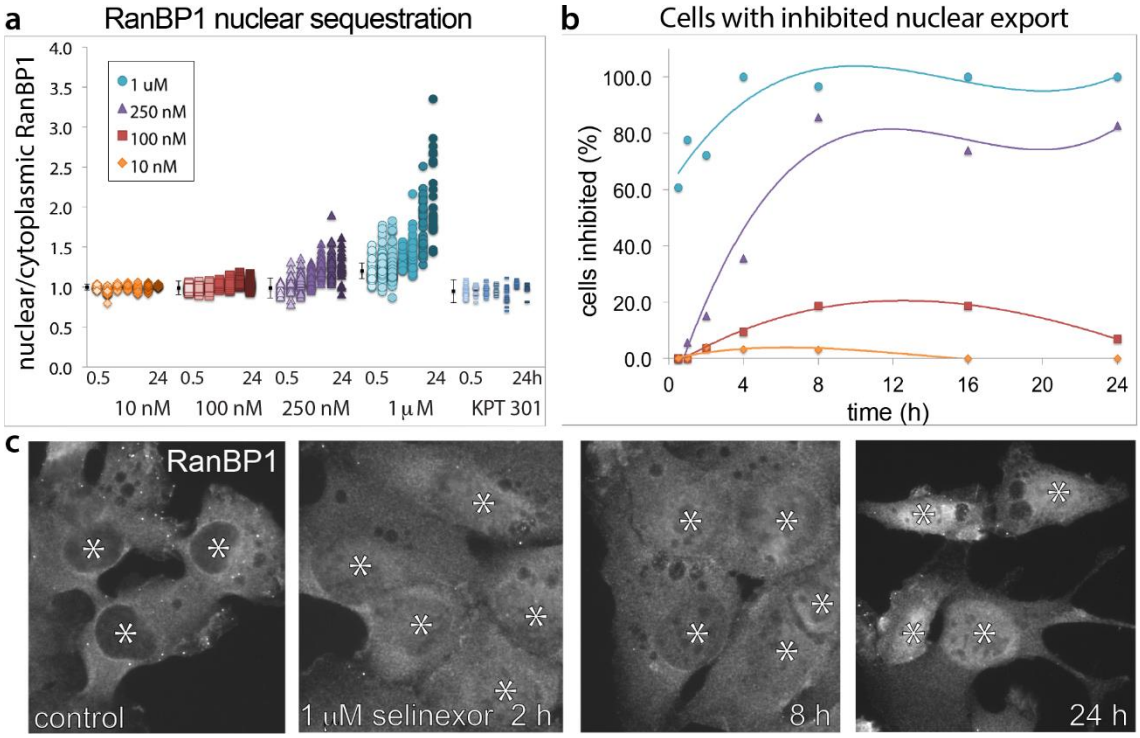

Figure 1.2: XPO1 inhibition by selinexor leads to rapid sequestration of cargo proteins. (A,B) HT-1080 cells were treated with varying concentrations of selinexor (10nM-1μM) over time (4-24 hours (h)). The inactive SINE compound (KPT-301) was included as a negative control. Cells were then stained with the XPO1 cargo protein RanBP1. The nuclear to cytoplasmic ratio was calculated to quantify nuclear sequestration of RanBP1. (C) Representative images are displayed. Asterisks (*) indicated nuclei. Figure adapted from Marcus et al., 2015.

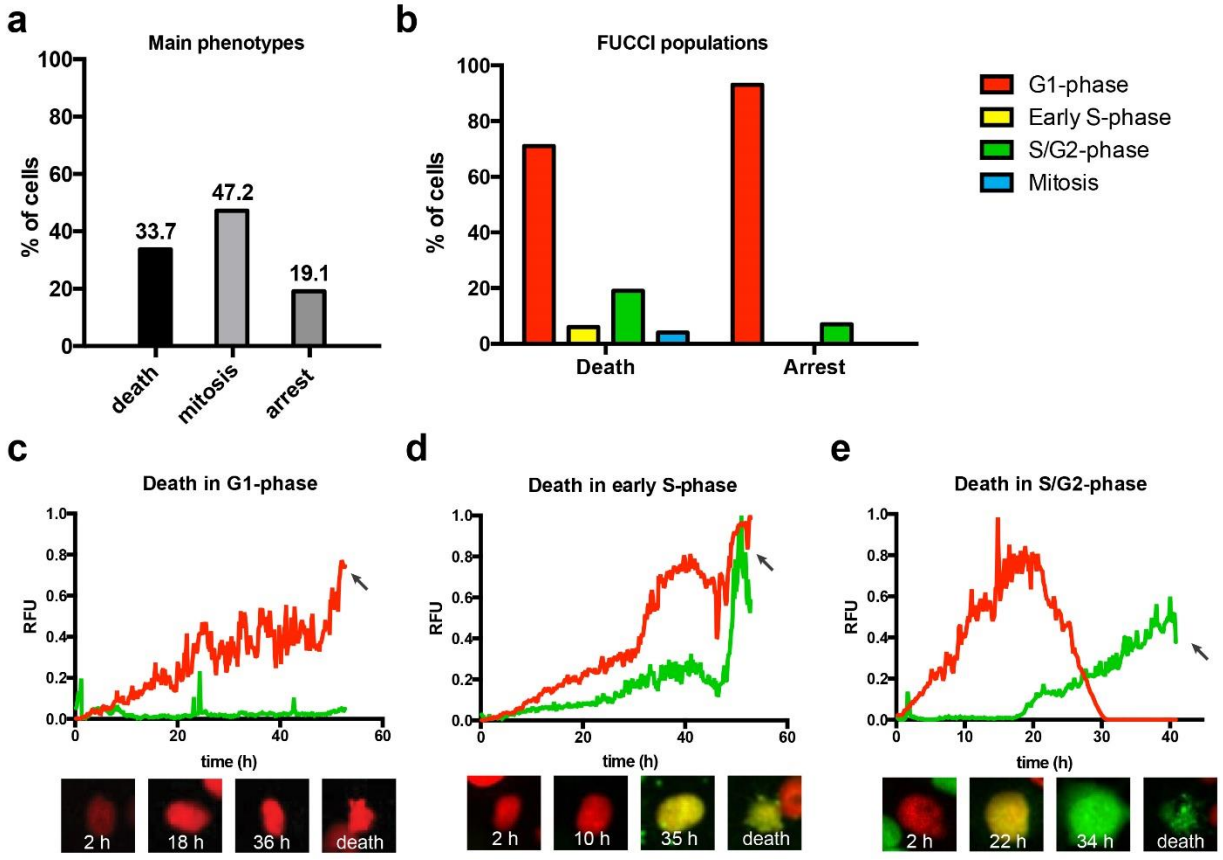

Figure 1.3: Response phenotypes of HT1080 cells after selinexor treatment. HT1080 cells expressing the fluorescent ubiquitin based cell cycle indicator (FUCCI) were treated with 1μM selinexor for 72 hours (h). Individual cells were longitudinally tracked and the mean fluorescence of the nuclear signal for both the FUCCI G1-phase probe (red) and S/G2-phase probe (green) were measured. (A) Different response outcomes are observed following selinexor treatment including death, progression through mitosis and cell cycle arrest. (B) Response is dependent on cell cycle status. (C-E) Individual cells are tracked after selinexor treatment. Death is seen in G-phase (C), S-phase (D) and S/G2-phase (E). Figure adapted from Marcus et al., 2015.

24 hours post-treatment (Tabe et al., 2015). Longitudinal tracking of cancer cells after selinexor treatment has revealed a variety of cell cycle effects including G1-phase arrest, prolonged S-phase and death within S-phase (Figure 1.3) (Marcus et al., 2015). The objective of this thesis is to determine the molecular basis of these differential response phenotypes of XPO1 inhibition.

1.4: DNA damage response in Eukaryotic cells

DNA double stranded breaks can occur after a variety of cell stress stimuli, including X-ray irradiation, replication stress and exposure to genotoxic agonists. Double strand breaks are detected by Ataxia telangiectasia mutated (ATM) kinase. The histone variant H2A.X is phosphorylated by ATM on serine 139 (also known as γH2A.X) (Kuo and Yang, 2008). γH2A.X serves as a scaffold to recruit other DNA damage repair proteins including the end binding protein complexes Mre11-Rad50-NBS1 (MRN) or Ku70/80 (Kim et al., 2005). Recruitment of these proteins as well as other repair proteins begin one of many different repair pathways, such as homologous recombination or non-homologous end-joining. The choice of repair pathway is largely dependent on the cell cycle status of the cell; non-homologous end joining occurring throughout interphase and homologous recombination occurring in S/G2-phase (Rothkamm et al., 2003). Pathway choice may also depend on chromatin structure and transcriptional status of the area surrounding the break site (Shibata et al., 2011).

Multiple DNA damage repair proteins are exported from the nucleus by XPO1. These include both BRCA1 and Chk1. In addition, proteins that are involved indirectly in DNA damage response to initiate cell cycle arrest, such as p53, are also XPO1 cargoes. It has been noted that treatment with selinexor reduces the expression of Chk1 and may lead to deficiencies in DNA

damage repair. The effects of these changes on DNA damage repair kinetics have not been well studied.

1.5: The nucleolus and ribosome biogenesis

The nucleolus is a non-membrane bound organelle within the nucleus of mammalian cells largely responsible for the transcription of ribosomal DNA (rDNA), processing of ribosomal RNA (rRNA), and subsequent formation of the 40S and 60S ribosomal subunits. rDNA is organized in multiple arrays consisting of rDNA gene repeats located on multiple different chromosomes that form the basis of nucleolar organizing regions (NORs). Mammalian cells respond to increased growth demands, including cell cycle progression, by increasing the number of active NORs to increase the number of ribosomes available for translation at any given time. In cancer, it is understood that nucleolar function is increased to account for a greater demand from growth of the tumor.

rDNA is transcribed by RNA polymerase I. Upstream binding factor (UBF) binds upstream of the transcription start site and is necessary for the recruitment of RNA polymerase I. A single polycistronic RNA is produced that includes the 18S, 5.8S and 25S rRNA species. Following transcription of the rRNA, many processing factors in the nucleolus are responsible for cleaving and processing the rRNA as well as recruiting and assembling the protein components of the 40S and 60S ribosomal subunits. The assembled ribosomal subunits are then transported out of the nucleus where they form the mature, translation-competent 80S. Nuclear export of the 60S subunit is dependent on XPO1 and is mediated through the chaperone NMD3 that contains a NES (Bai et al., 2013; Ho et al., 2000). While a NES-containing chaperone has

not been identified that binds the 40S subunit, nuclear export of the 40S subunit appears to be dependent on XPO1 function.

The effects of XPO1 inhibition on nucleolar function have been studied in a limited capacity. It has been noted that treatment of mammalian cells with leptomycin B leads to accumulation of the 60S chaperone protein, NMD3. Preventing the export of ribosomal subunits leads to defects in processing of the polycistronic rRNA (Bai et al., 2013). In addition, proteomic analysis of cells treated by the SINE molecule KPT-185 demonstrates that bulk ribosomal subunit amounts decrease (Tabe et al., 2015). The consequences of reduced nucleolar function following XPO1 inhibition on cell response and survival remain to be elucidated.

1.6: Research Goals and Thesis Scope

The work presented in this thesis began as a characterization of cell cycle effects observed following XPO1 inhibition, including a prolonged S-phase (Marcus et al., 2015). This thesis expands upon the molecular basis for variations in such response phenotypes. Beginning with characterization of the observed S-phase effects, we find that XPO1 leads to decreased frequency of cells in S-phase as well as defects in S-phase progression. Defects in DNA replication are known to cause DNA damage (Mazouzi et al., 2014). Staining for DNA damage repair proteins revealed the formation of large DNA damage break sites in response to XPO1 inhibition.

The first portion of this thesis concerns the timing of SINE-induced DNA damage within the cell cycle and the associated fates of those cells that acquire DNA damage. We find that DNA damage occurs in both G1-phase as well as S/G2-phase, although damage most often

occurs in G1-phase. In addition, the fate of cells is dependent on the timing of DNA damage within the cell cycle. Cells that acquire damage in G1-phase most often die, whereas those cells that acquire damage in S/G2-phase most often progress through mitosis.

The second half of this thesis explores the mechanism behind DNA damage formation. We find that DNA damage formation following XPO1 inhibition most often occurs within or proximal to nucleoli. Given previous nucleolar defects observed following XPO1 inhibition (Bai et al., 2013; Tabe et al., 2015), we explore the relationship between nucleolar dysfunction and DNA damage formation. We find that DNA damage formation is dependent on both active RNA polymerase I transcription and cell cycle progression. In addition, increasing the rate of rRNA transcription, through overexpression of the transcription factor, UBF, or loss of function of p53, leads to increased SINE-induced DNA damage formation.

A remaining question surrounding targeting XPO1, is the differences in effects of XPO1 inhibition on both cancer derived cells and normal cells. Given that nuclear export through XPO1 is a critical process for cell survival, it is crucial to study these differences. Throughout these studies, we find that DNA damage is not present in normal cell lines whereas DNA damage formation occurs to some degree in most of the cancer cell lines studied. However, nucleolar defects are observed in both normal and cancer cells. These effects are crucial to understand as the family of XPO1 inhibitors progresses further into clinical trials.

Chapter 2 : Inhibition of exportin-1 function results in rapid cell cycle-associated DNA damage

As published in Burke, R. T., Marcus, J. M., & Orth, J. D. (2017). Inhibition of exportin-1 function results in rapid cell cycle-associated DNA damage in cancer cells. Oncotarget, 8(24), 39460–39475. http://doi.org/10.18632/oncotarget.17063.

2.1: Introduction

Selective inhibitors of nuclear export (SINE) are a first-in-class family of compounds with potential clinical application in different disease states, including inflammation, autoimmunity, ALS and cancers (Aggarwal and Agrawal, 2014; Boeynaems et al., 2016; Freibaum et al., 2015; Gravina et al., 2015; Haines et al., 2015; Zerfaoui et al., 2010). SINE action works through direct, slowly-reversible covalent binding to the karyopherin exportin-1 (XPO1/CRM1) at cysteine-528 located in the cargo-binding cleft (Azmi et al., 2013; Crochiere et al., 2015; Turner et al., 2012). SINE binding to XPO1 prevents access of the cargo nuclear export sequence (NES) to the binding pocket, resulting in the subsequent nuclear accumulation and retention of cargo proteins (Crochiere et al., 2015).

Numerous studies use SINE to probe the anti-cancer potential of inhibiting XPO1 function (Azmi et al., 2013; Etchin et al., 2016; Lapalombella et al., 2012; Marcus et al., 2015). Within hours of SINE treatment, cargo sequestration, cell cycle arrest and progression defects, and activation of apoptosis are observed (Marcus et al., 2015; Zheng et al., 2014). Flow cytometry experiments in several studies report G1-phase accumulation and a rapid loss of the S-phase population after inhibition of XPO1 (Zheng et al., 2014). It is unclear from these studies what the fates of the cells accumulating in G1/S-phase are: progression and division, arrest, or

death. Cell cycle effects and apoptosis occur in many different cancer-derived cell lines and xenograft models with SINE, indicating potential broad efficacy of XPO1 as an anti-cancer target (Azmi et al., 2013; Salas Fragomeni et al., 2013; Zheng et al., 2014). Single cell longitudinal tracking using the fluorescent ubiquitin cell cycle indicator (FUCCI) system in HT-1080 fibrosarcoma cells shows that after acute treatment with selinexor (KPT-330) many cells treated in G1-phase exhibit G1-phase cell cycle arrest associated with cell death (Marcus et al., 2015). Some cells treated in G1-phase progress to cell division. These cells, and those treated in early S-phase, often show a protracted S-phase progression that is at least 2-fold longer than untreated cells, and some of these cells die in S-phase (Marcus et al., 2015). Cell stresses that may account for arrest and cell death in G1-phase and S-phase associated phenotypes –or– that in turn may be caused by abnormal S-phase progression, are unclear after selinexor treatment.

DNA damage can cause cell cycle arrest and death (Roos et al., 2016; Sperka et al., 2012). Likewise, abnormal DNA synthesis can result in DNA double-stranded breaks and S-phase arrest or progression defects (Dobbelstein and Sørensen, 2015; Helmrich et al., 2011; Mazouzi et al., 2014). Our and other's observations of G1-phase arrest and S-phase effects after SINE treatment prompted us to examine if there is a relationship between inhibition of XPO1 with SINE and DNA double-stranded damage.

2.2: Materials and Methods

Cell lines and plasmids

HT-1080 (ATCC) are grown in MEM with Earle's salt (Corning; 10-010-CV), sodium pyruvate (Sigma), non-essential amino acids (Sigma), penicillin/streptomycin (Sigma; P/S), and

10% FBS (Sigma). U2OS are grown in McCoys5a (Corning; 10-050-CV) with 10% FBS and 1% P/S. MCF7 are grown in RPMI (Corning; 10-040-CV), 10% FBS, and 1% P/S. HeLa, PANC-1 and human mesenchymal stem cells (MSC) are grown in DMEM (Sigma; D6429-500ML), 10% FBS, and 1% P/S. RPE1 are grown in DME/F-12 1:1 (Hyclone; SH30023.01), 10% FBS, and 1% P/S.

MSCs are obtained by a procedure adapted from Ahfeldt et al. (Ahfeldt et al., 2012). hiPSCs were cultured feeder free on Matrigel (Corning; 356234) in chemically defined E8 medium (Thermo; A1517001). For differentiation of hiPSCs into embryoid bodies, hiPSCs were disaggregated with 0.5mM EDTA into small clumps containing 5–10 cells and transferred to low-adhesion plastic 6-well dishes (Costar Ultra Low Attachment; Corning Life Sciences) in growth medium containing DMEM, 15% KOSR (Thermo; 10828010) and 1% GlutaMAX (Thermo; 35050061). After 7 days, embryoid bodies were collected and replated on gelatin-coated 6-well dishes in DMEM, 10% FBS, 1% GlutaMAX, 1% P/S. Upon confluency, cells were trypsinized in 0.25% trypsin:EDTA (Sigma; T4049) and replated on cell culture dishes and maintained as described above.

The HT-1080 mAG-hGem(1/110)/mCherry-BP1-2 expressing cell line was engineered by transfecting an HT-1080 mAG-hGem(1/110) cell line with the mCherry-BP1-2 expression plasmid (FuGENE 6, Promega; E2691) and selection in 1μg/ml puromycin. Cell lines expressing both probes were obtained via clonal selection in 96 well plates. The mAG-hGem(1/110) plasmid is from Sakaue-Sawano *et al.* (Sakaue-Sawano et al., 2008) via material transfer agreement. The mCherry-BP1-2 plasmid expresses a peptide fragment of the DNA damage response/transcriptional regulator protein 53BP1 that includes the γH2A.X binding domain and a mutated, non-functional Tudor domain, but lacks both BRCT domains. The peptide retains the

capacity to localize to sites of double-stranded DNA damage (Dimitrova et al., 2008). mCherry-BP1-2 pLPC-Puro was a gift from Titia de Lange (Addgene plasmid # 19835). Detection of DNA damage response using mCherry-BP1-2 was confirmed by treating expressing cells with 10μM etoposide and time-lapse microscopy.

Antibodies, immunofluorescence, and stains

Phospho-serine-139 H2A.X (γH2A.X) mouse monoclonal (Millipore JBW101) and rabbit monoclonal (Cell Signaling 20E3) are used at 1:500 dilution. Other antibodies are: 53BP1 (Cell Signal 4937, 1:200), NBS1 (Novus Biologicals 100-143. 1:500), pATM Ser1981 (Millipore 05-740. 1:1000), and RPA-70 (Santa Cruz 28304. 1:200). Goat and donkey anti-mouse or anti-rabbit secondary antibodies conjugated to AlexaFluor 488, 568, or 647 are from Invitrogen and used at 1:500 dilution. Cells were grown on #1.5 glass coverslips (VWR 48366-227). Cells were fixed in 3.7% formaldehyde in PBS (pH 7.4) for 20 minutes at room temperature, washed at least 3 times in PBS, permeablized in 0.2% Triton X100 (Sigma) in PBS, washed at least 3 times in PBS, blocked in 4% BSA in PBS for 60 minutes at room temperature, incubated in primary antibody diluted in 4% BSA/PBS for 60 minutes at room temperature, washed at least 3 times in PBS, incubated in secondary antibody diluted in 4% BSA/TBS for 60 minutes at room temperature, washed at least 3 times in PBS, and counterstained with 1μM DAPI for 5 minutes at room temperature, washed in distilled water, and mounted in ProLong Gold or Prolong Diamond antifade reagent (Invitrogen) on glass microscope slides (VWR, 16004-422).

Small molecules and treatment of cells

The SINE compounds KPT-185, KPT-330 (selinexor), and KPT-8602 and the inactive KPT-185 enantiomer, KPT-301, are from Karyopharm Therapeutics, Inc. (Newton, MA), and are

prepared in anhydrous DMSO (Sigma, Hybrimax) and used at the concentrations indicated. Etoposide and gemcitabine are from Selleckchem, dissolved in DMSO, and used at the concentrations indicated. Cisplatin (Sigma) is dissolved in dimethylformamide (Sigma), and used at the concentrations indicated. 5-fluorauracil (5-FU) (Sigma) is dissolved in DMSO and used at the concentrations indicated. Olaparib (LC laboratories) is dissolved in DMSO and used at the concentrations indicated. For FUCCI fixed cell experiments, 10μM Cdk4/6 inhibitor PD-0332991 (Selleckchem) for 16 hours is used as a G1-phase arrest standard, and 10μM etoposide (Selleckchem) for 8 hours is used as an S/G2-phase arrest standard as previously described for HT-1080 cells (Marcus et al., 2015). Cells are approximately 70% confluent at the time of drug treatments.

Microscopy, FUCCI scoring, cell tracking, and quantification

Fixed cell, immunofluorescence microscopy was performed using an inverted Olympus IX81 microscope with Prior Lumen200 Pro metal halide lamp, Hamamatsu ORCA R2 CCD camera, motorized Prior ProScan III stage, and 20X 0.70NA, 40X 0.75NA, and 100X oil immersion 1.40NA objectives using optical filters for DAPI (Chroma), Alexa488/EGFP (Chroma), Alexa568/mCherry (Chroma) and Alexa647/Cy5 (Semrock). High-resolution, structured illumination microscopy (SIM) was performed using a Nikon A1/N-SIM microscope with 100X oil immersion 1.49NA TIRF objective and 405, 488, 561, and 647 lasers and optical filters from Chroma. SIM images were reconstructed using Nikon Elements software. Two investigators scored the FUCCI status in fixed cell experiments. Briefly, nuclei (DAPI) were identified using the Analyze Particles tool in FIJI (NIH). Fluorescence intensity values in the red and green channels were measured and based on signal over background cells were scored as G1- (red), G1/S (yellow), or S/G2-phase (green). For DNA damage foci in fixed cells, the “Find

Maxima' tool in FIJI using appropriate thresholding based on positive control cells treated with 10μM etoposide to isolate DNA damage foci above background was used, and cells were scored as positive or negative. Live-cell microscopy was performed using an inverted Olympus IX81, 20X 0.70NA objective, and stage-top incubation chamber (InVivo Scientific) as described previously (see [10, 21]). Autofocusing was performed using phase-contrast. To minimize acquisition delay between green and red channels, EGFP/mCherry dual optical filters (Semrock) and filter wheels were used. Control conditions are included in each experiment to confirm normal growth. Two investigators independently tracked all live cells. For DNA damage foci formation, puncta matching the properties of those found in fixed cells were identified by eye and validated by a second investigator. Each cell was tracked longitudinally and fates were defined as; 1) death, cell rounding accompanied with blebbing and cell fragmentation, 2) arrest, cells remain in interphase, and 3) cell division, cell enters mitosis and completes division. The cell numbers analyzed in each case are provided in the respective figure legends.

Neutral DNA comet assay

The Trevigen DNA comet assay kit was used following the manufacturer's protocol. Briefly, drug treated cells are resuspended with 0.5% Trypsin and $3x10^6$ cells/ml were suspended into low melting point agarose. Cells were placed onto glass slides provided with the kit. Prepared slides were placed in 1X TAE running buffer and electrophoresed at 22 volts for 35 minutes, per the manufacturer's protocol. DNA was stained using Sybr Gold (Invitrogen). Glass coverslips were mounted on top of the sample using Prolong Gold anti-fade reagent. DNA comets were imaged using an Olympus IX81 inverted epifluorescence microscope and 10X 0.40NA objective with a YFP filter set (Omega). Tail length and tail moment were calculated using the ImageJ plugin OpenComet (Gyori et al., 2014). All tail-lengths and tail moments are

plotted using box and whisker plots, the median is indicated. Significant differences between the populations are calculated using a two-tailed student's T-test. Comet number is >100 for each condition from two experiments.

Drug combination effects

Selinexor was combined with gemcitabine, 5-FU, etoposide, cisplatin, or olaparib. Briefly, 500-1000 HT-1080 cells were plated into 96 well white-walled plates (Thermo Scientific) with glass or optical plastic bottoms, grown overnight, and treated with the indicated conditions for 72 hours. ATP luminescence (CellTiter-Glo 2.0, Promega) was read using a Biotek plate reader within 10 minutes of sample preparation. Effects on cell survival over equimolar dose combinations were calculated using the median effect model (Chou and Talalay, 1983, 1984). Statistical modeling of combination effects was determined using a script in R based on previous methods, and using the software package CompuSyn (Burke et al., 2013; Chou and Martin, 2005; Lee et al., 2007). For the selinexor and gemcitabine combination, luminescence values were also measured at 24, 48, and 72 hours. For an x-irradiation control, cells in 96 well plates were exposed to 3 Gy.

2.3: Results

2.3.1: DNA damage after SINE treatment depends on XPO1 Cysteine-528

Cell-based effects after XPO1 inhibition by SINE begin within hours of treatment, including the nuclear sequestration of cargos, cell cycle effects, and cell death (Etchin et al., 2016; Gravina et al., 2015; Marcus et al., 2015). The cell cycle effects are complex, including arrest and progression defects as characterized by flow cytometry and time-lapse microscopy with longitudinal tracking of cells (Marcus et al., 2015; Zheng et al., 2014). After 8 hours of acute treatment with SINE, we observe cell cycle progression defects, including in S-phase cells, before cell death occurs (Marcus et al., 2015). Cell cycle effects and cell death often associate with DNA damage. We asked whether DNA damage occurs after treatment with SINE. Fixed cell analyses of HT-1080 cells after 8 hours of SINE indicate dose-dependent double-stranded DNA damage in 35-40% of cells via immunostaining for the phosphorylated serine-139 histone variant H2A.X (γH2A.X) (Figure 2.1). Three different SINE compounds – selinexor (KPT-330), KPT-8602, and KPT-185 – each cause foci formation to the same extent (Figure 2.1C). The KPT-185 enantiomer, KPT-301, at 1μM shows no increase in the number of cells with DNA damage foci over mock treated cells (0.05% DMSO) (data not shown).

Many previous studies use 1μM to study SINE response and it can be achieved in vivo (Azmi et al., 2013; Kim et al., 2016; Lapalombella et al., 2012). Unless noted otherwise, 1μM selinexor is used. In HT-1080, foci formation after 1μM selinexor treatment peaks after 8 hours and remains elevated over mock at 24 hours (Figure 2.2). In addition to HT-1080 cells, MCF7 breast carcinoma, U2OS osteosarcoma, HCT116 colon carcinoma, HeLa cervical carcinoma, and PANC-1 pancreatic carcinoma, cells show DNA damage foci after treatment with selinexor (Figure 2.3A-J). Interestingly, two proliferative, non-transformed human cell lines, telomerase

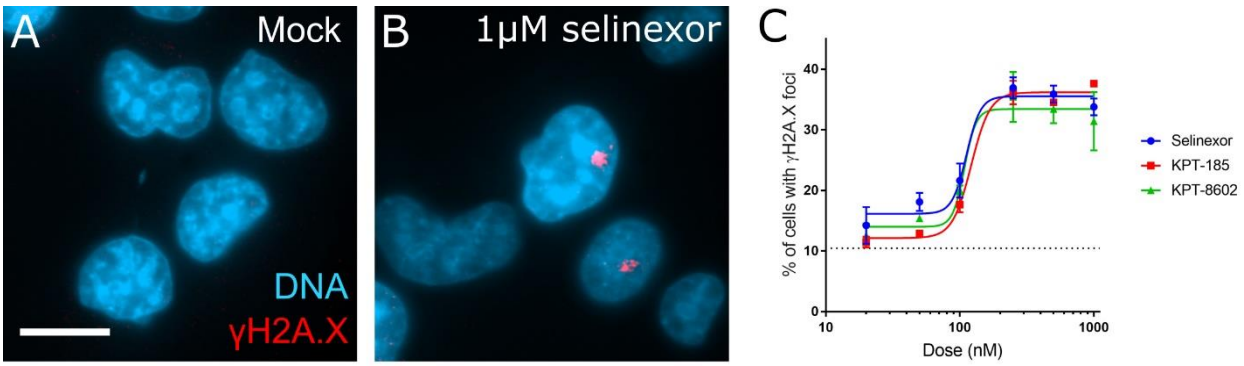

Figure 2.1. DNA damage foci formation is dose-dependent in response to SINE treatment. (A, B) HT-1080 cells were treated for 8 hours with DMSO (mock) or 1μM selinexor. Cells were fixed and stained for the phosphorylated histone variant γH2A.X (red) and DNA (blue). Prominent damage foci are present in selinexor treated cells. (C) Multiple XPO1 inhibitors show dose-dependent foci formation. Points represent the mean percent of cells at each dose with γH2A.X foci. The dotted line is the mock treated population. Error bars are the SEM from three replicate experiments, at least 100 cells scored in each. Note: The KPT-185 enantiomer KPT-301 does not cause foci formation (not shown). Scale bar in A = 10μm for all panels.

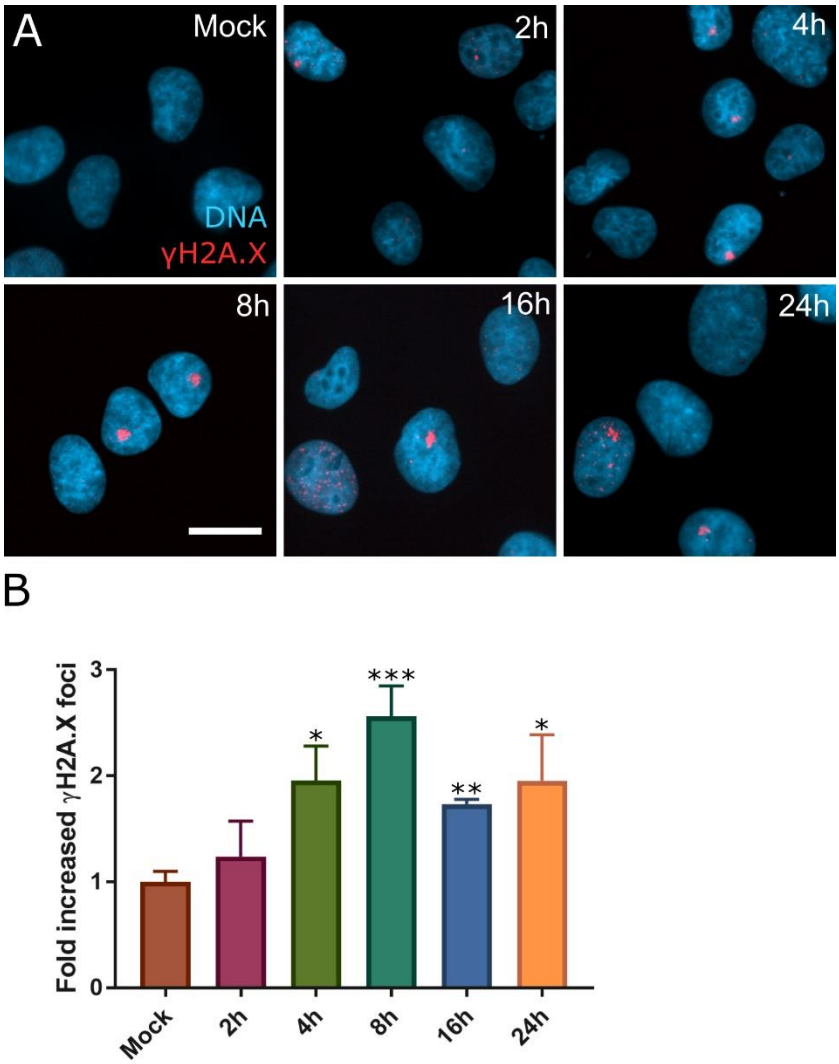

Figure 2.2. DNA damage foci form rapidly after SINE treatment. (A) HT-1080 cells were treated with DMSO (mock) or 1μM selinexor for 2, 4, 8, 16, or 24 hours. Cells were fixed and stained for γH2A.X (red) and DNA (blue). (B) Mean fold increase in cells with γH2A.X foci over mock treated cells for each time point was scored. Error bars are the SEM from three replicate experiments, at least 100 cells scored in each. A Student's t-test was performed comparing time points to mock treated. *** is $p<0.001$, ** is $p<0.01$ and * is $p<0.05$. Scale bar = 10μm for all panels.

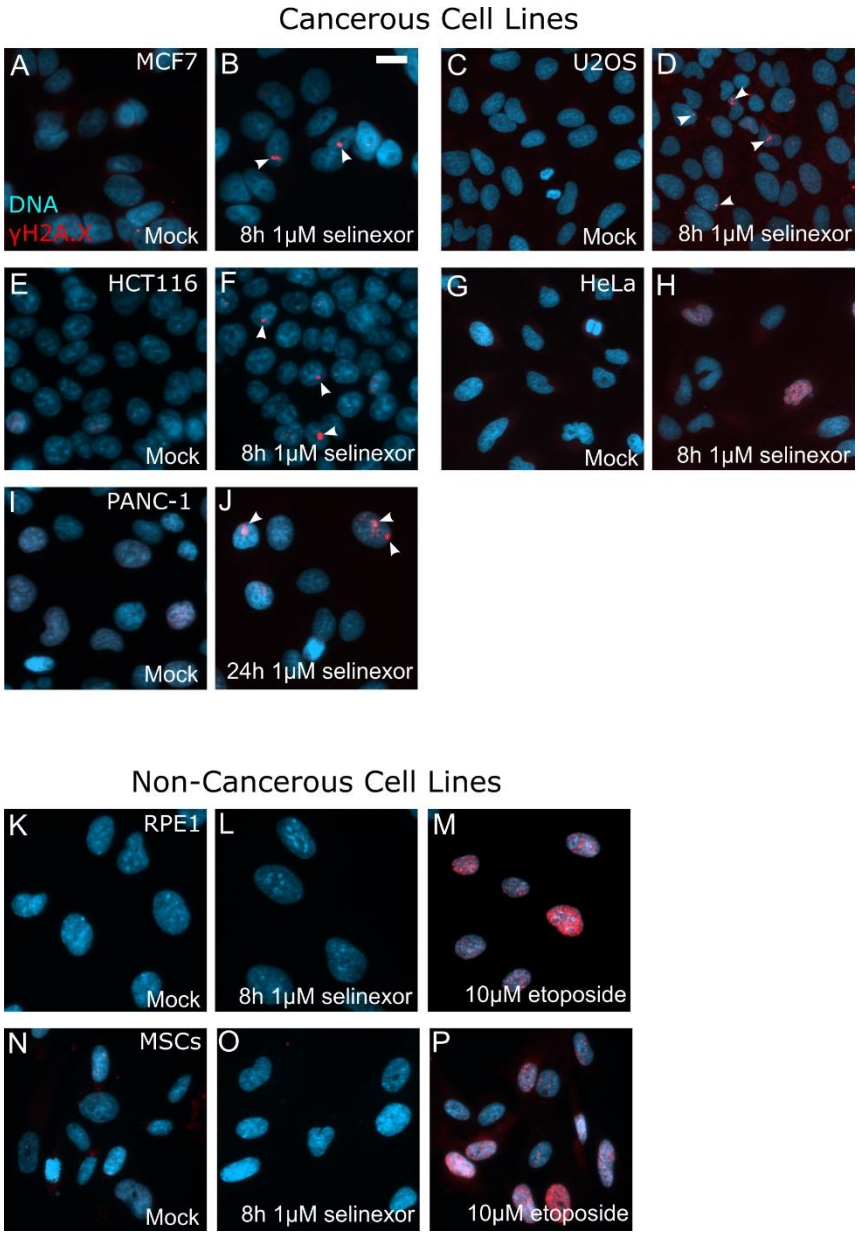

Figure 2.3. Several cancer-derived cell lines show increased, large DNA damage foci after selinexor treatment while non-cancer lines do not. Cells were treated with DMSO (control) or 1μM selinexor for the time indicated and stained for γH2A.X (red) and DNA (blue). White arrows indicate DNA damage foci. (A, B) MCF7 breast cancer derived cells show foci after 8 hours treatment. (C, D) U2OS bone cancer derived cells show foci after 8 hours treatment. (E, F) HCT116 colon cancer derived cells show foci after 8 hours treatment. (G, H) HeLa cervical carcinoma cell show increased damage after 8 hours treatment. (I, J) PANC-1 pancreatic cancer derived cells show foci after 24 hours treatment. (K-M) RPE1, non-transformed human telomerase immortalized cells derived from retinal epithelium, show no strong foci formation after 8 hours and 24 hours (not shown) treatment. DNA damage is present after 8 hours of 10μM etoposide. (N-P) Human mesenchymal stem cells (MSC) show no obvious increase in γH2A.X foci formation after 8 hours and 24 hours (not shown). DNA damage is present after 8 hours of 10μM etoposide. Scale bar in B = 10μm for all panels.

immortalized retinal pigment epithelial (RPE1) and mesenchymal stem cells (MSC), show no strong increase in γH2A.X foci staining after treatment with 1μM selinexor (Figure 2.3K-P). SINE molecules bind to XPO1 via the cysteine-528 residue (Azmi et al., 2013; Crochiere et al., 2015; Turner et al., 2012). To validate that DNA damage formation is specific to XPO1 inhibition by SINE, we transfected cells and expressed XPO1 mutated from a cysteine to a serine at residue 528 (XPO1 C528S). XPO1 C528S cannot bind SINE but is functional to export cargos (Neggers et al., 2015, 2016). Mutant transfected cells were treated for 8 hours with 1μM selinexor and the number of cells that form the γH2A.X foci compared to mock transfected cells, transfected cells expressing soluble mRFP, and transfected cells expressing wildtype XPO1 was quantified (Figure 2.4A). Treated control (1μM selinexor) or XPO1 wildtype expressing (XPO1, 1μM selinexor) cells show a 4-fold increase in γH2A.X foci formation over untreated (mock) cells after SINE treatment (Figure 2.4B-D, F). Cells expressing the XPO1 C528S mutant show only a 1.5-fold increase in cells with γH2A.X foci (Figure 2.4E, F). XPO1 C528S expression also significantly inhibited γH2A.X foci formation in U2OS cells (Figure 2.5), further demonstrating that DNA damage formation occurs downstream of SINE binding to cysteine-528 of XPO1.

We next characterized and validated the γH2A.X foci in HT-1080 as sites of double-stranded DNA damage. Co-immunofluorescent staining shows the γH2A.X foci also label for 53BP1, NBS1, phospho-(S1981)-ATM and RPA70, which are proteins that mediate the double-stranded DNA damage response (Figure 2.6). Line-scans through representative co-stained foci and plotting of the fluorescent intensity profiles indicates these damage response proteins are strongly localized, supporting these are damaged sites that cells may attempt to repair (Figure 2.6). Standard, low-magnification epifluorescence microscopy (e.g. 20X 0.70 NA air objective),

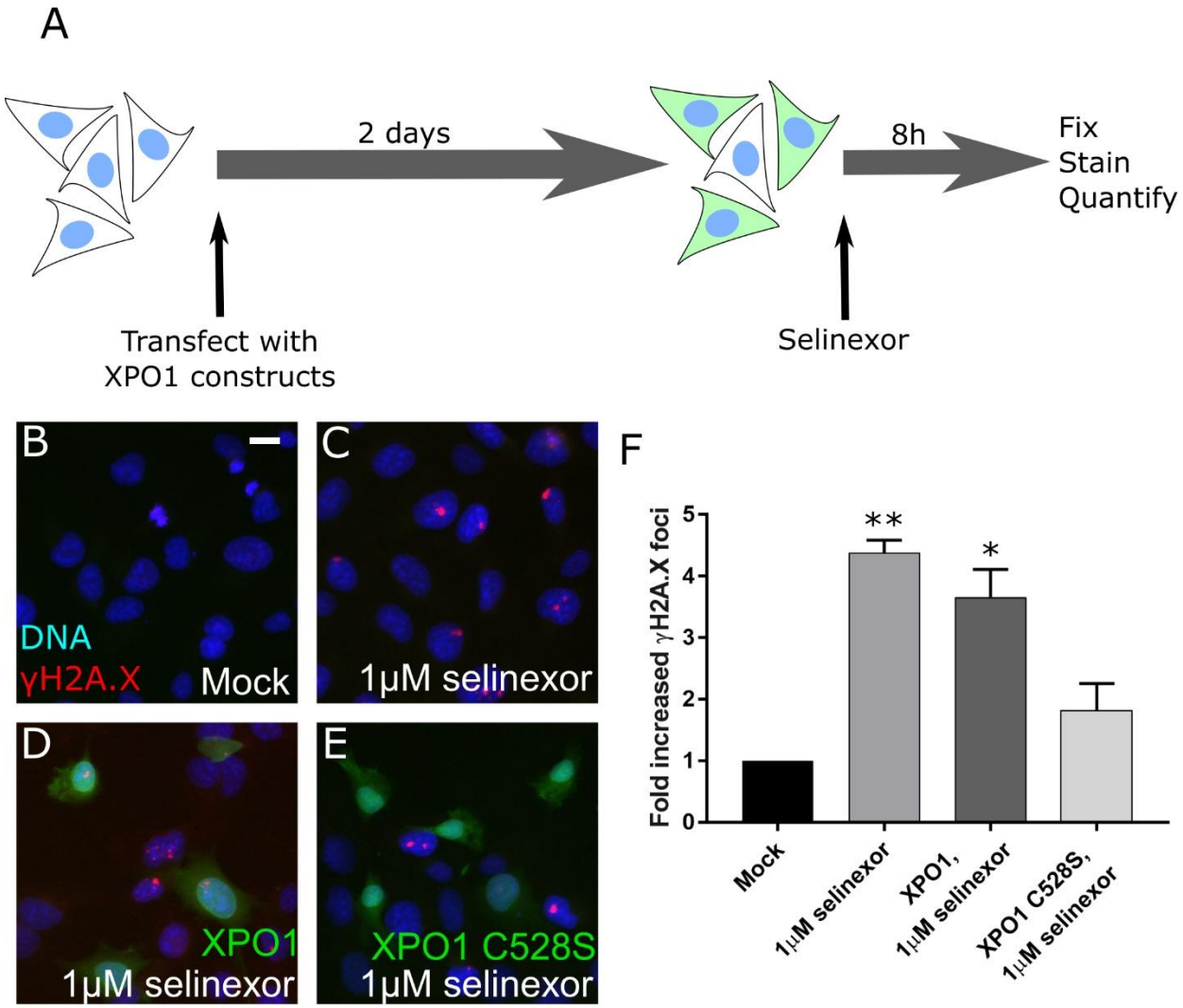

Figure 2.4. SINE treatment resulting in DNA damage foci requires XPO1 binding. (A) Experimental scheme. Cells are transfected, treated, and the DNA damage formation is quantified. (B, C) HT-1080 cells were mock transfected or (D) transfected with XPO1-RFP or (E) XPO1 C528S-RFP expression plasmids. Cells were treated with DMSO (mock) or 1μM selinexor for 8 hours. Cells were fixed and stained for γH2A.X (red) and DNA (blue). Transfected cells are shown in green. (F) The mean fold increase in DNA damage foci over mock was quantified. Error bars are the SEM from two replicate experiments, at least 50 cells scored in each. ** is $p<0.01$ and * is $p<0.05$ compared to mock. Scale bar in B = 10μm for all panels.

A

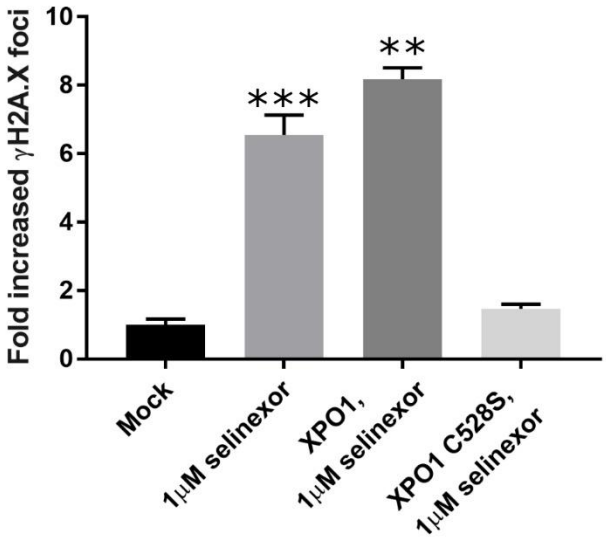

Figure 2.5. SINE treatment resulting in DNA damage foci requires XPO1 binding in U2OS cells. Experimental scheme is as Figure 2.4A. U2OS cells were mock transfected or transfected with XPO1-RFP or XPO1 C528S-RFP expression plasmids. Cells were treated with DMSO (mock) or 1μM selinexor for 8 hours. Cells were fixed and stained for γH2A.X and DNA. (A) The mean fold increase in DNA damage foci over mock was quantified. Error bars are the SEM from two replicate experiments, at least 150 cells scored in each. *** is $p<0.001$ and ** is $p<0.01$ compared to mock.

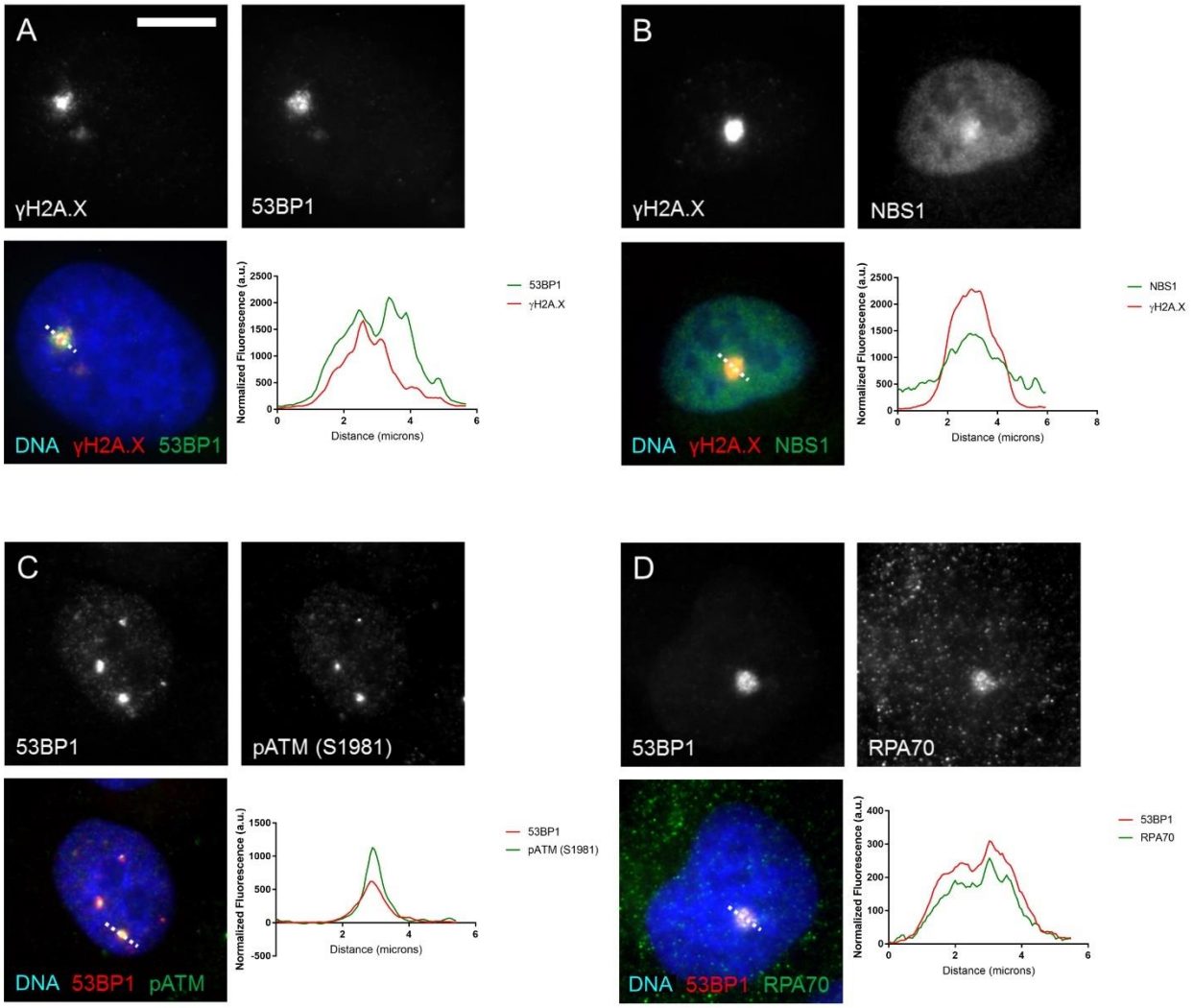

Figure 2.6. Double-stranded DNA damage response/repair proteins colocalize with γH2A.X. Cells were treated with 1μM selinexor for 8 hours, fixed and stained. Representative images are displayed with line scans through foci showing fluorescence intensities along the line. (A) 53BP1 (green) colocalizes with γH2A.X (red). (B) NBS1 (green) colocalizes with γH2A.X (red). (C) pATM S1981 (green) colocalizes with 53BP1 (red). (D) RPA70 (green) colocalizes with 53BP1 (red). Scale bar in A = 5μm for all panels.

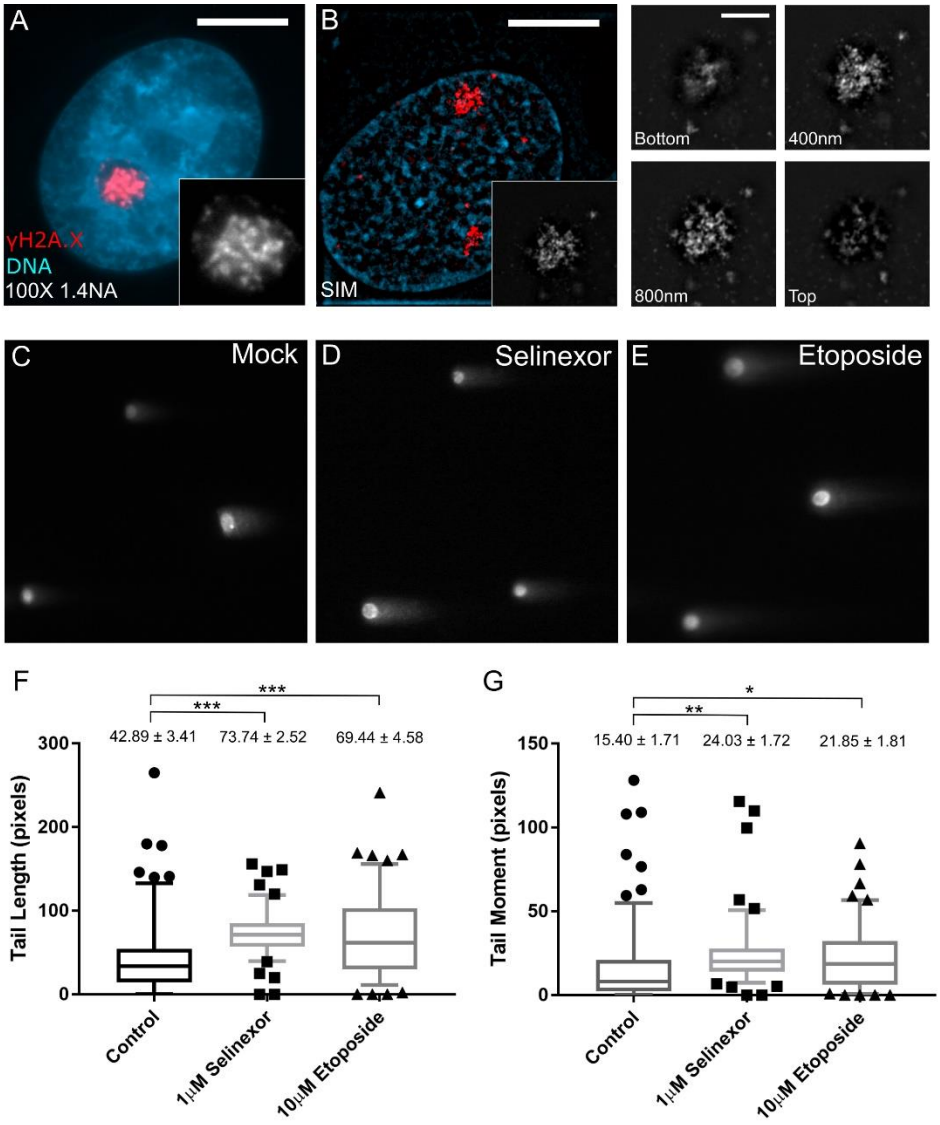

Figure 2.7. High-resolution microscopy and comet assay reveal multiple, clustered DNA double-stranded break sites. HT-1080 cells were treated with 1μM selinexor for 8 hours. (A) An example of a cell with DNA damage taken with widefield epifluorescence using a 100X 1.40NA objective. Scale bar = 3μm. (B) An example of a cell with DNA damage taken with structured illumination microscopy. Scale bar = 3μm. Four optical Z-sections are shown through the DNA damage structure. Individual foci are resolved within the cluster. Scale bar for Z-sections = 1μm. (C, D, E) A comet assay was performed on the cells treated with DMSO (mock), 1μM selinexor or 10μM etoposide for 8 hours. Representative images of comets are shown. (F) Quartile analyses of comet tail length. Horizontal line in each population is the median value. The tail length is significantly longer in both selinexor and etoposide treated cells. (G) Quartile analyses of the comet tail moment. Horizontal line in each population is the median value. The moment is significantly increased in both the selinexor and etoposide treated populations. Outliers from the 5th and 95th percentile are shown as individual points. Data is from two experiments, total of >100 cells. *** is $p<0.001$, ** is $p<0.01$ and * is $p<0.05$.

shows the γH2A.X stain as dense, with the structures measuring 1-3 microns in their largest x-y dimension after 8 hours treatment (e.g. Figure 2.1B or Figure 2.6A). It is unclear whether the structures are a single focus with a large accumulation of γH2A.X staining, or multiple distinct foci that are tightly clustered. High magnification (100X, 1.40NA oil) resolves some structural detail within the γH2A.X foci (Figure 2.7A). Three-dimensional, high-resolution SIM with a lateral resolution of approximately 100nm and axial resolution of approximately 300nm suggests of treatment with selinexor there is a significant increase in the length of associated comet tails and in the comet tail moment compared to spontaneous damage in control cells, indicating increased double-stranded damage to a similar extent using these measures as is caused by 8 hours of 10μM etoposide (Figure 2.7C-G).

2.3.2: DNA damage associates with G1- and S-phase cells with decreased DNA replication

DNA damage can occur throughout the cell cycle and lead to different cellular responses, including cell cycle arrest and death. We first sought to define if γH2A.X foci are cell cycle associated after treatment with selinexor. Using the FUCCI reporter system (Chittajallu et al., 2015; Marcus et al., 2015; Sakaue-Sawano et al., 2008), etoposide (topoisomerase IIα; S/G2-phase inhibition) and PD-0332991 (Cdk4/6; G1-phase inhibition) controls confirm the reporters accurately report on cell cycle phase (Figure 2.8A and (Marcus et al., 2015)). FUCCI expressing HT-1080 cells treated with selinexor for 2, 4, 8, 16, and 24 hours were fixed and stained for DNA and γH2A.X. Nuclei with the γH2A.X foci are classified as red only (G1-phase), red and green (yellow, G1/S-phase), and green only (S/G2-phase) (see Methods); cells in mitosis are excluded from this analysis. At 2 hours treatment, 15-20% of cells have the γH2A.X foci (Figure 2.2B); at this time, approximately 60% of cells are in G1- or G1/S-phase, regardless of damage

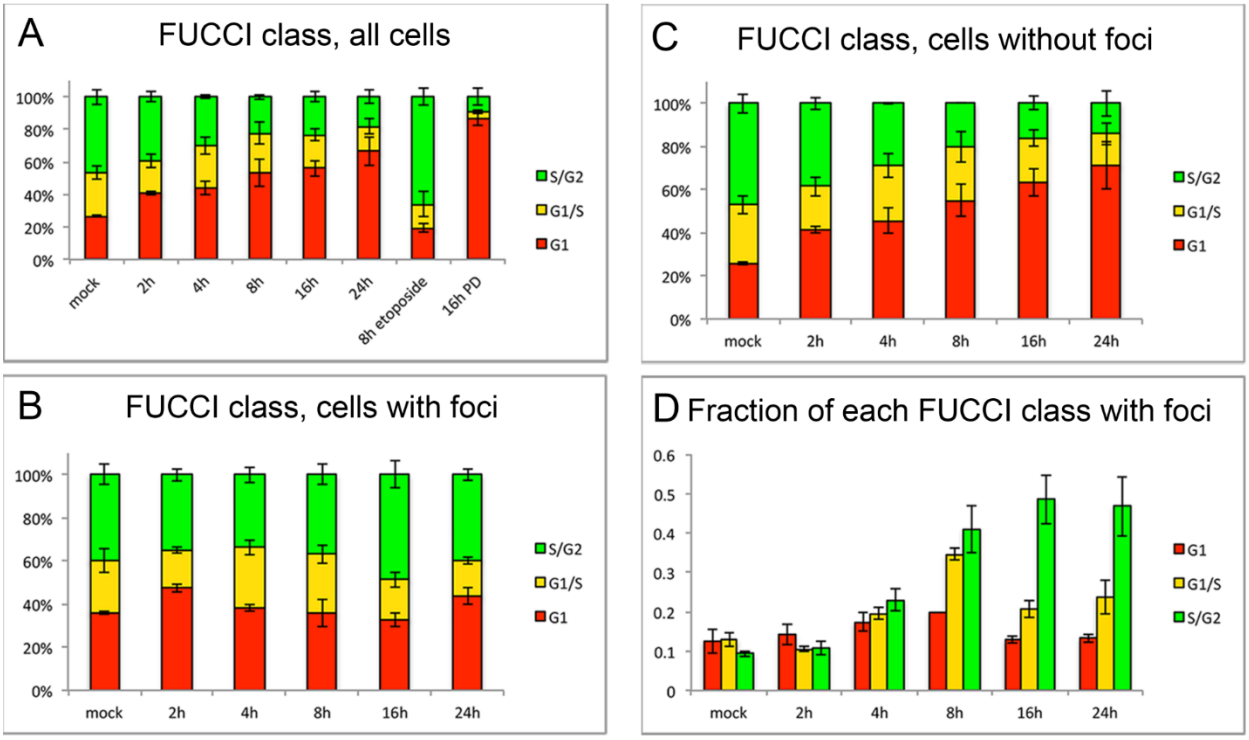

Figure 2.8. Cell cycle effects in HT-1080 correlate with DNA damage status. HT-1080 mKO2-hCdt1(30/120)/mAG-hGem(1/110) cells were treated with 1μM selinexor for increasing amounts of time, and then fixed and immunostained for γH2A.X to detect foci. 10μM etoposide (8 hours) and 10μM PD-0332991 (PD, 16 hours) were included as controls to ensure proper cell cycle response (see Methods). (A) The FUCCI class distribution (FUCCI signature) of the entire population of treated cells where cells are in G1-phase (red), G1/S-phase (yellow) or S/G2-phase (green). There is a steady accumulation of G1-phase cells to approximately 70% by 24 hours. (B) Cells with detectable damage foci were analyzed for FUCCI signature. Approximately 60% of cells with foci at early timepoints are present in G1- or G1/S-phase. (C) Those cells without detectable damage were analyzed for FUCCI signature. This population of cells shows a signature distinct from cells with damage, and steadily accumulates to approximately 70% G1-phase by 24 hours. (D) The cell population at each time point was analyzed for the fraction of each FUCCI class that show foci. At early timepoints, cells in G1- or G1/S-phase together show more foci, by 24 hours S/G2-phase cells more often show foci. For more detail see the text. N > 5000 cells for each time point and condition. Error bars are SEM from three experiments.

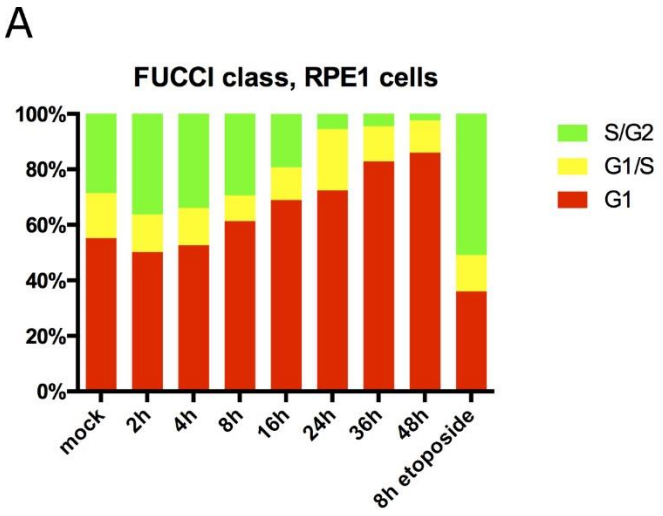

Figure 2.9. Cell cycle effects in RPE1 cells. RPE1 mKO2-hCdt1(30/120)/mAG-hGem(1/110) FUCCI cells were treated with 1μM selinexor for increasing amounts of time and the FUCCI classes were quantified. RPE1 cells do not form significant DNA damage foci after treatment with selinexor (Figure 2.3 K versus L). Over time, the population shifts toward a G1-phase FUCCI signature. By 48 hours, the population is >80% G1-phase. This FUCCI signature is similar to that seen in HT-1080 cells that do not show DNA damage foci (Figure 2.8C).

status (Figure 2.8A). Over time, the combined percentage of G1- or G1/S-phase cells with foci is relatively constant (Figure 2.8B). In contrast to cells with the γH2A.X foci, cells without DNA damage foci in the same population, shifts persistently and strongly to a G1-phase (red) state over time (Figure 2.8C), in agreement with the cell cycle arrest observed for this cell line previously (Marcus et al., 2015). We also calculated the fraction of each FUCCI class with γH2A.X foci over time. Between 2–8 hours after treatment, the fraction of G1- and G1/S-phase cells with foci increases from approximately 0.25 to 0.55, before decreasing at 16 and 24 hours (Figure 2.8D). The fraction of S/G2-phase cells with the γH2A.X foci accumulates after 4 hours, and remains elevated at 24 hours when approximately 70% of the total population is in a G1-phase state (Figure 2.8D and A). These data support that foci can form in G1- and S-phase, and may associate with prolonged S-phase and/or S/G2-phase arrest. Normal RPE1 cells do not accumulate DNA damage foci (Figure 2.3L) and respond rapidly to selinexor treatment by arresting in G1-phase (Figure 2.9) similar to the population in HT-1080 FUCCI that do not form damage (Figure 2.8C).

DNA damage can cause –or– be caused by S-phase progression defects (Mazouzi et al., 2014). We evaluated a potential relationship between DNA damage foci and S-phase after treatment with selinexor (Figure 2.10A). Following 8 hours of selinexor treatment, fewer HT-1080 cells are actively replicating their DNA and replication is significantly decreased based on quantification of EdU incorporation – even after 2 hours of EdU incubation (Figure 2.10B, C, Figure 2.11). Cells treated in a time course with selinexor, followed by a 15min EdU pulse were co-stained for γH2A.X. Mean incorporation of EdU per cell begins to decrease after 2h of selinexor exposure (Figure 2.10D), suggesting a rapid impact on S-phase progression. By 24h of SINE treatment, EdU incorporation is negligible. EdU – γH2A.X foci correlation analysis

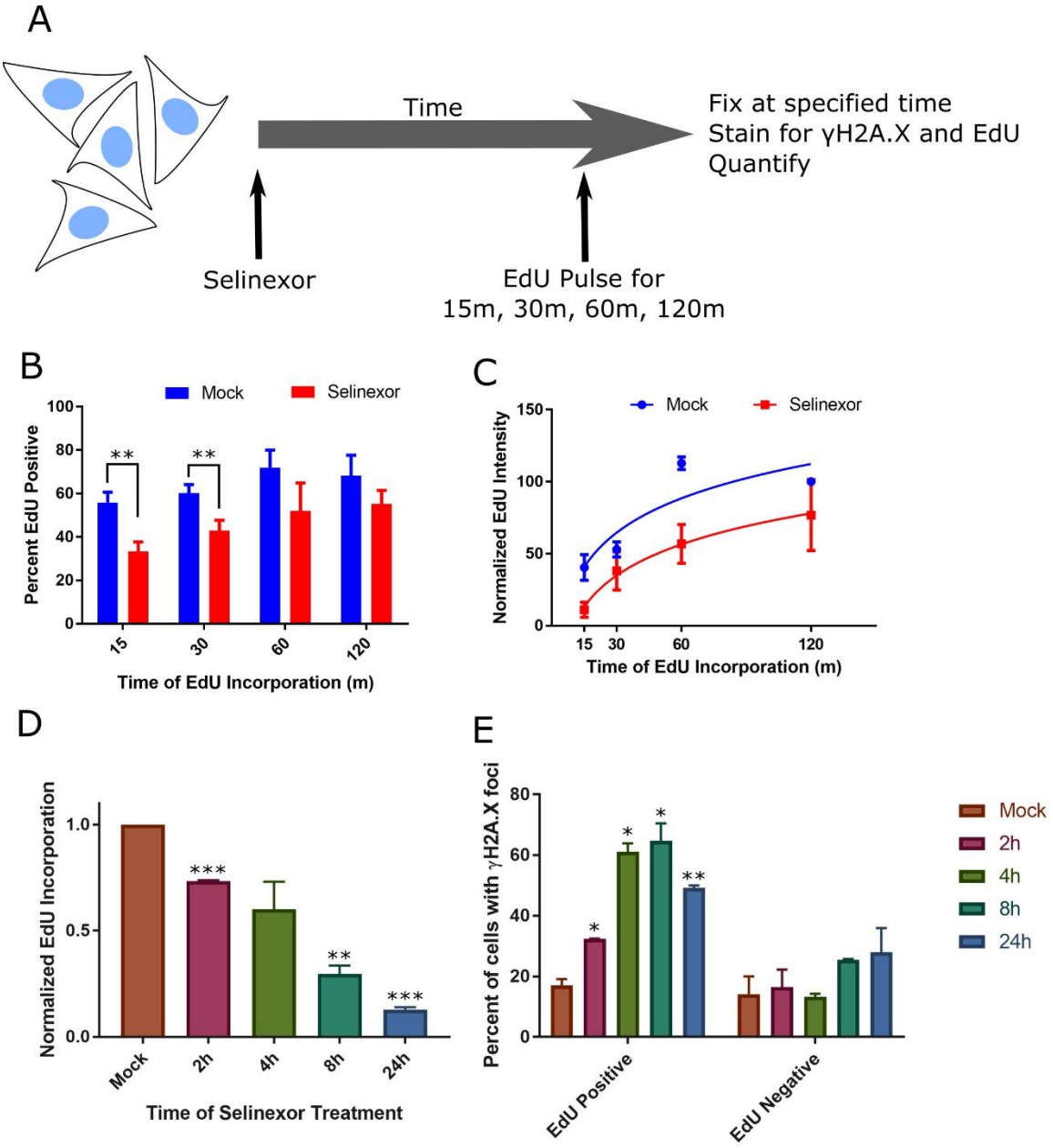

Figure 2.10. Cells with DNA damage foci associate strongly with S-phase cells and S-phase progression defects. (A) Experimental scheme. Cells treated with 1μM selinexor are pulse-labeling with EdU for varying times at the end, and quantified. (B, C) HT-1080 cells were treated with DMSO (mock) or 1μm selinexor for 8h and pulse-labeled with EdU for the last 15 minutes, 30 minutes, 1 hour, or 2 hours. Cells were fixed and stained for γH2A.X, DNA and EdU. Please see Supplemental Figure 7 for representative images. (B) The mean percentage of EdU positive cells after 8h selinexor is decreased compared to mock, regardless of EdU pulse length. Error bars are the SEM from three replicate experiments, at least 100 cells scored for each time point. (C) The mean integrated EdU signal intensity per cell is decreased after 8h of 1μM selinexor even after long EdU incorporation times. Error

bars are SEM from three replicate experiments, at least 100 cells scored for each time point. (D, E) HT-1080 cells were treated with 1μM selinexor for 2, 4, 8, and 24 hours and labeled with EdU for the final 15min of each time point. (D) The mean fluorescence of EdU decreases as the duration of treatment increases. Error bars are the SEM from two replicate experiments, at least 100 cells measured for each time point. (E) The population of analyzed cells was divided into two groups, EdU positive and EdU negative. γH2A.X foci were identified and the percentage of cells in each group with foci was quantified. EdU positive cells show damage foci more frequently than EdU negative cells. After 8 hours of selinexor treatment, 70% of EdU positive cells show foci compared to 25% of EdU negative cells. Error bars are the SEM from two replicate experiments, at least 100 cells measured for each time point. *** is $p<0.001$, ** is $p<0.01$ and * is $p<0.05$.

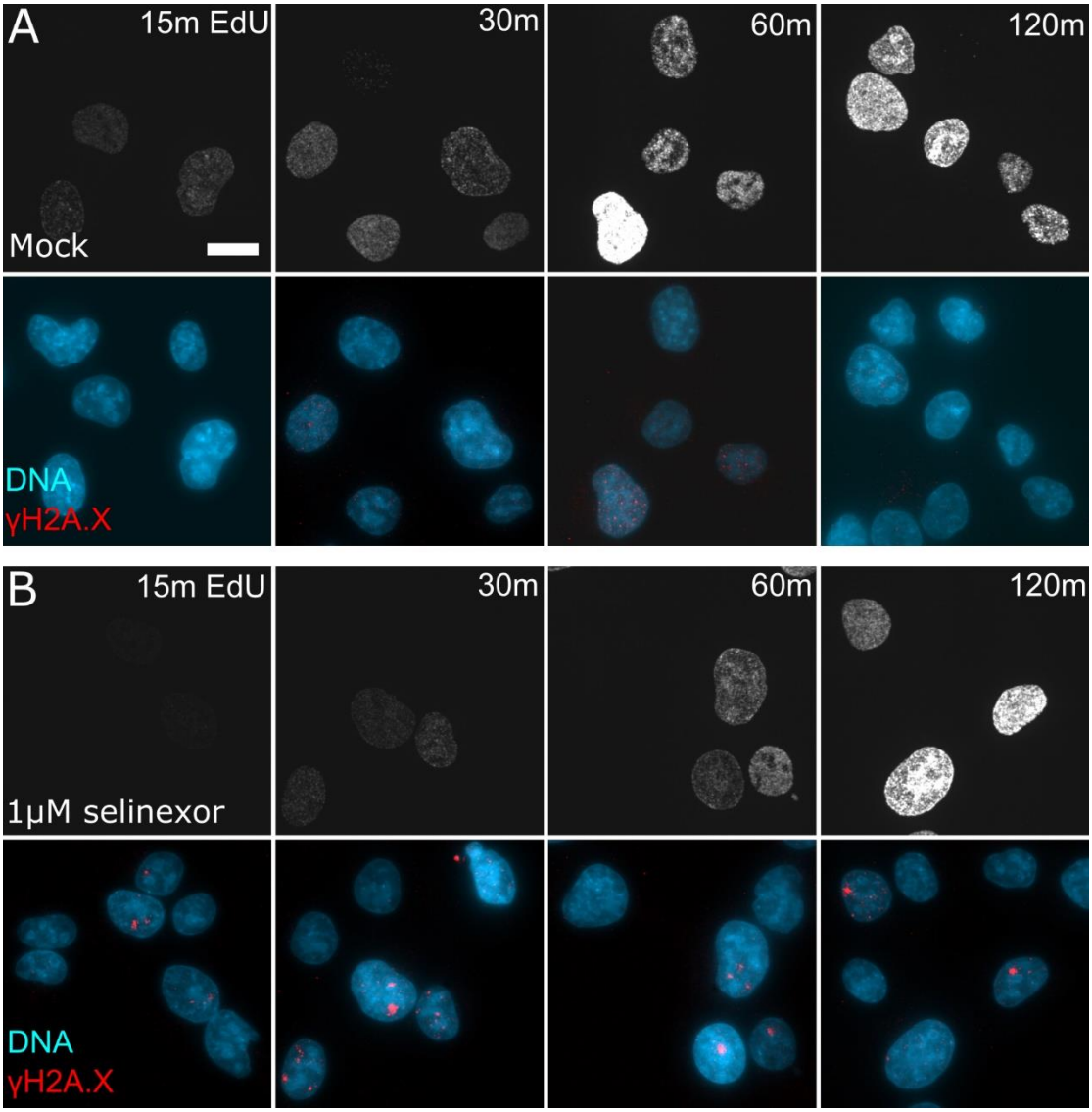

Figure 2.11. Representative images of HT-1080 cells from Figure 4. (A) HT-1080 cells were treated with DMSO (mock) or (B) 1μm selinexor for 8h and pulse-labeled with EdU for the last 15 minutes, 30 minutes, 1 hour, or 2 hours. Cells were fixed and stained for γH2A.X (red), DNA (blue) and EdU (white). Prominent DNA damage foci are observed in cells that also show some EdU labeling. Scale bar in A = 10μm for all panels.

indicates a positive association between positive, but decreased EdU labeling and the presence of γH2A.X foci that increases until 8 hours after treatment (Figure 2.10E). EdU negative cells in the same treated population show no strong association with γH2A.X foci status, but it does appear to somewhat increase over time compared to the EdU negative cells in the mock treated population (Figure 2.10E), indicating dead cells or that at least some cells with foci become arrested. In U2OS cells, selinexor treatment also results in decreased DNA replication based on EdU incorporation, and γH2A.X foci associate strongly with S-phase status after 8 hours of treatment (Figure 2.12); foci are present in approximately 30% of cells fixed after 8 hours of treatment. EdU incorporation in cells is nearly absent altogether after a 24 hour treatment (Figure 2.12A). These results in U2OS are consistent with HT-1080. Taken together, the FUCCI and EdU data indicate an association between DNA damage formation and the cell cycle, but the precise timing of the damage cannot be resolved nor does it allow for the direct determination of cell fate in cells with and without damage.

2.3.3: Longitudinal tracking shows that nearly 50% of all cells become damaged, mostly in G1- and S-phase, and >90% of cells damaged in G1-phase subsequently die

Fixed cell experiments show DNA damage increases within hours after treatment with 1μM SINE. For HT-1080, the peak percentage of cells with damage occurs at 8 hours and remains elevated at 24 hours, and the damage associates with G1- and S-phase (Figures 2.2, 2.4 and 2.11). To precisely define the timing of DNA damage formation with regard to G1- and S-phase directly in the same cell, we employed an HT-1080 reporter cell line stably co-expressing the double-stranded DNA damage probe, mCherry-BP1-2 (red, see Materials and Methods for detail), and the S/G2-phase FUCCI probe, mAG-hGem(1/110) (green), and time-lapse

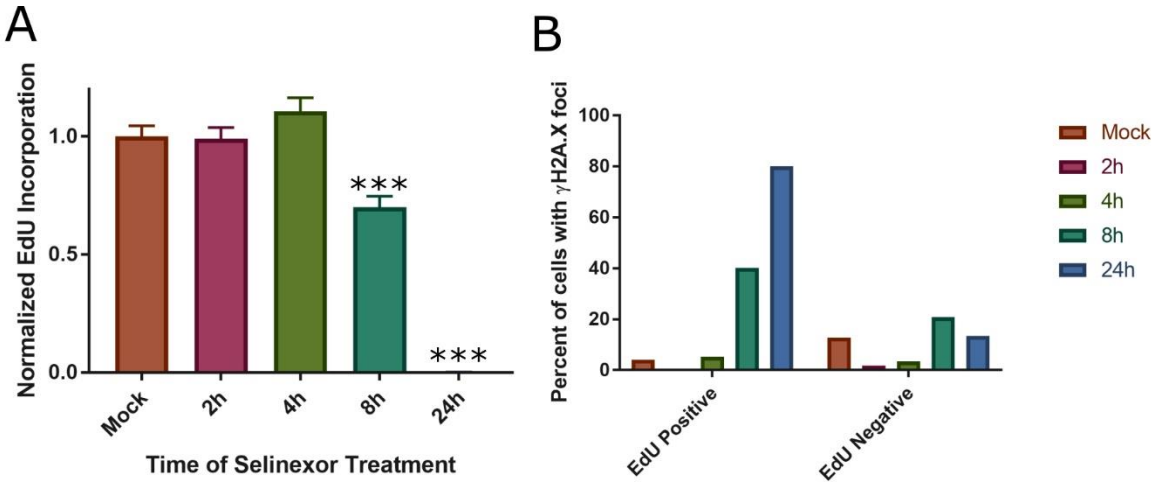

Figure 2.12. Cells with DNA damage foci associate strongly with S-phase cells and S-phase progression defects. U2OS cells were treated with DMSO (mock) or 1μM selinexor for specified times. Cells were pulse labeled for 15min with EdU at the end of treatment. Experimental scheme is as Figure 2.10A. Cells were then stained for γH2A.X and DNA. (A) The mean EdU incorporated in cells is decreased by 8 hours and negligible by 24 hours. Error bars are the SEM from >150 cells analyzed per condition. *** is $p<0.001$. (B) The population of analyzed cells was divided into two groups, EdU positive and EdU negative. γH2A.X foci were identified and the percentage of cells in each group with foci was quantified. EdU positive cells show damage foci more frequently than EdU negative cells.

microscopy and longitudinal tracking was performed (Figure 2.13A) (Burke and Orth, 2016; Marcus et al., 2015). After treatment with SINE, nearly 75% of cells that form DNA damage do so in G1-phase (absence of green signal); the remaining 25% are in S/G2-phase (green) (Figure 2.13B versus C, and Figure 2.13D). Cells that acquire DNA damage in G1/S-phase (yellow in FUCCI system, Figure 2.8) are represented in the S/G2-phase population using this reporter cell line. Longitudinal tracking reveals that close to 50% of all treated cells acquire damage within the first 24 hours after treatment with SINE, and approximately half of this occurs by 8 hours (Figure 2.13F). Timing analysis of damage formation in the damaged population indicates a rapid increase to approximately 15 hours after treatment, in support of a tight association with the cell cycle (Figure 2.13G). The cell cycle association of DNA damage and fraction of treated cells with damage foci over time suggest these cells are gradually lost and/or that the damage is repaired (Figures 2.2, 2.8, 2.12 and 2.13).

When SINE treated cells acquire DNA damage they are not dead. Rather, cells with DNA damage may undergo death, cell cycle arrest or senescence, or they may continue proliferating. Longitudinal tracking of treated HT-1080 mAG-hGem(1/110)/mCherry-BP1-2 cells shows that by 48 hours after treatment, 30% of all cells died and 26% divided (Figure 2.13D); over 40% of cells are classified as arrest/undetermined due to the end of imaging or movement from the analysis field; previous work indicates these cells may remain arrested (Marcus et al., 2015). The treated cell population can be parsed into populations that become damaged versus those that do not. Cells that acquire damage are more likely to die (33.9%) than to progress to cell division (19.1%) (Figure 2.13D). By comparison, treated cells that do not acquire damage divide more frequently divide (36.5%) than they die (24.3%). SINE treatment causes death with and without damage, but death is elevated in cells that become damaged (33.9% versus 24.3%).

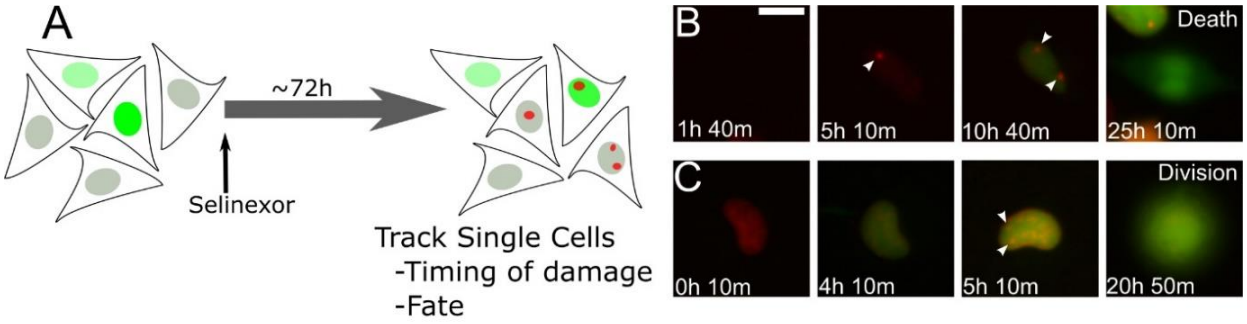

D

	Death	Division	Arrest/Unknown
All cells	30.2%	25.9%	43.9%
Cells that acquire damage	33.9%	19.1%	47.0%
Cells without damage	24.3%	36.5%	39.2%

	Cell Cycle Phase	
	G1-phase	S/G2-phase
All cells that have damage		
When damage occurs	74.3%	25.7%
At death/cell cycle arrest	47.7%	52.3%
Cells that Die		
When damage occurs	93.4%	6.6%
At death	54.5%	45.5%
Cells that Divide		
When damage occurs	23.8%	76.2%
At division	0%	100%

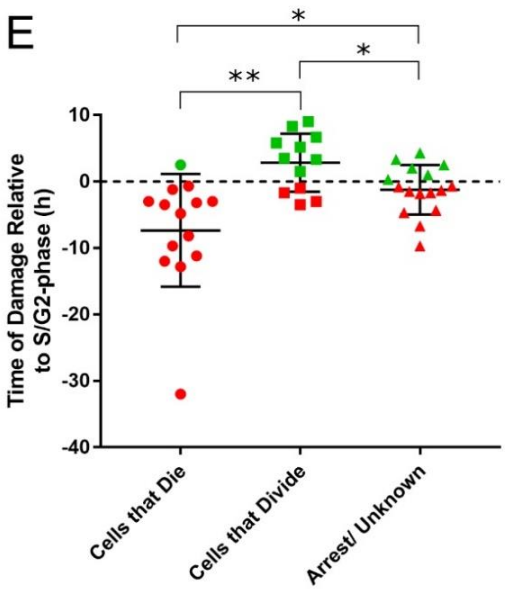

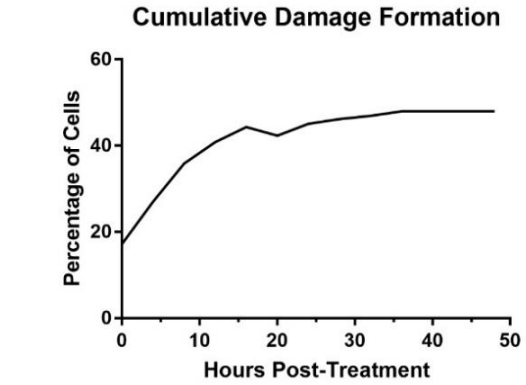

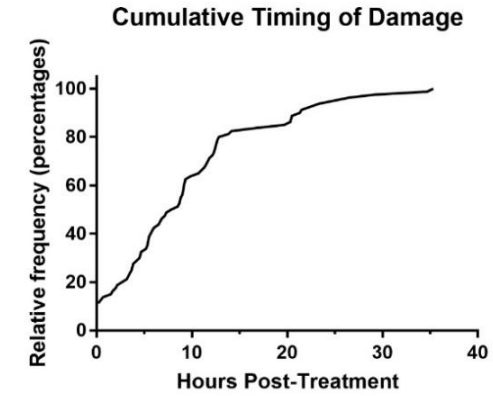

Figure 2.13. Live cell tracking of SINE treated cells reveals cell cycle associated DNA damage and cell fates. (A) Experimental scheme. HT-1080 cells that express mAG-hGem(1/110) and mCherry-BP1-2 were treated with 1μM selinexor and imaged every 10 minutes for 72 hours. DNA damage foci formation, cell cycle stage and cell fate were analyzed. (B, C) Representative examples of cells that acquire DNA damage foci are presented. (B) This cell acquires damage 5h 10m after treatment. The cell then enters S-phase (accumulation of mAG-hGem(1/110) probe) at 10h 40m and dies at 25h 10m. (C) The second example enters S-phase at 4h 10m, acquires damage foci at 5h 10m and progresses to cell

division at 20h 50m. White arrows indicate DNA damage foci. (D) Tables summarize the fate and cell cycle stages of 189 individually tracked cells. Over 70% of cells that become damaged, are damaged in G1-phase (absence of mAG-hGem(1/110) probe). For cells that die, over 90% are damaged in G1-phase, those cells that acquire damage and progress to cell division become damaged in S/G2-phase. (E) Cells that progress to S/G2-phase were analyzed to determine the timing of DNA damage accumulation in relation to the S/G2-phase transition and cell fate. The dotted line is S/G2-phase entry, designated time=0. Each point is an individual cell. The bars are the mean with standard deviation. Cells that become damaged and die in S/G2-phase are typically damaged several hours before S/G2-phase entry, where those that become damaged but divide are damaged shortly before or after S/G2-phase entry. ** is $p<0.01$ and * is $p<0.05$. (F) Cumulative damage formation within the entire tracked population. Nearly 50% of all cells acquire damage, mostly by 15 hours after treatment, and approximately 36% after 8 hours, in good agreement with fixed cell experiments. (G) The cumulative timing of damage for all cells that acquire damage is displayed. Damage formation is rapid until approximately 15 hours and slower thereafter. Scale bar in B = 10μm for all panels.

Of the damaged cells that die, greater than 90% show damage initially in G1-phase (Figure 2.13D); 58.0% remain in G1-phase and die and 42.0% progress to S/G2-phase and die. Of the damaged cells that progress to cell division, 76.2% were damaged in S/G2-phase (Figures 2.13 C,D). Next, we characterized the timing of DNA damage with relation to S-phase entry and cell fate for cells that form damage and progress to S/G2-phase (Figure 2.13E). For cells that form damage and die in S/G2-phase, damage most often occurs in G1-phase, 7-8 hours on average before entering S-phase (increasing mAG-hGem(1/110) probe). For cells that form damage and progress to cell division, DNA damage on average forms 2-3 hours after S-phase entry. The timing of DNA damage is on average 1-2 hours before entering S-phase for cells that arrest or whose fate could not be determined (Figure 2.13E). The ultimate fate of cells that acquire DNA damage and maximizing their death is an important consideration for how to most effectively use SINE against cancer.

2.3.4: Multiple classes of agents that compound DNA damage show combination effects with selinexor

DNA damage is a critical avenue to clinical efficacy for many cancer treatments, especially in combination chemotherapies that compound DNA damage to enhance the anti-cancer effect (Hosoya and Miyagawa, 2014; Ranganathan et al., 2016; Turner et al., 2016). Nearly 50% of all cells form DNA damage after treatment with SINE (Figure 2.13F). While cells that acquire damage show modestly elevated frequency of death than their undamaged counterparts, over 60% arrest or progress to cell division (Figure 2.13D). We tested equimolar combinations of selinexor with multiple different DNA damage agonists in an attempt to find combination effects that significantly decrease cell survival. We used nucleoside analogs, a

platinum-based DNA intercalator, a topoisomerase IIα poison, and a poly-ADP-ribose polymerase-1 (PARP1) inhibitor that are all approved for the treatment of human cancers in combination with other agents (Figures 2.14, 2.15 and 2.16). Further, clinical trials are planned that combine selinexor with these or highly related chemotherapy compounds (ClinicalTrials.gov).

The median effect model was used to calculate the combination effects. Both CompuSyn and an R based analysis package (see Materials and Methods) were used to calculate the combination effect indices using ATP as a surrogate for cell survival (Figures 2.14 and 2.16). Results from both methods were the same, and results using CompuSyn are shown as it is widely available. Applying the guidelines of Chou and Martin (Chou and Martin, 2005) regarding drug combination effects, there is significant synergy (combination index <1.0) of selinexor with each of these agents in at least some equimolar combinations (Figure 2.14A-D and Figure 2.16B). The concentrations of selinexor used are 31.25nM-1μM in each combination series. The other compounds were used at equimolar ratios depending on the effect of the compound alone (1:10, 1:1 or 10:1, see Figures 2.15 and 2.16).

The nucleoside analogs gemcitabine and 5-FU show strikingly similar combination effects across the dose combinations tested (Figure 2.14A, B). Gemcitabine shows combination indices <1.0 for the four lowest concentration combinations. We chose concentrations that were approximately half the EC50 to characterize the selinexor– gemcitabine combination over time (30nM selinexor, 3nM gemcitabine) (Figures 2.14 and 2.15). As single agents, there is no significant decrease in cell survival by 72 hours compared to untreated. The combination has a significant decrease in viability compared to untreated at 48h and 72h, with an approximate 25% decrease in survival at 48 hours, and nearly a 50% decrease at 72 hours (Figure 2.14E).

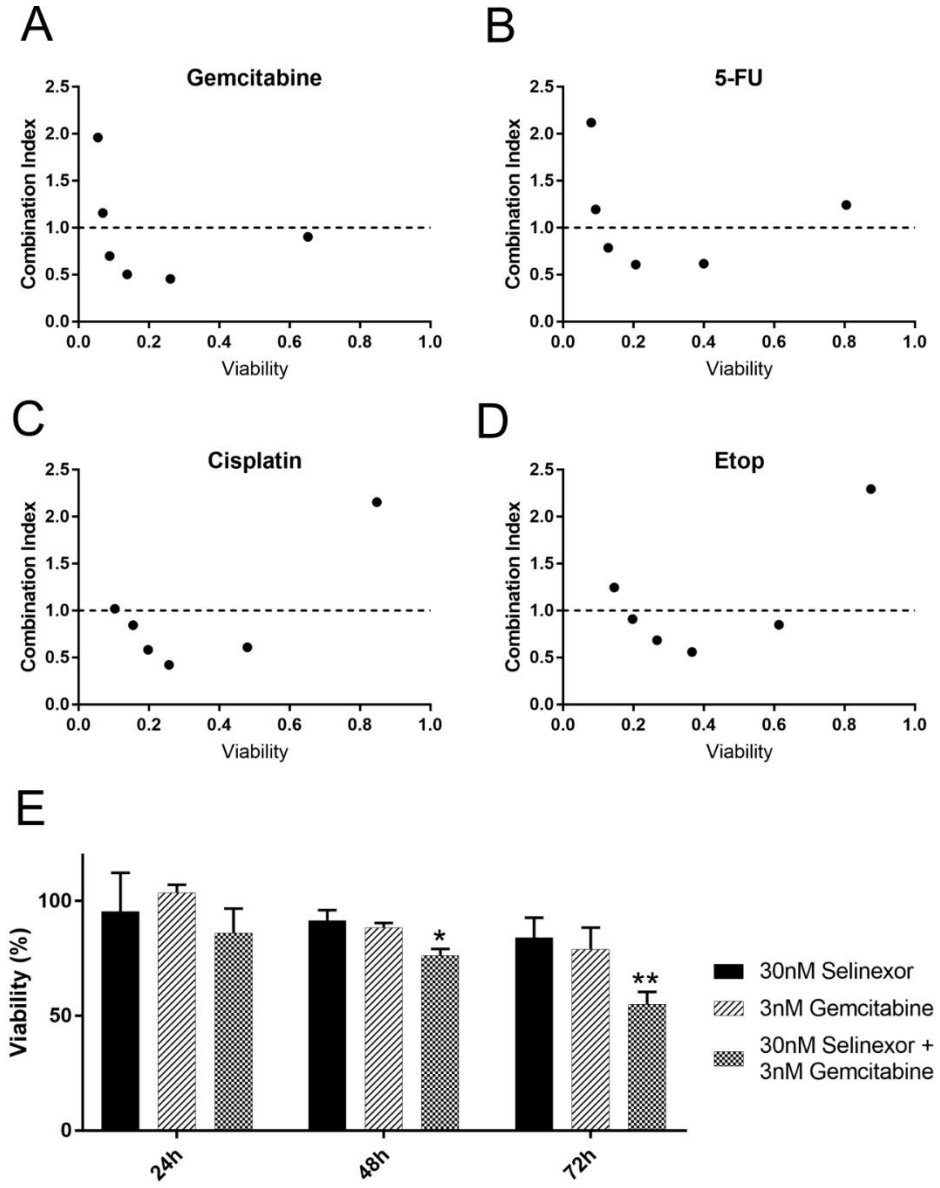

Figure 2.14. Selinexor combines synergistically with different classes of DNA damage agents. HT-1080 cells were treated with selinexor and the FDA approved therapeutics in equimolar concentrations (A-D). Relative cell survival was detected with CellTiter-Glo after 72h. Combination indices for each combination were calculated using the median effect model. The dotted line represents a combination index of 1. Points less than 1 are synergistic whereas points greater than 1 are antagonistic. (E) A time course with selinexor or gemcitabine alone and in combination was performed at half the EC_{50} concentration. Survival at each time point is determined via normalization to DMSO (mock) treated wells. A significant decrease in survival compared to mock treated is seen at 48h and 72 hours post treatment in the combination. Error bars are SEM from 3 experiments. ** is $p<0.01$ and * is $p<0.05$.

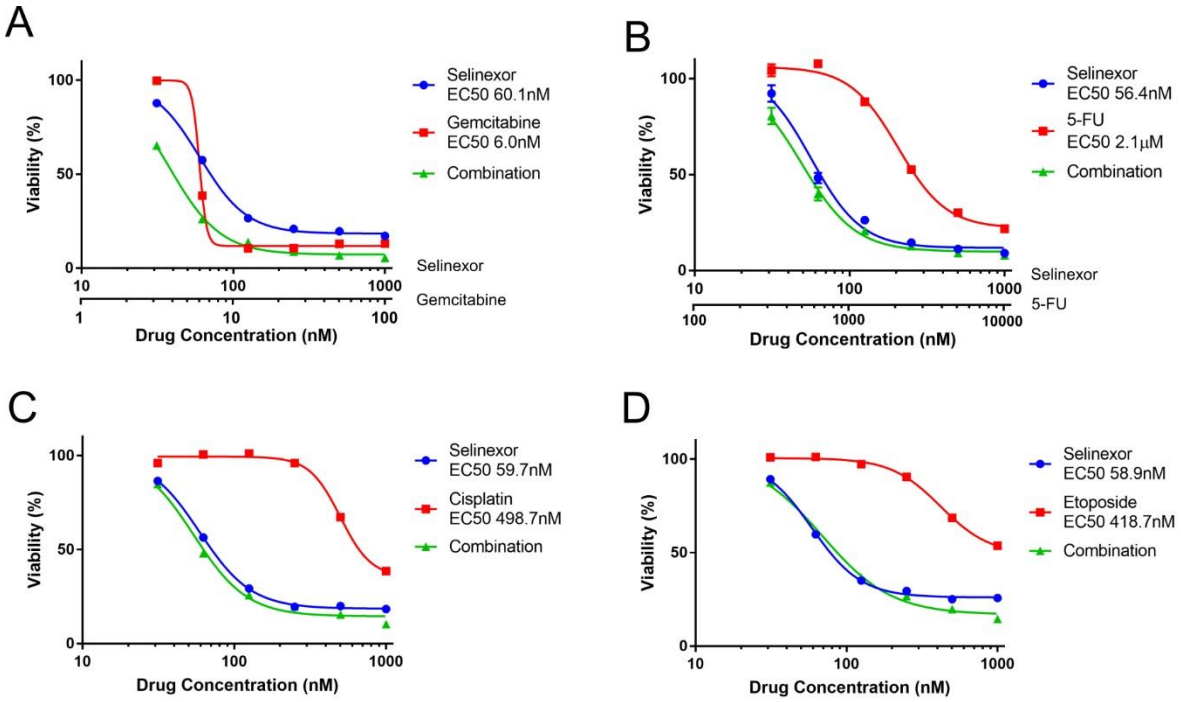

Figure 2.15. Single agent and combination dose responses of selinexor and different classes of DNA damage agents. (A-D) After 72 hours, ATP was measured as a surrogate for cell survival. Survival curves were performed for single agents alone and in combinations with selinexor. EC_{50} concentrations are noted in the respective figure key. Combination indices were calculated in Figure 2.14 for each equimolar combination dose.

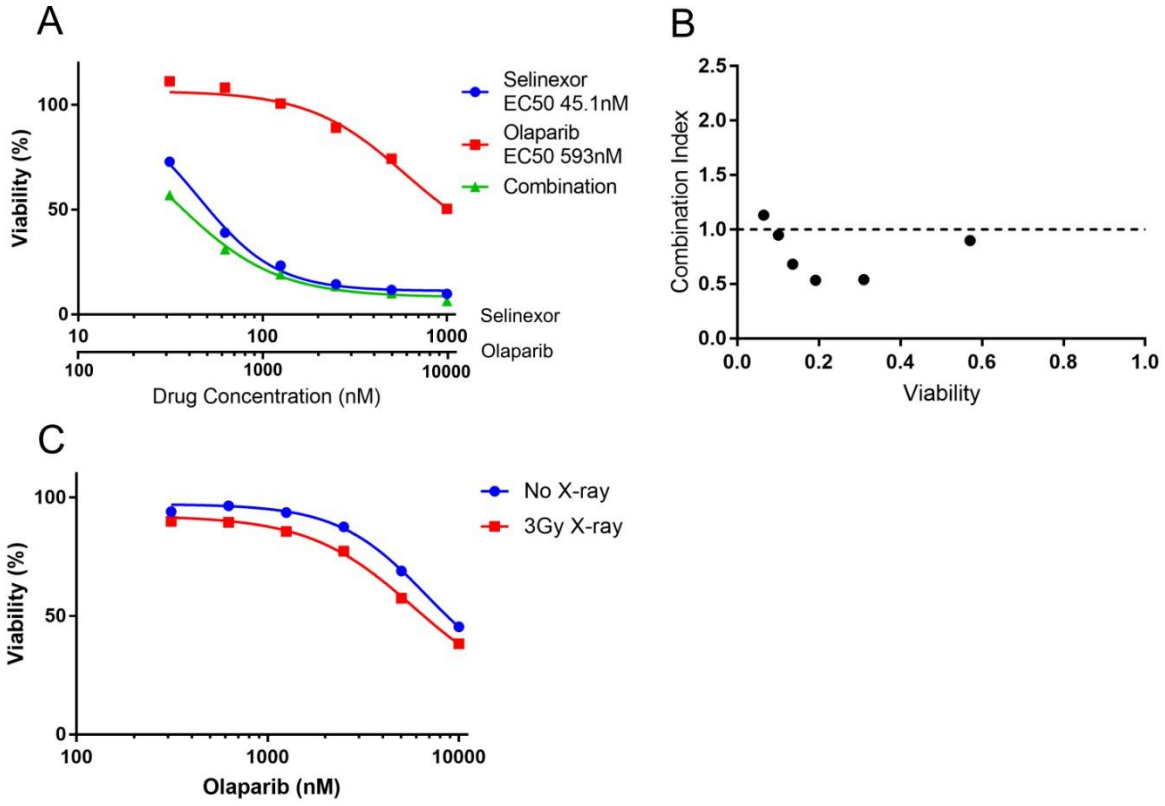

Figure 2.16. Selinexor combines synergistically with the PARP1 inhibitor olaparib. (A) Dose-response curves were performed for selinexor and olaparib alone and in combination. After 72 hours, ATP was measured as a surrogate for cell survival. EC_{50} concentrations are noted in the figure key. (B) Combination indices for each combination were calculated using the median effect model. The dotted line represents a combination index of 1. Points less than 1 are synergistic whereas points greater than 1 are antagonistic. (C) As a control, olaparib was combined with 3Gy of x-irradiation. After 72 hours, ATP was measured as a surrogate for cell survival and apparent combination effects are observed across the olaparib concentration range.

The DNA intercalator cisplatin combines well with selinexor at four of the tested combinations (Figure 2.14C). The topoisomerase IIα poison, etoposide has been combined with selinexor in chronic lymphocytic leukemia (Lapalombella et al., 2012) and acute myeloid leukemia (Ranganathan et al., 2016), and also shows combinations effects here with HT-1080 cells (Figure 2.14D). The EC50 for cell survival for cisplatin and etoposide are approximately 498.7nM and 59.7nM, respectively (Figure 2.15). The PARP1 inhibitor olaparib combines well DNA damaging treatments and other chemotherapies (Hijaz et al., 2016; Xu et al., 2015) and shows combination effects with selinexor in triple negative breast cancers cells independent of BRCA1 status (Marijon et al., 2015). When combined with selinexor in HT-1080 cells (BRCA1 wildtype, (Slebos and Taylor, 2001)), olaparib shows combination effects in five different combinations; olaparib also combines well with x-irradiation as a positive control, although combination indices cannot be calculated in this case (Figure 2.16A-C). Taken together, selinexor combines well with chemotherapy agents that each induce double-stranded DNA damage through distinct molecular mechanisms (gemcitabine, 5-FU, cisplatin, and etoposide) and that perturb DNA repair and apoptosis signaling (olaparib).

2.4: Discussion

Treatment of cells with SINE compounds results in multiple cell fates, including cell cycle arrest, cell cycle progression defects, and apoptosis (Azmi et al., 2013; Marcus et al., 2015; Turner et al., 2012). The mechanisms by which SINE compounds exert these effects need to be understood if we are to best utilize these agents to treat cancers. The sequestration of some XPO1 cargos, the functions of some proteins, and gross cell fates after treatment with SINE indicate that nuclear export is blocked rapidly and the cell responses are highly complex

(Gravina et al., 2015; Kashyap et al., 2016; Kim et al., 2016; Marcus et al., 2015). For example, recent studies document decreased ribosome biogenesis (Tabe et al., 2015), disrupted nuclear architecture of telomeres (Taylor-Kashton et al., 2016), synthetic lethality with oncogenic K-Ras (Kim et al., 2016), and NFκB/IκB regulation after treatment with SINE (Kashyap et al., 2016).

Here, we show that double-stranded DNA damage occurs in some cells within hours of treatment with SINE (Figures 2.1 and 2.2) and longitudinal tracking experiments in one cell model indicate nearly half of the population becomes damaged by 24 hours and correlates strongly with eventual cell death and arrest, particularly if the damage occurs when cells are in G1-phase (Figure 2.13). Over time, cells with DNA damage show a strong association with S-phase based on positive, but decreased EdU staining (Figures 2.10, 2.11 and 2.12). The DNA damage foci stain for multiple DNA damage repair proteins consistent with double-stranded damage (Figure 2.6). Indeed, based on single cell tracking (Figure 2.13D), while 34% of cells with damage progress to cell death, 66% appear to either repair the foci in a protracted S/G2-phase (and divide) or remain in an arrested state.

High-magnification, high-resolution microscopy and the neutral DNA comet assay reveal there are multiple, clustered DNA damage foci after treatment with SINE (Figure 2.7); a small number of breaks does not generate tails in the comet assay. Notably, the population of HT-1080 cells at 8 hours of treatment with SINE that is used in the comet assay contains very few apoptotic cells (Marcus et al., 2015), indicating the tails are not due to DNA fragmentation associated with cell death. Cells expressing the functional XPO1 C528S point mutant that cannot bind SINE show decreased DNA damage foci formation compared to cells expressing wildtype XPO1 (Figures 2.4 and 2.5); DNA damage formation is not completely inhibited by expression of XPO1 C528S, likely due to the continued expression of normal XPO1. These data indicate

that SINE binding to XPO1 is causal to a subsequent mechanism of DNA damage and that the SINE molecules themselves are not directly causing the damage.

DNA damage in general can result from many different mechanisms. The data indicate that multiple, clustered, double-stranded breaks occur within hours after treatment with SINE (Figures 2.2 and 2.7). Given the pattern of the foci and timing of their formation it is unlikely that global DNA replication defects are responsible. It is possible that an early replicating gene cluster at the G1/S-phase transition is prone to damage after XPO1 inhibition, but attempts to co-localize the damage foci with EdU shows little if any colocalization (not shown). DNA damage foci localized at telomeres and centromeres are known (Guerrero et al., 2010; Takai et al., 2003). Damage localized with centromeres is reported to be associated with mitotic defects (Guerrero et al., 2010) and XPO1 does have reported roles at centrosomes and in chromosome attachment to the centromere that could potentially perturb mitosis when inhibited (Funabiki et al., 1993; Knauer et al., 2006). However, the clustered foci studied here after treatment with 1μM selinexor are observed to form predominantly in G1-phase cells without any obvious association with mitosis (Figures 2.2 and 2.13). Telomere dysfunction-induced foci (TIFs) (Takai et al., 2003) are found in small numbers in some cell lines growing in culture, label with double-stranded break markers (Dimitrova et al., 2008) and associate with decreased cell proliferation and increased senescence (Flach et al., 2014). It is conceivable that SINE treatment impacts telomere signaling or length, given that a component of the telomere cap, TPP1, may bind XPO1 (Chen et al., 2007). The TPP1 is disrupted by dominant inhibitor expression numerous TIF form that scattered throughout the nucleus (Chen et al., 2007). HT-1080 express telomerase and telomere length is stable (Kim et al., 1999), and uncapping did not cause growth defects until >4 days (Gomez et al., 2006). The acute nature of the experiments here and the pattern of damage staining indicate a

telomere-based mechanism is unlikely. Future work will focus on the molecular mechanism of DNA damage formation.

DNA damage foci are observed in multiple cancerous cell lines after selinexor treatment (Figure 2.3). Interestingly, two non-cancer cell lines, RPE1 and MSCs, show no appreciable increase in damage foci (Figure 2.3). The identification of underlying sensitizing factors to DNA damage formation after treatment with selinexor will make an important future contribution to how these molecules work on cells. Based on experiments with RPE1 and MSC cells, possibilities include that at least some normal cells respond very rapidly to SINE treatment and arrest in early G1-phase (e.g. RPE1 FUCCI, Figure 2.9), prior to DNA damage formation, and show little death. These data agree with earlier observations showing less cytotoxicity of normal cells to selinexor (Azmi et al., 2013; Etchin et al., 2016; Tyler et al., 2017). Taken together, there is likely a common mechanism underlying the DNA damage, but it does not mean that the foci form at the same frequency or with the same kinetics in all cell lines. This may be especially true given the G1- and G1/S-phase association of the damage, that cell cycle progression is different between cell lines, and that some cells are more capable of strong G1-phase arrest and DNA repair than others based on signaling pathways. It is possible that overall response to selinexor response is directly affected by the functionality of various XPO1 cargos, such as p53 (Chen et al., 2016; Clewell et al., 2014). Due to p53 being an XPO1 cargo involved in cell cycle arrest and cell death after DNA damage, it will be important to investigate p53 loss of function as it relates to the DNA damage and cell fate observed here. Other mechanisms in cancer cells may also impact response and fate after selienxor treatment. For example, oncogenic Ras signaling, which impacts telomere dysfunction, ribosome biogenesis, and DNA replication, has been observed to

decrease cell survival after selinexor treatment (Bai et al., 2013; Kim et al., 2016; Suram et al., 2012).

DNA damage after treatment with SINE correlates with cell death in 34% of the cells, other cells appear to repair the damage and continue proliferation or undergo cell cycle arrest, and still others show no DNA damage, but also die or arrest (Figure 2.13). Cell fate appears to be dependent on the timing of DNA damage, with death occurring most often in cells that acquire damage in G1-phase (38%) compared to those that acquire damage in S/G2-phase (7%) (Figure 2.17). These features of the response to SINE may enable the combination effects found when SINE is combined with different classes of DNA damage agents. Combination treatments are an essential part of anti-cancer therapies and are an important part of future research (Figure 2.17). Of note, gemcitabine, platinum-based agents, topoisomerase inhibitors and PARP1 inhibitors are each being evaluated with selinexor in clinical trials (NCT02178436, NCT02269293, NCT02299518, NCT02419495, ClinicalTrials.gov). Our data suggest that SINE combined with DNA damaging drugs may significantly decrease cell survival and, optimistically, some combination will result in a stronger initial response in cancer therapy.

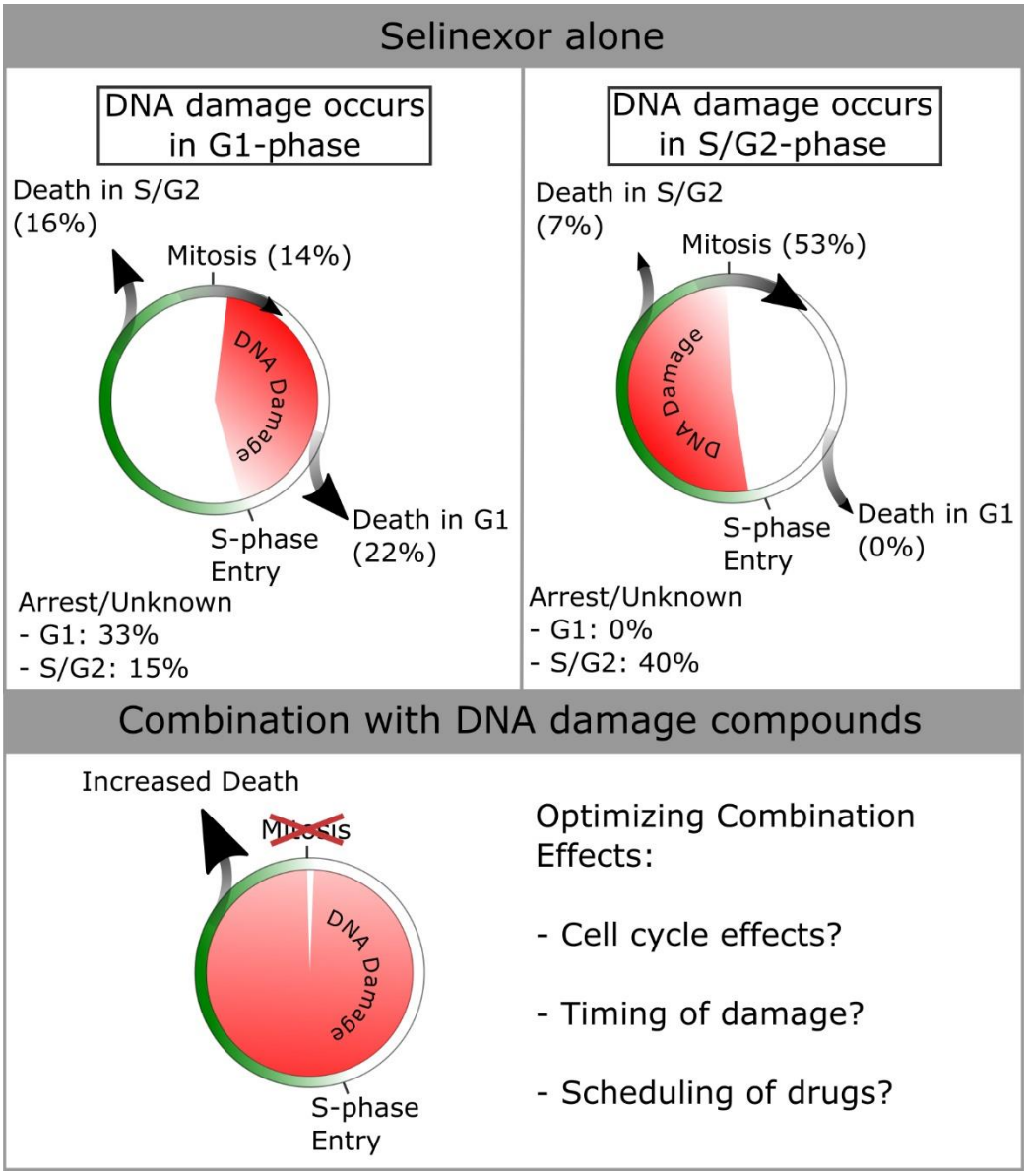

Figure 2.17. Summary of main cell cycle, DNA damage, and associated cell fates in HT-1080. Data from Figure 2.13 were used to compile cell fates dependent on when damage occurs in the cell-cycle. More death is seen in cells that acquire damage in G1-phase (total of 38% versus 7% for damage in S/G2-phase). Cells that accumulate damage in S/G2-phase most often progress through mitosis (53% versus 14% for damage in G1-phase). Given the synergistic effects of combining selinexor with DNA damage agonists [see Figure 2.14], cell death is increased across the entire population. The mechanisms of optimizing combinatorial effects should be studied, and are hypothesized to be cell cycle effects caused by either/both compounds, the timing of DNA damage within the cell cycle, and/or the scheduling of drugs to maximize the combinatorial effects.

Chapter 3 : Nucleolar stress concomitant with DNA damage after inhibition of exportin-1

As submitted Burke, R.T., Marcus, J.M. and Orth, J.D. (2018) Nucleolar stress concomitant with DNA damage after inhibition of exportin-1.

3.1: Introduction

Selective inhibitors of nuclear export (SINE) are a family of small molecules in development for the treatment of a wide range of hematological and solid cancers including sarcoma, breast, ovarian and prostate cancers (Etchin et al., 2016; Gravina et al., 2014; Lapalombella et al., 2012; Nakayama et al., 2016; Zheng et al., 2014). SINE molecules covalently bind the nuclear transporter exportin-1 (XPO1) at cysteine 528, and prevent the binding of cargo proteins with nuclear export signals (NESs). Inhibition of XPO1 leads to rapid nuclear sequestration of cargo proteins including key cell cycle and cell death regulators (Azmi et al., 2013; Crochiere et al., 2015; Turner et al., 2012).

The effect of cargo retention following XPO1 inhibition is a growing field of study to understand anti-cancer mechanisms of SINE molecules. Recent NES containing cargos of interest include IκB, p53, cyclinD1 and FoxO-1 (Corno et al., 2017; Gravina et al., 2015; Kashyap et al., 2016; Yang et al., 2014). In addition to the nuclear export of individual cargos, XPO1 also transports assembled ribosome subunits from the nucleolus to the cytoplasm (Ho et al., 2000). Inhibiting XPO1 with the molecule leptomycin B, that like SINE binds to cysteine 528, leads to accumulation of the XPO1-ribosome chaperone NMD3 at nucleoli and nuclear retention of ribosomal subunits (Bai et al., 2013; Thomas and Kutay, 2003). Further, inhibiting ribosomal RNA (rRNA) transcription with the RNA polymerase I inhibitor, Actinomycin D (ActD), causes accumulation of XPO1 and NMD3 within nucleoli (Bai et al., 2013). Previous

studies have shown that inhibition of XPO1 with both leptomycin B and SINE leads to defects in rRNA processing (Bai et al., 2013) and decreased production of ribosomal protein subunits (Tabe et al., 2015).

Our previously published work shows clusters of DNA double strand breaks occur within four hours after XPO1 inhibition using multiple SINE molecules (Burke et al., 2017). We present data here showing that inhibition of XPO1 by the clinical SINE, selinexor (KPT-330), perturbs nucleolar structure and function in cells, similar to previous work with non-clinically viable leptomycin B. Nucleolar disruption after XPO1 inhibition is dependent on the cysteine 528 drug binding site and occurs concomitant with increased DNA damage formation at or proximal to nucleoli. Supporting a direct link between nucleolar stress and DNA damage formation after treatment with selinexor, further disruption of nucleolar stability by the overexpression of a rRNA transcriptional regulator, upstream binding factor (UBF), or loss of p53, a crucial mediator of nucleolar stress response, exacerbates both the nucleolar and DNA damage response after treatment. The mechanism of selinexor is complex, and potentially involves the activities of many cargo proteins and signaling pathways. The data here reveal that a nuclear domain fundamental to cellular life, the nucleolus, is a target of SINE activity. This observation is important in a clinical context given that nucleoli and ribosome biogenesis are often dysregulated in transformed cells and tissues, perhaps providing selectivity for SINE inhibitors (Quin et al., 2014).

3.2: Materials and Methods

Cell lines, plasmids

HT1080 cells (ATCC) were used at passage 30 or less. HT1080 are grown in minimum essential medium (MEM; Corning 10-010-CV) modified with Earle's salts, sodium pyruvate (Sigma), non-essential amino acids (Sigma), penicillin/streptomycin (Sigma; P/S), and 10% fetal bovine serum (Sigma). mCherry-BP1-2 pLPC-Puro was a gift from Titia de Lange (Addgene plasmid # 19835). pEGFP-C1-UBF was a gift from Sui Huang (Addgene plasmid # 26672). pEGFP-C1-Fibrillarin was a gift from Sui Huang (Addgene plasmid #26673). For the HT1080 mCherry-BP1-2/EGFP-UBF and mCherry-BP1-2/EGFP-Fibrillarin cell lines, a cell line stably expressing mCherry-BP1-2 was transfected with expression plasmids for either EGFP-UBF or EGFP-Fibrillarin. Plasmid DNAs were purified via Qiagen maxi-prep kit. Cells were transfected using Fugene 6 (Promega). Transient transfectants were expanded into a 10 cm dish and subjected to selection using 1μg/ml puromycin (Gold Biotechnologies; mCherry-BP1-2) and 1 mg/ml G418-sulfate (Gold Biotechnologies; EGFP-UBF and EGFP-Fibrillarin) until population out-growth. This polyclonal population was subjected to dilution subcloning and a dual expressing stable cell lines were picked and expanded. Fresh aliquots were used throughout the research project.

Antibodies, EU, EdU

γH2A.X rabbit monoclonal antibody (Cell Signaling) or γH2A.X mouse monoclonal (Millipore) are used at 1:500 dilution in blocking buffer, 4% BSA fraction V in PBS. RPA194 mouse monoclonal antibody (Santa Cruz Biotechnology) is used at 1:200 dilution. Fibrillarin rabbit polyclonal antibody (Santa Cruz Biotechnology) is used at 1:100 dilution. Secondary

antibodies, goat anti-mouse, donkey anti-rabbit conjugated to AlexaFluor 488, 568, or 647 (Molecular Probes) are used at 1:500 dilution. For Click-iT EU labeling, 0.5-1mM 5-ethynyl uridine was pulsed for 1h following manufacturer protocol (Thermo Fisher Scientific). For Click-iT EdU labeling, 1mM 5-ethynyl-2'-deoxyuridine was pulsed for 30min following manufacturer protocol (Thermo Fisher Scientific). Staining for both EU and EdU samples was completed normally following the Click-iT procedure.

Immunofluorescence

Cells are fixed at the desired time point in 3.7% formaldehyde (37% Mallincrokdt stock) in PBS for 20 minutes at room temperature. Cells are washed in PBS several times over 5-10 minutes. Cells are permeabilized in 0.5% triton X-100 (Sigma) in PBS for 10 minutes at room temperature. Cells are washed in PBS several times over 5-10 minutes. Cells are blocked in blocking buffer (4% BSA fraction V in PBS) for 60 minutes. For γH2A.X or RPA194, cells are incubated in diluted primary antibodies for 60 minutes at room temperature in a humid chamber. For fibrillarin, cells are incubated in diluted primary antibody overnight at 4 degrees Celsius in a humid chamber. After primary antibody incubation, cells are washed in PBS several times over 5-10 minutes. Cells are incubated in secondary antibodies for 60 minutes and then washed several times over 5-10 minutes. The stained and washed cells are stained when appropriate with 1μg/ml DAPI in PBS for 5 minutes at room temperature. Cells are washed several times in PBS over 5-10 minutes, rinsed in distilled water and mounted onto glass microscope slides (VWR) in 15-20 microliters of Prolong Gold anti-fade (Life Technologies). Slides are cured for at least 16 hours at room temperature before imaging.

Microscopy

Fixed cell, immunofluorescence microscopy was performed using an inverted Olympus IX81 microscope with Prior Lumen200 Pro metal halide lamp, Hamamatsu ORCA R2 CCD camera, motorized Prior ProScan III stage, and 20X 0.70NA and 40X 0.75NA objectives using optical filters for DAPI (Chroma), Alexa488/EGFP (Chroma), Alexa568/mCherry (Chroma) and Alexa647/Cy5 (Semrock). Confocal microscopy was performed on a Yokogawa CV1000 spinning disk confocal with Olympus 20X 0.75NA and 60X 1.35NA objectives. Live-cell microscopy was performed using an inverted Olympus IX81, 20X 0.70NA objective, and stage-top incubation chamber (InVivo Scientific) as described previously (see (Burke and Orth, 2016; Marcus et al., 2015)) and autofocusing was performed using phase-contrast. To minimize acquisition delay between green and red channels, EGFP/mCherry dual optical filters (Semrock) and filter wheels were used. Control conditions are included in each experiment to confirm normal growth.

Quantification

Image analysis was performed using FIJI (ImageJ; NIH). Nuclei (DAPI) were identified using the Analyze Particles tool. Nucleolar masks were created using a variance filter to detect the edges of the nucleoli followed by morphological transformations to capture the entirety of the nucleolus. Masks of the fluorescence channels were compared to the phase microscopy images to ensure accuracy of the mask creation. For γH2A.X foci in fixed cells, the "Find Maxima" tool in FIJI using appropriate thresholding based on positive control cells treated with 10μM etoposide to isolate DNA damage foci above background was used, and cells were scored as positive or negative. Foci detection and scoring was performed by a second investigator to ensure accuracy.

3.3: Results

3.3.1: XPO1 inhibition by selinexor leads to decreased rRNA transcription and nucleolar dysfunction in cancer and normal cells

Previous studies using the XPO1 inhibitors leptomycin B and KPT-185, show decreased ribosome protein subunit levels after 18 hours of treatment (Tabe et al., 2015). Using the fibrosarcoma-derived cell line, HT1080, the nucleolar response to XPO1 inhibition by selinexor was studied. 1μM selinexor was used throughout these studies unless otherwise stated; 1μM has been used in many published works and has been shown to be a clinically relevant concentration (Azmi et al., 2013; Kim et al., 2016; Lapalombella et al., 2012). Transcription of nascent RNA was detected using 5-ethynyl uridine (EU) and the RNA polymerase I inhibitor Actinomycin D (ActD) was used as a control to interrupt ribosomal RNA (rRNA) transcription. Quantification of nucleolar EU signal shows that compared to mock treated cells (DMSO), there is essentially no detectable EU incorporation at nucleoli following 8 hours of 50ng/ml Actinomycin D treatment (Figure 3.1A,B). Following 8 hours of 1μM selinexor, EU incorporation at nucleoli is reduced 70% to approximately one-third the level of mock cells, indicating reduced rRNA transcription (Figure 3.1 A,B) (Bai et al., 2013; Tabe et al., 2015). EU incorporation in non-nucleolar regions, accounting mostly for mRNA transcription, is minimally decreased, by approximately 3% compared to mock (Figure 3.2A). The area of each nucleus that is occupied by nucleolar EU incorporation is also decreased in selinexor treated cells compared to mock, suggesting possible effects on nucleolar organization (Figure 3.2B).

Nucleoli reorganize in response to stress, for example acute inhibition of RNA polymerase I in cells by Actinomycin D collapses the actively transcribed rRNA genes into nucleolar caps (Reynolds et al., 1964) or after DNA double strand breaks caused by ionizing

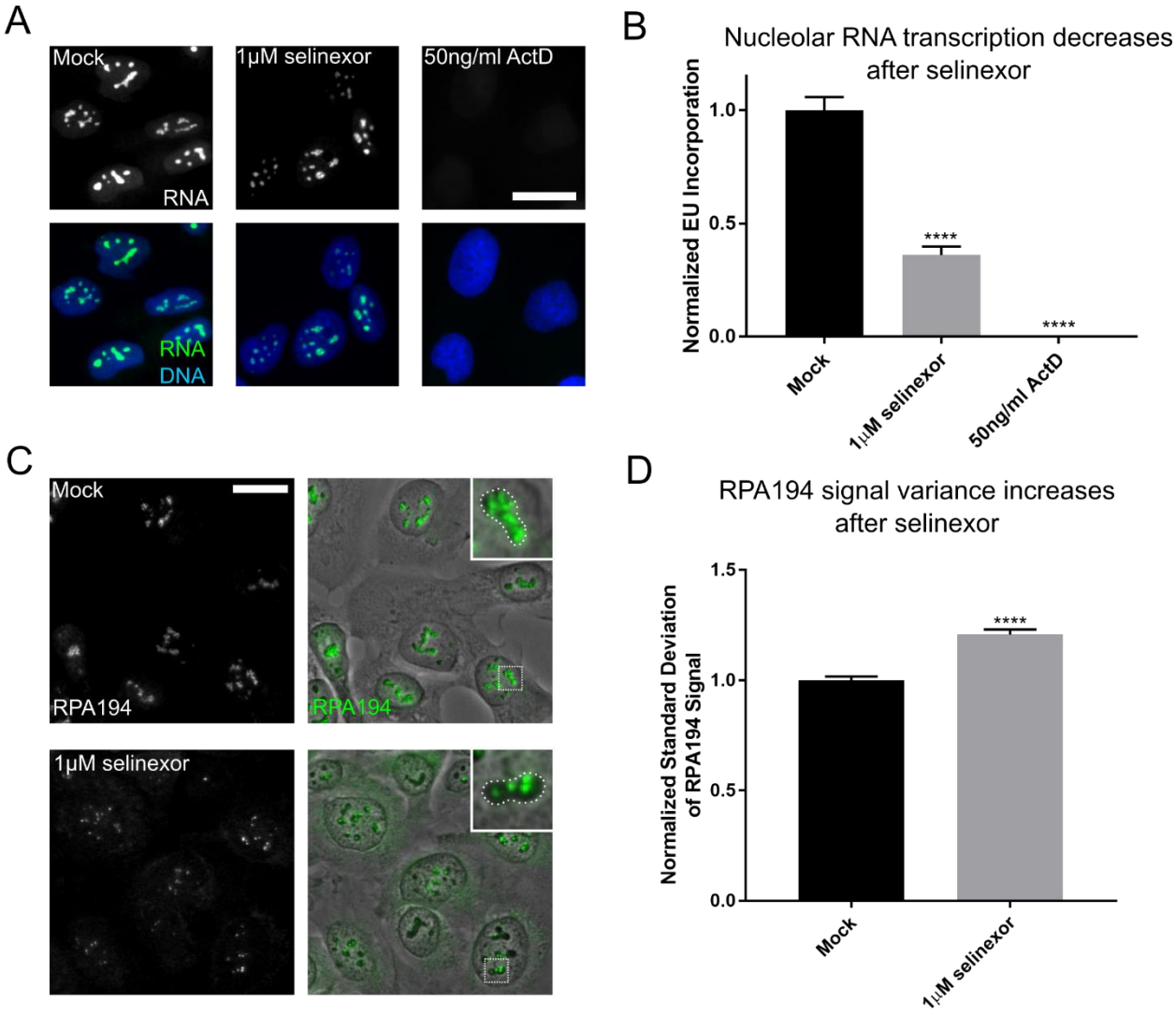

Figure 3.1. Nucleolar transcription and structure is disrupted following XPO1 inhibition. HT1080 cells were pulsed for 1 hour with 1mM Click-iT EU after 8 hours of treatment with mock (DMSO), 1μM selinexor and 50ng/ml Actinomycin D (ActD). (A) Representative images are shown with incorporated EU (green) and counterstained for DNA (blue). (B) Nucleolar masks were created and the amount of EU fluorescence incorporated in nucleoli was quantified. n > 75 cells per condition. (C,D) HT1080 cells were treated with mock (DMSO) or 1μM selinexor for 8 hours. Cells were immunostained for the RNA polymerase 1 subunit, RPA194 (green). Phase microscopy is included to emphasize the change in RPA194 distribution within the nucleolus. Insets are displayed to highlight the redistribution. (D) Nucleolar masks were created and the signal for RPA194 was quantified. Standard deviation of the signal is displayed. The variance of the RPA194 signal increases after selinexor treatment indicative of disrupted nucleolar structure. n > 300 cells per condition. Scale bars = 10 micrometers (μm). **** is p-value < 0.0001.

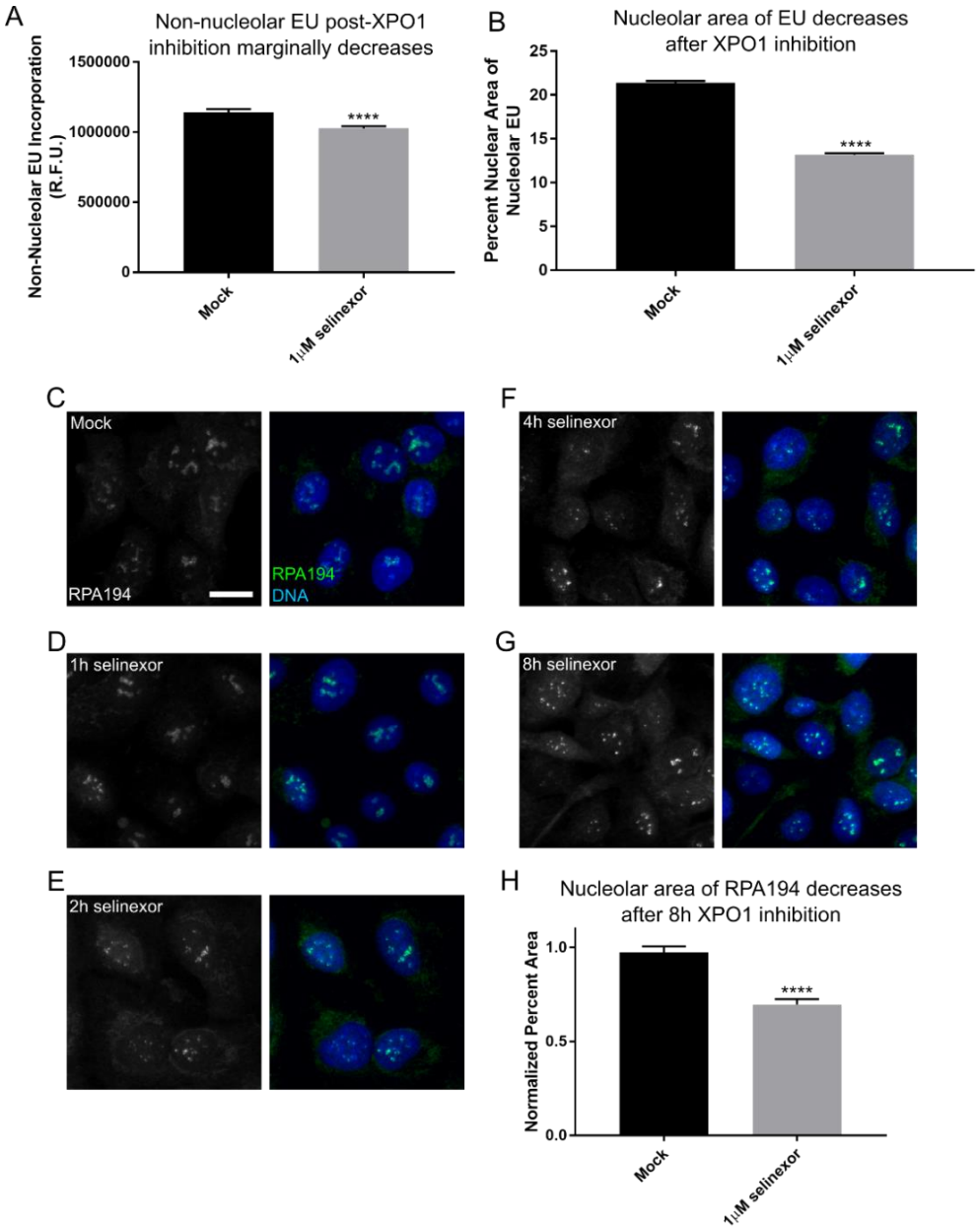

Figure 3.2. Inhibition of XPO1 nucleolar structure and function in a time dependent manner. (A,B) HT1080 cells were treated with mock (DMSO) and 1μM selinexor for 8 hours (h) and pulse labeled with EU for 1 hour at the end of treatment. (A) Non-nucleolar EU incorporation decreases slightly after selinexor treatment. n > 75 cells per condition. (B) The percent area of nucleolar-associated EU decreases, indicative of changing nucleolar structure. n > 200 cells per condition. (C-H) HT1080 cells were treated over a time course with 1μM selinexor. The cells were then fixed and stained for RPA194 (green). Representative images are displayed. Redistribution of RPA194 is detectable as early as 2 hours (E) and persists through 4 hours (F) and 8 hours (G). (H) The percent area of RPA194 was quantified after isolation with a nucleolar mask. These data coincide with an increase in the variance of RPA194 signal across the nucleolus (Figure 3.1D). n > 200 cells per condition. Scale bar = 10μm. **** is p-value < 0.0001.

radiation (Kruhlak et al., 2007). We immunostained the catalytic RNA polymerase I subunit, RPA194, after treatment with selinexor to detect if there are any changes in its distribution in nucleoli that could be congruent with the area effects evident in the EU stain, and possibly EU incorporation (Figure 3.2B). As early as 2 hours after treatment with 1μM selinexor, redistribution of RPA194 is broadly evident across the population (Figure 3.1C and Figure 3.2C-G). To quantify the RPA194 changes, the nucleoli were isolated in the images by creating a nucleolar mask (see Materials and Methods) and the fluorescent signal was quantified (Figure 3.1C,D). Redistribution of RPA194 was detected by changes in the standard deviation of the pixel intensities distributed across the nucleolus (Moore et al., 2011; Orth et al., 2012). The mean standard deviation of RPA194 signal increases after XPO1 inhibition as the protein distribution becomes more punctate (Figure 3.1 D and C, respectively). Further, as with the EU stain (Figure 3.2B), nucleolar sizes decrease relative to nuclear sizes after 8 hours (Figure 3.2H). These data together suggest that nucleoli respond rapidly to XPO1 inhibition and are under stress as indicated by a redistribution of nucleolar proteins concomitant with nucleolar collapse and decreased EU incorporation.

XPO1 is a critical mediator of nuclear export in all cell types, and response to XPO1 inhibition has been noted in cancer and normal cell lines (Burke et al., 2017; Marcus et al., 2015). Retinal pigment epithelial cells, RPE1, are immortalized with human telomerase, and are used to investigate the nucleolar response of XPO1 inhibition in a normal cell type. RPE1 cells were treated with 1μM selinexor for 8 hours and immunostained for RPA194 (Figure 3.3B). Actinomycin D and the topoisomerase IIα inhibitor, Etoposide, were included as controls for nucleolar stress response (Figure 3.3C,D) (Govoni et al., 1994; Reynolds et al., 1964); RPE1 show strong G1-phase arrest no increase in DNA damage after selinexor (Burke et al., 2017).

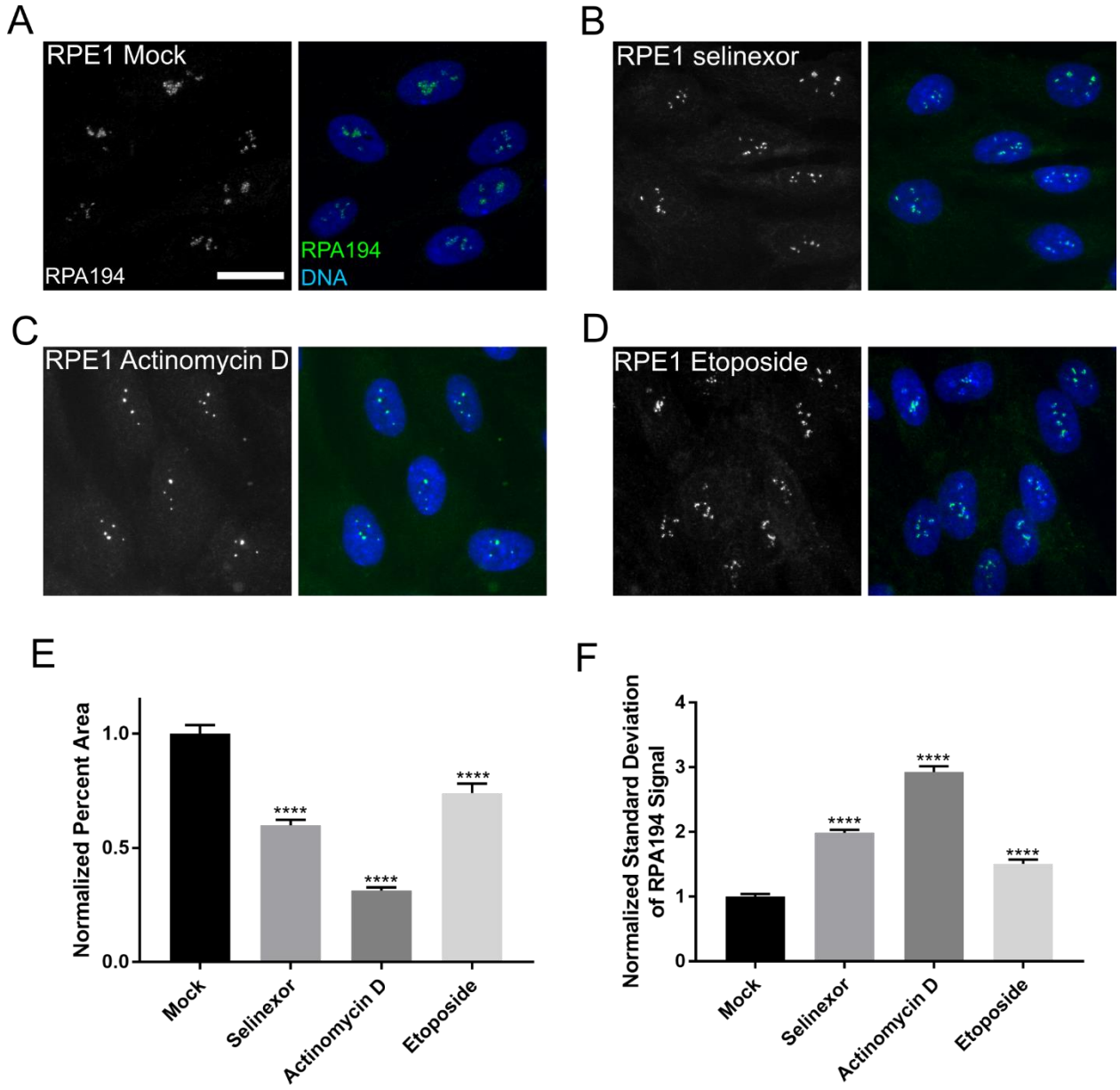

Figure 3.3. Normal cells have disrupted nucleolar structure after XPO1 inhibition. Immortalized retinal pigment epithelial cells, RPE1, were treated for 8 hours with mock (DMSO), 1μM selinexor, 50ng/ml actinomycin D and 10μM etoposide. Cells were then fixed and stained for RPA194 (green) and DAPI (blue). (A-D) Representative images displaying disrupted nucleolar structure after selinexor (B) and ActD (C). (E) Nucleolar masks were created and the percent area of the nucleolus was quantified. There is a significant reduction in percent area after selinexor, ActD and etoposide. (F) The signal variance of RPA194 across the nucleolus was quantified to describe redistribution of the protein within the nucleolus. The standard deviation is significantly increased over mock for all three compounds. n >200 cells per condition. Scale bar = 10μm. **** is p-value < 0.0001.

Similar to HT1080, RPE1 have significantly decreased nuclear area of RPA194 and increased standard deviation of the RPA194 signal (Figure 3.3E,F). These data indicate that the effects of XPO1 inhibition on nucleolar structure and function are likely not limited to cancer cells.

The binding of selinexor to XPO1 is via a covalent bond formed with the sulfhydryl group of cysteine 528 in the cargo binding pocket of XPO1 (Azmi et al., 2013; Crochiere et al., 2015; Turner et al., 2012). Mutation of the cysteine to a serine (XPO1 C528S) prevents binding of selinexor, but conserves the function of XPO1 to bind and export cargos out of the nucleus (Neggers et al., 2015, 2016). Previous studies have shown that both homozygous and heterozygous mutation of XPO1 C528S confers resistance to SINE molecules (Neggers et al., 2015, 2016), including against SINE-induced DNA double strand break formation (Burke et al., 2017). Transient expression of XPO1 or XPO1 C528S in HT1080 cells was used to establish dependence of selinexor binding to XPO1 to cause nucleolar defects. XPO1 or XPO1 C528S expressing cells were treated with 1μM selinexor for 8 hours, fixed and immunostained for RPA194. The percent area of RPA194 signal relative to the nuclear size decreased in mock transfected cells and those cells expressing wildtype XPO1 (Figure 3.5B,D, and E). The percent area of RPA194 did not decrease in cells expressing XPO1 C528S, indicating protection against selinexor induced effects on nucleoli (Figure 3.4D,E). These data support that the observed disruptions to nucleolar structure and function are dependent on binding of selinexor to XPO1.

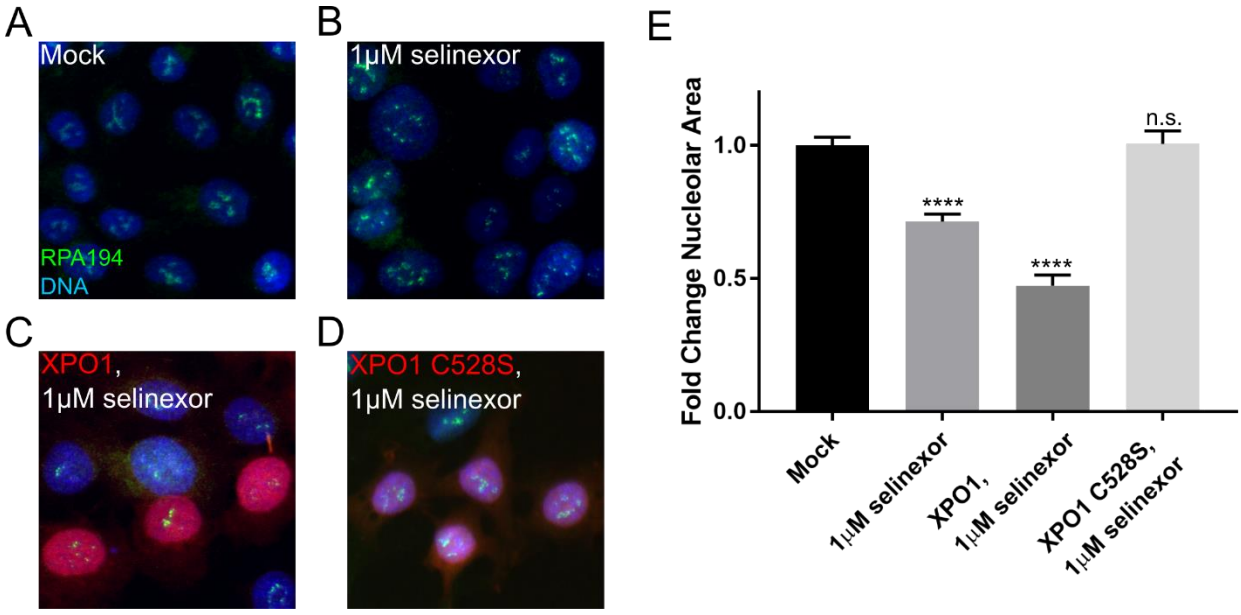

Figure 3.4. Transient expression of XPO1 C528S prevents nucleolar disruption following XPO1 inhibition. HT1080 were transiently transfected with XPO1 mRFP and XPO1 C528S mRFP. Cells were then treated with mock (DMSO) and 1μM selinexor for 8 hours. Cells were then stained for RPA194 (green) and DAPI (blue). (A,B) Representative images of control transfected cells with no plasmid. (C) Representative image of cells transfected with wildtype XPO1 mRFP (red). (D) Representative image of cells transfected with XPO1 C528S mRFP (red). (E) Nucleolar area of RPA194 staining within the nucleus was quantified. There is a significant decrease in nucleolar area in the control transfected and wildtype XPO1 transfected cells treated with 1μM selinexor. There is no significant difference in the XPO1 C528S transfected cells treated with 1μM selinexor (n.s.), indicating binding of selinexor to XPO1 is necessary for nucleolar disruption to occur. $n > 200$ cells per condition. Scale bar = 10μm. **** is p-value < 0.0001.

3.3.2: SINE induced DNA damage occurs within and proximal to nucleoli in cancer cells

Inhibition of XPO1 by selinexor has been shown to induce DNA damage in large, distinct clusters of foci (Burke et al., 2017). This pattern of DNA damage is unique from the distributed damage foci resulting from DNA damaging agonists like etoposide and cisplatin, for example (Rappold et al., 2001). Nucleoli are discrete bodies within the nucleus that are highly dynamic, prone to DNA damage, and in the same size range as the clustered DNA damage foci after selinexor. Due to the effects of selinexor on nucleoli and in causing a unique DNA damage pattern, we began to test for an association of the two responses. Using the phosphorylated histone variant, γH2A.X, to mark DNA double strand breaks, we immunostained HT1080 cells following selinexor treatment and overlaid the fluorescence images onto the corresponding phase contrast microscopy images where nucleoli are clearly evident. The fixed cell images after 8 hours of treatment with 1μM selinexor show large clusters of induced DNA damage foci are both within and proximal to nucleoli in most cases (Figure 3.5A).

To further investigate the proximity of DNA damage to nucleoli, cells were coimmunostained for both γH2A.X and nucleolar proteins. The RNA polymerase I catalytic subunit, RPA194, overlaps with selinexor induced DNA damage in many cells (Figure 3.5B). In addition, the rRNA processing ribonucleoprotein fibrillarin shows overlap with selinexor induced DNA damage (Figure 3.5C). The RNA polymerase I transcription factor, upstream binding factor (UBF), also displays an overlap with γH2A.X in cells (Figure 3.5D). It is important to note that consistent with phase-contrast microscopy, some selinexor treated cells show DNA damage clusters in close proximity with the nucleolar-associated proteins. The nucleolus is a highly dynamic structure and responds rapidly to cellular stresses including DNA damage (Franek et al., 2016; Moore et al., 2011). To probe the temporal relationship between the

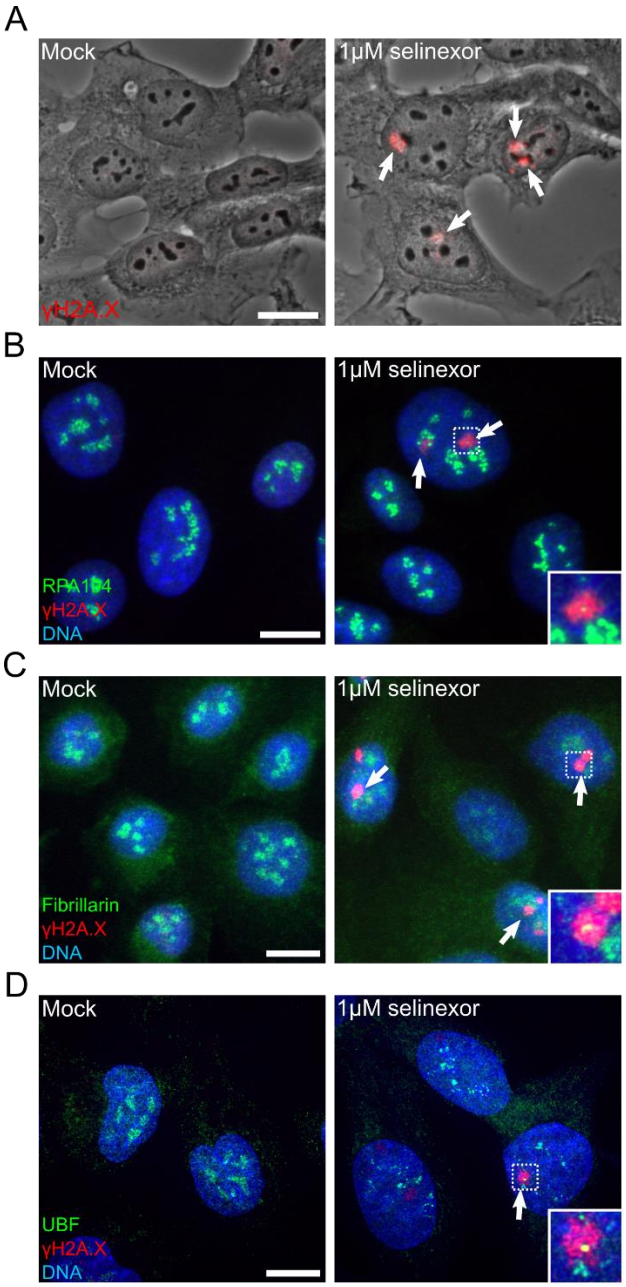

Figure 3.5. Selinexor induced DNA damage is proximal to and overlapping with components of the nucleolus. HT1080 were treated for 8 hours with mock (DMSO) or 1μM selinexor. Cells were then fixed and immunostained for γH2A.X, RPA194 and fibrillarin. (A) Phase contrast microscopy reveals selinexor induced γH2A.X foci proximal to and within nucleoli (white arrows). (B) Confocal imaging of cells with γH2A.X and RPA194 reveals a close association of selinexor induced DNA damage foci and the catalytic subunit of RNA polymerase I, RPA194 (white arrows). (C) Cells immunostained for γH2A.X and fibrillarin show colocalization of DNA damage and fibrillarin within the nucleolus (white arrows). (D) Cells immunostained for γH2A.X and the RNA polymerase I transcription factor, UBF, show colocalization of DNA damage and UBF staining (white arrows). Insets are included to emphasize the colocalization of the fluorescent signals. Scale bars = 5μm.

observed nucleolar reorganization and DNA damage formation events, live cell imaging is required.

3.3.3: Longitudinal time lapse microscopy shows nucleolar redistribution and DNA damage

A dual expressing HT1080 cell line was created that expresses the DNA double strand damage reporter mCherry-BP1-2 and the RNA polymerase I transcription factor EGFP-UBF. Live cells were imaged every 3 minutes overnight after addition of 1μM selinexor. A qualitative analysis of EGFP-UBF redistribution indicates similar results to immunostaining with RPA194 (Figure 3.6A,B and Figure 3.1C, respectively) where the protein becomes more punctate within the nucleolus indicative of stress. Early DNA damage events indicated by accumulation of mCherry-BP1-2 puncta in a pattern like reported for γH2A.X foci show a strong association with EGFP-UBF within 1-4 hours after treatment (Figure 3.6A,B). Additionally, HT1080 cells were transfected with mCherry-BP1-2 and the nucleolar protein EGFP-Fibrillarin (Figure 3.6C,D). Live cells were imaged every 4 minutes after addition of 1μM selinexor and mCherry-BP1-2 foci appear near or within nucleoli labeled with EGFP-Fibrillarin. In both reporter cell lines, the mCherry-BP1-2 foci increase in size equal to what is seen with γH2A.X staining in cells. These data indicate that selinexor induced DNA damage occurs proximal to or within nucleoli.

We observe in time-lapse that expression of EGFP-UBF in HT1080 appears to enhance DNA damage foci formation (Figure 3.6). HT1080 mCherry-BP1-2/ EGFP-UBF and parental HT1080 cells were treated for 8 hours with 1μM selinexor and then immunostained for γH2A.X (Figure 3.7A). The percent of cells with DNA damage foci were quantified (see methods in (Burke et al., 2017)). Approximately 35-40% of HT1080 parental cells after selinexor treatment

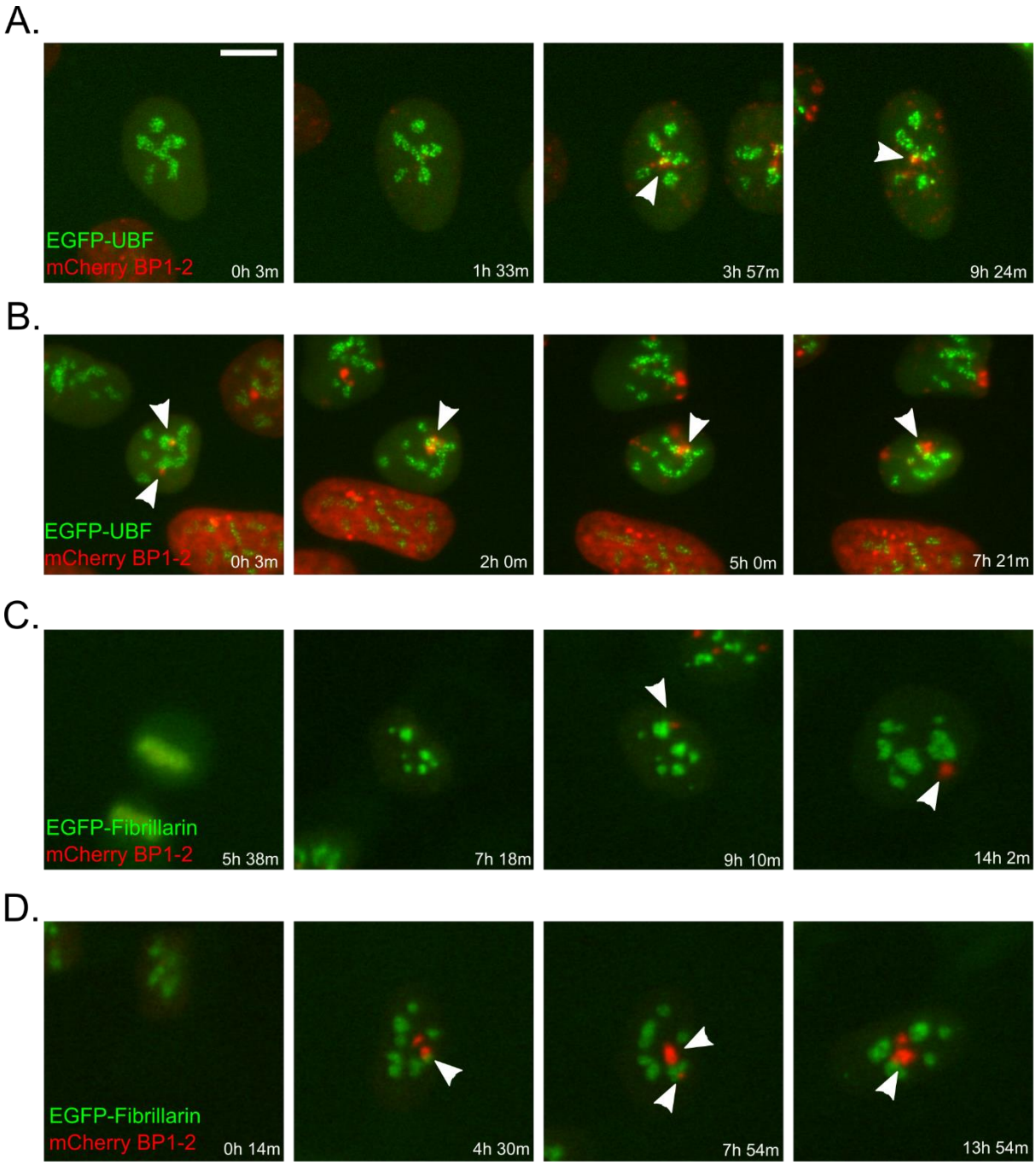

Figure 3.6. Live cell longitudinal tracking of cells after selinexor reveals a tight association of DNA damage and nucleolar proteins. HT1080 EGFP-UBF/mCherry BP1-2 were imaged overnight at 3 minute intervals. (A,B) Representative examples of cells that form DNA damage (red) colocalizing with the RNA polymerase I transcription factor UBF (green) (white arrows). (C,D) HT1080 EGFP-Fibrillarin/mCherry BP1-2 cells were imaged overnight at 4 minute intervals after 1μM selinexor. Representative images of cells that form DNA damage (red) colocalizing with the nucleolar protein fibrillarin (green) (white arrows). Time is noted in hours (h) and minutes (m) and represents time after selinexor addition. Scale bar = 5μm for all panels.

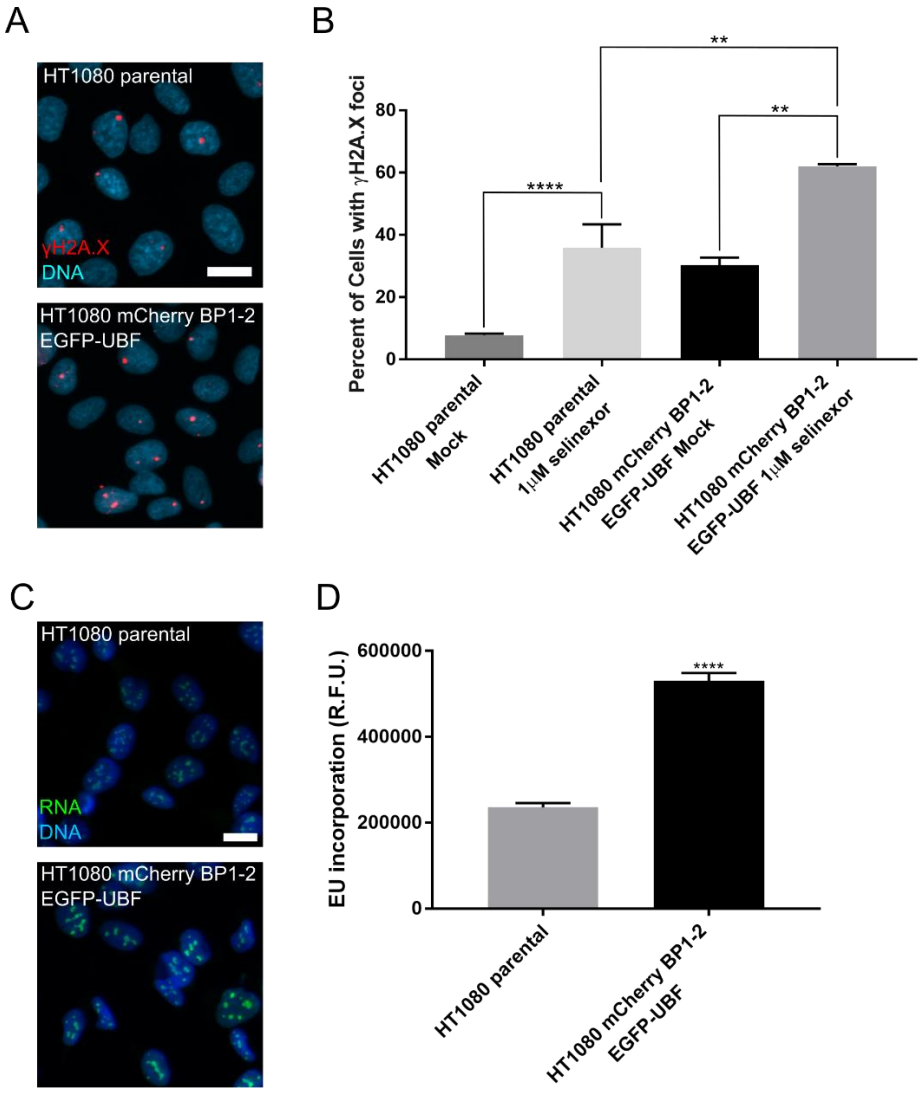

Figure 3.7. Overexpression of EGFP-UBF increases selinexor induced DNA damage and nucleolar EU incorporation. (A) Parental HT1080 and HT1080 EGFP-UBF mCherry BP1-2 cells were treated with 1μM selinexor for 8 hours. Cells were then fixed and immunostained for γH2A.X (red). Representative images are shown. (B) Percent of cells with γH2A.X foci were quantified. HT1080 EGFP-UBF/mCherry BP1-2 show an increase in DNA damage foci in the mock treated over parental HT1080. HT1080 cells have an increase in the frequency of DNA damage following selinexor treatment as has been reported previously (Burke et al., 2017). HT1080 EGFP-UBF/mCherry BP1-2 have a higher frequency of DNA damage following selinexor over the parental line as was observed in live cell microscopy (Figure 3.6). n > 200 cells per condition across 2-3 biological replicates. (C) Parental HT1080 and HT1080 EGFP-UBF/mCherry BP1-2 cells were pulsed with 1 hour of EU (green). Representative images are shown. (D) EU incorporation at the nucleolus was quantified. HT1080 EGFP-UBF/mCherry BP1-2 cells have a more than 2 fold increase in the amount of EU incorporated at nucleoli compared to parental HT1080. n >200 cells per condition. Scale bars = 10μm. ** is p-value < 0.01 and **** is p-value < 0.0001.

show γH2A.X foci; this result parallels our previously published study (Burke et al., 2017). HT1080 mCherry-BP1-2/ EGFP-UBF cells have a higher background amount of DNA damage compared to parental cells (Figure 3.7B) and XPO1 inhibition increases this amount approximately 3-fold to 60% of the population at 8 hours; these data corroborate what is seen in the timelapse microscopy data of this cell line (Figure 3.6). Since UBF is a transcription factor for RNA polymerase I, the effects of overexpressing EGFP-UBF were assayed using EU incorporation at nucleoli. HT1080 mCherry-BP1-2/ EGFP-UBF cells show a more than 2 to 3-fold increase in nucleolar EU incorporation over parental HT1080, indicating rRNA transcription is enhanced in these cells by overexpression of UBF (Figure 3.7D), consistent with previous studies (Hannan et al., 1996; Panov et al., 2006). Importantly, mCherry-BP1-2 expression alone does not increase DNA damage in untreated and selinexor treated cells (Burke and Orth, 2016; Burke et al., 2017).

3.3.4: Acute inhibition of RNA polymerase I prevents selinexor induced DNA damage independent of cell cycle effects

Given that selinexor induced DNA damage occurs within and/or proximal to nucleoli, and that increased nucleolar activity via UBF expression increases the damage, the function of the nucleolus could be important for DNA damage formation. Cells were left untreated, treated with 1μM selinexor alone, or in combination with different, specific RNA polymerase inhibitors (Figure 3.8 and Figure 3.9). DNA damage was then assessed by immunostaining for γH2A.X. The RNA polymerase II selective inhibitor, α-amanitin, shows no significant effects on selinexor induced DNA damage formation (Figure 3.9A). However, the RNA polymerase I selective inhibitor ActD results in a significant decrease in the percentage of cells with selinexor induced

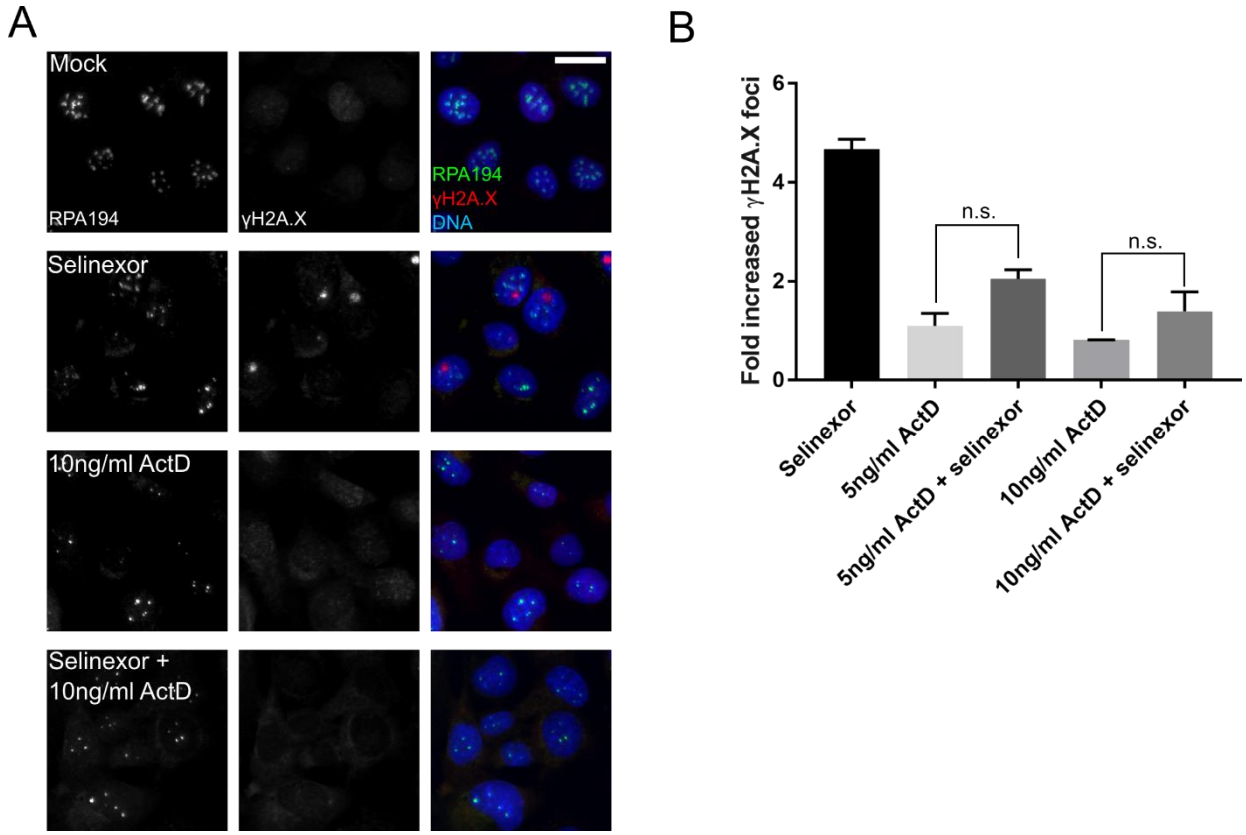

Figure 3.8. Inhibition of RNA polymerase I prevents selinexor induced DNA damage. (A) HT1080 cells were treated for 8 hours with mock (DMSO), 1μM selinexor, 5ng/ml Actinomycin D (ActD) and 10ng/ml ActD and the combination. Cells were then fixed and immunostained for RPA194 (green) and γH2A.X (red). Representative images are shown. (B) Treatment of HT1080 with selinexor alone increases DNA damage foci formation. Treatment of HT1080 with both 5ng/ml and 10ng/ml ActD alone does not increase DNA damage formation over mock. ActD combined with selinexor prevents selinexor induced DNA damage formation and no significant difference in formation is observed between the combination and mock (n.s.). n > 200 cells across 2-3 biological replicates. Scale bar = 10μm.

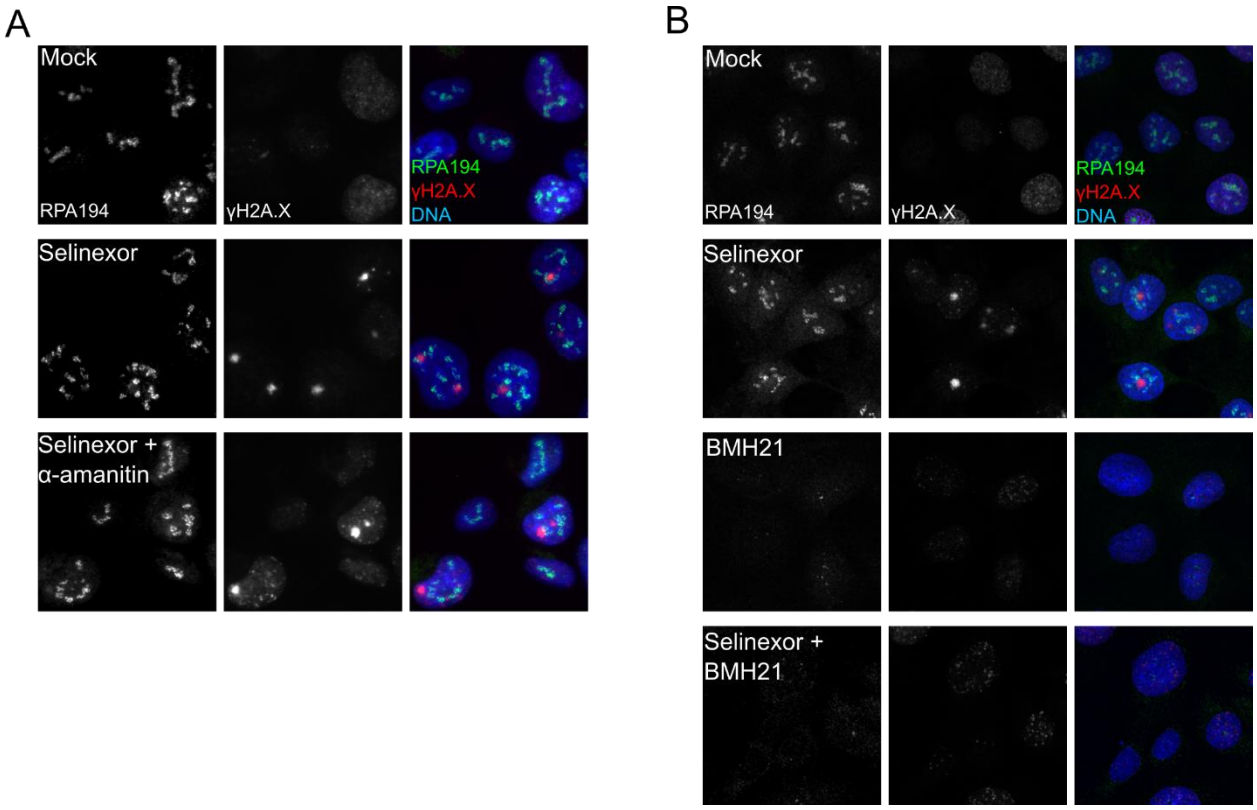

Figure 3.9. Inhibition of RNA polymerase I prevents selinexor induced DNA damage. (A) HT1080 cells were treated with mock (DMSO), 1μM selinexor and a combination of 1μM selinexor and 10μg/ml α-amanitin. Cells were then fixed and immunostained for RPA194 (green) and γH2A.X (red). Inhibition of RNA polymerase II by α-amanitin does not prevent selinexor induced DNA damage foci. (B) HT1080 cells were treated with mock (DMSO), 1μM selinexor, 10μM BMH21 and a combination of 1μM selinexor and 10μM BMH21. Cells were then fixed and immunostained for RPA194 (green) and γH2A.X (red). Inhibition of RNA polymerase I by BMH21 prevents formation of selinexor induced DNA damage similar to Actinomycin D (ActD) (Figure 3.8). Scale bars = 10μm.

DNA damage (Figure 3.8A,B). Importantly, α-amanitin alone causes no clear effect on nucleoli based on RPA194 (Figure 3.9A), while ActD treatment results in the rapid collapse of nucleoli and potent inhibition of rDNA transcription as revealed by EU incorporation (Figure 3.8A and Figure 3.1B, respectively). Another molecule that blocks rDNA transcription via a different mechanism from ActD, BMH-21 (Colis et al., 2014), also results in rapid nucleolar collapse and blocks selinexor-induced DNA damage formation (Figure 3.9B).

Previous studies have indicated a cell cycle association of DNA damage formation with selinexor (Burke et al., 2017). To test the effects of cell cycle progression on selinexor-induced DNA damage formation, the CDK4/6 inhibitor, PD 0332991, was used to hold HT1080 in G1-phase (Marcus et al., 2015). HT1080 cells were left untreated or synchronized in G1-phase with 10μM PD 0332991 for 16 hours before adding in 1μM selinexor. 10μM etoposide was included as a DNA damage positive control. γH2A.X staining was used to detect DNA damage formation and the Ran-specific GTPase-activating protein, RanBP1, was included to show XPO1 cargo sequestration as an indicator of selinexor action. Mock treatment shows largely cytoplasmic RanBP1 and little DNA damage (Figure 3.10A). Treatment for 8 hours with 1μM selinexor induces DNA damage and XPO1 cargo sequestration (Figure 3.10B). Treatment with 10μM PD 0332991 alone does not induce DNA damage nor does it perturb export of RanBP1 (Figure 3.10C). Treatment with 10μM PD 0332991 for 16 hours followed by 8 hours cotreatment of PD 0332991 and selinexor still demonstrates RanBP1 nuclear sequestration, but DNA damage does not form (Figure 3.10D). Cotreatment of PD 0332991 and etoposide following 16 hours PD 0332991 alone still has DNA damage formation indicating that G1-phase arrest with PD 0332991 does not affect DNA damage response (Figure 3.10E). These data suggest that selinexor induced DNA damage is dependent on cell cycle progression.

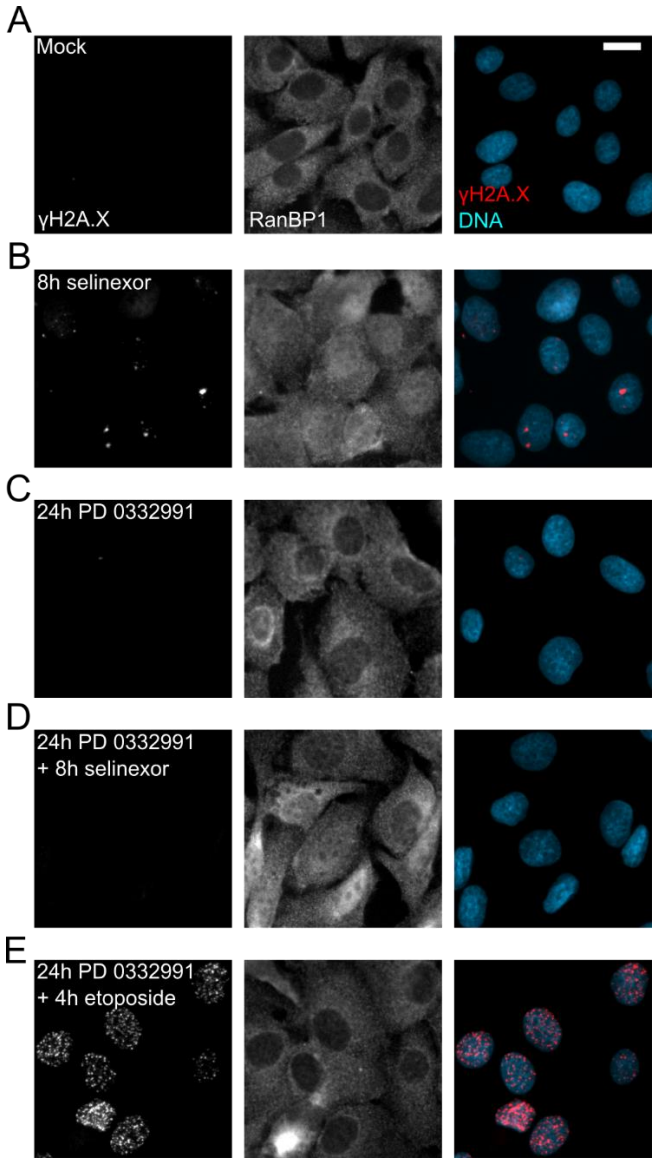

Figure 3.10. Inhibition of CDK4/6 prevents selinexor induced DNA damage. HT1080 cells were treated with mock (DMSO) (A), 8 hours (h) of 1μM selinexor (B), 24 hours of 10μM PD 0332991, a CDK4/6 inhibitor (C), 16 hours of 10μM PD 0332991 followed by the combination of 10μM PD 0332991 and 1μM selinexor for 8 hours (D), and 20 hours of 10μM PD 0332991 followed by the combination of 10μM PD 0332991 and 10μM etoposide for 4 hours (E). Cells were then immunostained for γH2A.X and the XPO1 cargo, RanBP1. (B) Treatment with selinexor alone causes both DNA damage and RanBP1 nuclear sequestration. (C) Treatment with PD 0332991 alone causes no increase in DNA damage over mock and no RanBP1 nuclear sequestration. (D) Overnight treatment with PD 0332991 to arrest cells in G1-phase followed by a combination of PD 0332991 and selinexor causes RanBP1 cargo sequestration, but DNA damage is not increased over mock. (E) Cells arrested in G1-phase by PD 0332991 followed by a combination of PD 0332991 and etoposide still form DNA damage, indicating that halting cell cycle progression prevents selinexor induced DNA damage but does not prevent XPO1 cargo sequestration.

In addition, ActD can cause cell cycle arrest (Ma and Pederson, 2013; Xu and Krystal, 2010). To test whether ActD perturbs DNA damage formation due to inhibition of RNA polymerase I versus cell cycle effects, the dose of ActD was titrated and cell proliferation was quantified using incorporation of the thymidine analog 5-ethynyl-2'-deoxyuridine (EdU). EdU incorporation in cells was measured both by percentage of cells within the population that are EdU positive and the mean total integrated EdU that was incorporated (Figure 3.11A,B). Previous studies have shown that a dose of 50ng/ml ActD is specific for RNA polymerase I (Penman et al., 1968; Perry, 1962). We show that a dose of 50ng/ml also shows cell proliferation effects on HT1080 cells at 8 hours (Figure 3.11A,B). Titration of ActD shows that 5 and 10ng/ml shows less cell cycle effects than 50ng/ml on both percentage of cells that are EdU positive and the amount of EdU incorporated in each nucleus (Figure 3.11 A and B, respectively). Immunostaining of cells treated with either 5ng/ml or 10ng/ml ActD with RPA194 shows strong nucleolar collapse indicating rRNA transcription is inhibited strongly while there are minimal effects to the cell cycle (Figure 3.8). These data taken together suggest that DNA damage formation after inhibition of XPO1 is dependent RNA polymerase I activity and/or functional or intact nucleoli (Figures 3.8, 3.9 and 3.11), in addition to showing a cell cycle association (Figure 3.10 and (Burke et al., 2017)).

3.3.5: Loss of p53 leads to increased rRNA transcription and increased selinexor induced DNA damage

A major component of the nucleolar stress response is the transcription factor p53. p53 accumulates in the nucleus after nucleolar stress induced by either ActD treatment or direct DNA damage of the rDNA gene arrays (reviewed in (Quin et al., 2014)). p53 has also been shown to

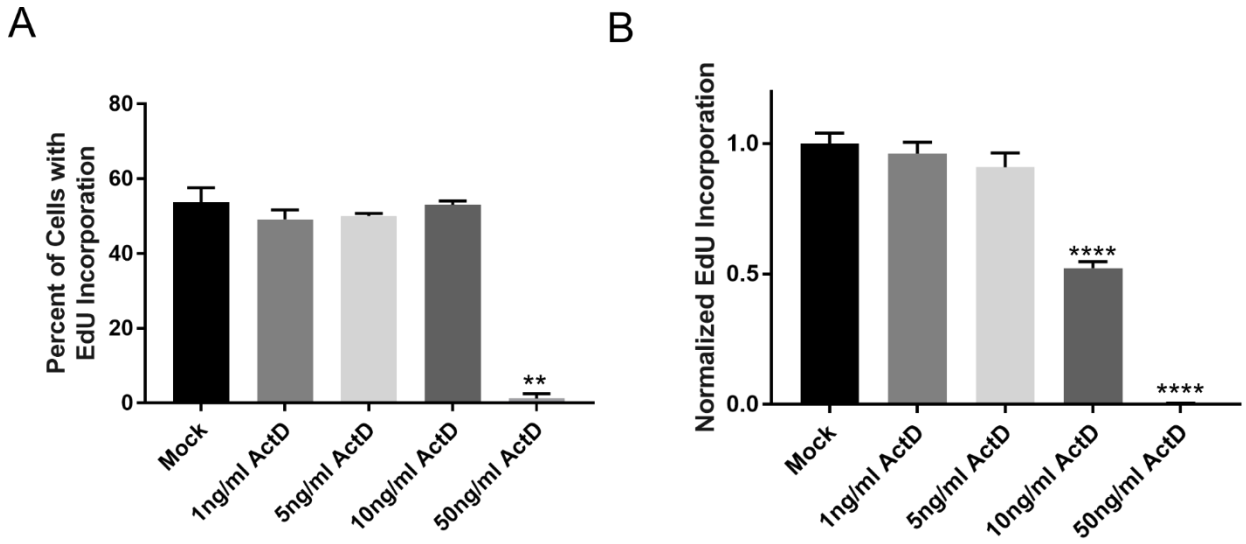

Figure 3.11. Inhibition of RNA polymerase I prevents cell cycle progression in high doses. (C,D) HT1080 cells were treated with a titration of ActD for 8 hours. EdU was pulsed for 1 hour at the end of treatment. (C) The percent of cells with EdU incorporation decreases only at the highest dose of ActD (50ng/ml). (D) The amount of EdU incorporated into each nucleus decreases with both 10ng/ml and 50ng/ml ActD. n > 200 cells per condition across 2-3 biological replicates. ** is p-value < 0.01 and **** is p-value < 0.0001.

accumulate in the nucleus after XPO1 inhibition and may be important for selinexor response (Gravina et al., 2015; Yang et al., 2014; Yoshimura et al., 2014). A matched HT1080 cell line was created using CRISPR/cas9 directed mutagenesis to obtain a p53 loss of expression mutant (HT1080 TP53*). The effects of p53 loss on selinexor induced cell cycle responses and cell fate is described elsewhere (Marcus et al. 2018, in review). When p53 expression is removed, nucleolar structure and function is altered compared to HT1080 parental cells (Figure 3.12A,B). The percent nuclear area of RPA194 signal decreases in HT1080 TP53* compared to parental (Figure 3.12A). After a 1 hour pulse of EU, nucleolar incorporation of EU is increased about 2-fold in the HT1080 TP53* mock cells compared to parental mock (Figure 3.12B). Interestingly, a similar increase in nucleolar transcriptional activity was also observed in the HT1080 mCherry-BP1-2/EGFP-UBF cell line (Figure 3.7D).

When treated with 1μM selinexor, a decrease in the percent area of the nucleolus relative to the nuclear size occurs in both HT1080 parental cells and HT1080 TP53* (Figure 3.12A). This suggests that despite differences in nucleolar structure in mock treated cells, inhibition of XPO1 perturbs nucleolar structure independent of wildtype p53 expression. The activity of nucleoli to transcribe rDNA was measured next. EU was pulsed for 1 hour following selinexor treatment and the level incorporated into each selinexor treated cell line is decreased approximately 50% compared to respective mock treated partner (Figure 3.12B). The result that EU incorporation is blocked after selinexor treatment in p53 wildtype and HT1080 TP53* cells, further supports this action on nucleoli is independent of p53.

Increased DNA damage formation following XPO1 inhibition was evident in cells that overexpress the RNA polymerase I transcription factor UBF (Figure 3.6A,B and Figure 3.7B). This increase in damage correlates with an increase in EU incorporation at nucleoli before

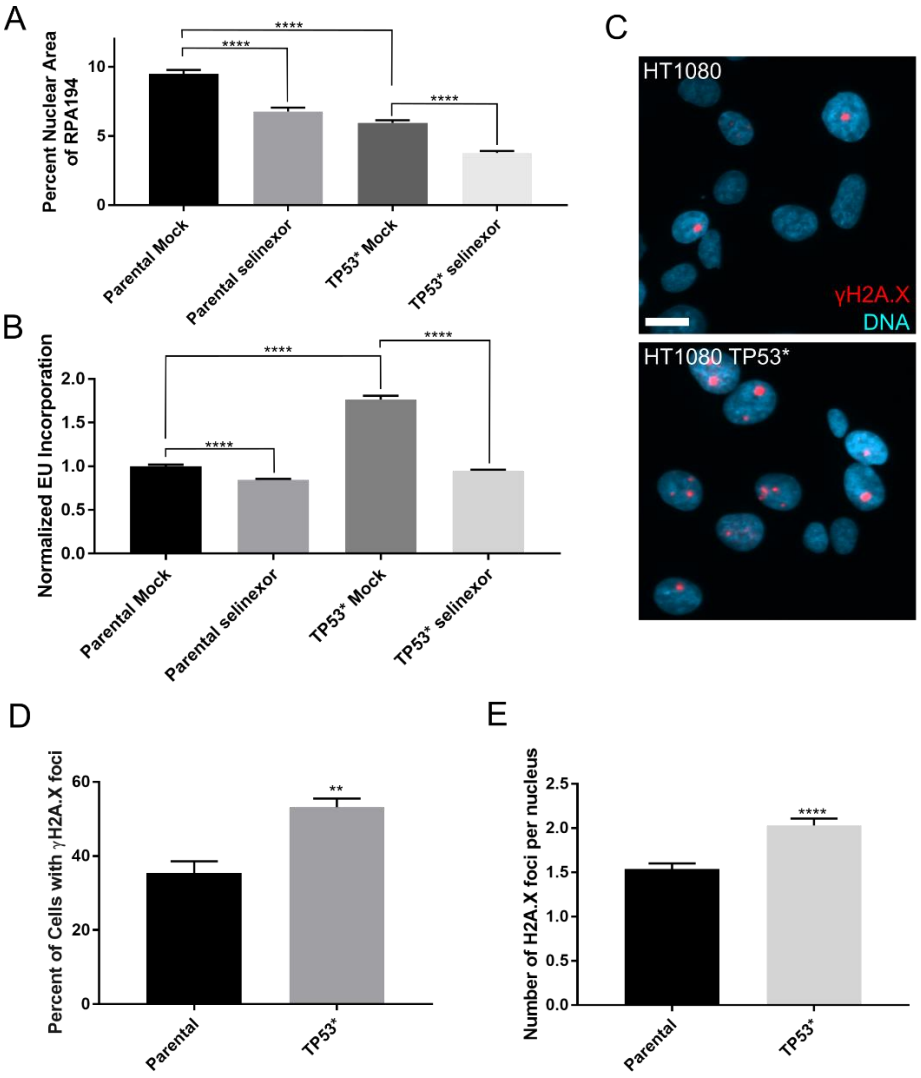

Figure 3.12. DNA damage and nucleolar defects are enhanced in p53 loss of expression mutant cells. HT1080 and HT1080 TP53* cells were treated for 8 hours with mock (DMSO) or 1μM selinexor. Click-iT EU was pulsed in for 1 hour at the end of treatment. Cells were then immunostained for RPA194 and γH2A.X (red). (A) Nucleolar masks were created and the percent area of RPA194 stain within each nucleus was quantified. The percent area of untreated HT1080 TP53* is decreased compared to parental HT1080. XPO1 inhibition causes a decrease in the nuclear area of RPA194 in both cell lines compared to the corresponding mock treatment. (B) Masks for nucleolar EU were made. The amount of nucleolar EU increases about 1.7 fold in HT1080 TP53* compared to the parental cell line. The amount of EU incorporated at nucleoli decreases by about 50% in both the parental and TP53* cell lines. (C) Representative images of selinexor induced DNA damage show an increase in the frequency and number of foci per cell in the HT1080 TP53* compared to the parental line. (D) The frequency of cells with DNA damage increases in HT1080 TP53*. (E) The number of DNA damage foci per cell increases significantly in HT1080 TP53* compared to parental HT1080. n > 200 cells per condition across 2-3 biological replicates. Scale bar = 10μm. **** is p-value < 0.0001.

treatment with selinexor (Figure 3.7D). A similar increase in EU incorporation at nucleoli is observed in cells lacking p53 expression (Figure 3.12B). DNA damage formation was tested in cells lacking p53 expression. HT1080 parental and HT1080 TP53* were treated with 1μM selinexor and both the percent of cells with DNA damage clusters and the number of clusters increase when p53 is absent (Figure 3.12D,E). These data suggest that perturbances to nucleolar structure and function by either overexpressing the transcription factor UBF, or loss of p53 which is involved in nucleolar stress response, increase the overall DNA damage response following XPO1 inhibition.

3.4: Discussion

Inhibition of XPO1 as a target for anti-cancer therapeutics displays a variety of responses including cell cycle arrest, DNA damage and apoptosis (Azmi et al., 2013; Burke et al., 2017; Marcus et al., 2015). The complexities of response are likely due in part to the over 200 protein cargos whose export from the nucleus are dependent on XPO1 (Xu et al., 2012). Recent work has focused on the importance of select cargos as a targetable node that determine response, including IκB, FOXO3a, Cyclin D1, survivin and p53 (Conforti et al., 2017; Corno et al., 2017; Gravina et al., 2015; Nair et al., 2017; Yoshimura et al., 2014). A second node may be the nucleolus, where XPO1 through some binding partners has a role in ribosome biogenesis (Ho et al., 2000; Moore et al., 2011). Here we show that transcription within the nucleolus is significantly inhibited concurrent with redistribution of nucleolar proteins within hours of XPO1 inhibition and DNA damage clusters form within and proximal to these nucleoli. Formation of DNA damage requires RNA polymerase I-dependent transcription and/or normal nucleolar function (Figures 3.8 and 3.9). Finally, increased rRNA transcription in nucleoli through either

overexpression of the rDNA transcription factor, UBF, or loss of p53 expression enhances both nucleolar phenotypic response and DNA damage formation following XPO1 inhibition (Figures 3.6, 3.7 and 3.12).

The nucleolus is a highly dynamic and complex organelle within the nucleus. Our previous studies have shown that clusters of DNA double strand breaks occur in a cell cycle associated manner that affects cell fate (Burke et al., 2017). In this study, we demonstrate that nucleolar-associated selinexor-induced DNA damage foci (Figure 3.5) form either following or concomitant with nucleolar protein redistribution and inhibited rRNA synthesis (Figures 3.1 and 3.2). This study reveals that DNA damage formation is associated with nucleolar dysfunction. Accordingly, RNA polymerase I inhibitors, either actinomycin D or BMH21, when combined with selinexor, potently block DNA damage formation independent of any effect on DNA synthesis (Figures 3.8 and 3.9). The data here, together with our previous work support a mechanism where nucleolar stress after XPO1 inhibition intersects with cell cycle progression from G1- into S-phase leading to DNA double strand breaks, potentially at dynamically active chromatin sites such as rDNA gene arrays. Increasing the transcription rate at nucleoli through overexpression of UBF or removal of p53 also enhances the DNA damage response (Figures 3.7 and 3.12, respectively), further supporting a direct association of DNA damage and transcription in rDNA gene arrays. In separate works, p53 plays a significant role in initial cell cycle response after selinexor treatment (Marcus et al., 2018, in review) and it is well documented that p53 removal allows for continued proliferation under stress (Drosten et al., 2014; Li et al., 2012), and UBF expression has been associated with accelerated cell growth (Huang et al., 2002). This information together with data here are consistent with increased DNA damage via nucleolar stress and/or cell cycle progression. There are other genomic areas that tether to and associate

with nucleoli that may be sensitized sites of selinexor-induced DNA damage. Centromeres have been shown to tether to the periphery of nucleoli, and XPO1 is known to function at these sites during mitotic spindle assembly (Funabiki et al., 1993; Knauer et al., 2006). DNA damage can form in centromeres after perturbations to mitosis (Guerrero et al., 2010), however selinexor-induced DNA damage appears to form directly in interphase as soon as 2 hours after treatment, independent of any mitotic response (Figure 3.6 and (Burke et al., 2017)). Further studies are needed to identify the precise chromatin regions of selinexor induced DNA damage.

Published work indicates that DNA damage formation either occurs at a very low level in normal cell models, or perhaps not at all (Burke et al., 2017). We observe that normal RPE1 cells show a nucleolar phenotype after treatment with selinexor based on RPA194 staining, like HT1080 cells (Figure 3.3). This indicates that the nucleolar response can occur without a subsequent significant increase in DNA damage. RPE1 cells treated in G1-phase remain arrested there and as a population these cells accumulate in G1-phase and arrest after treatment with almost no cell death (Burke et al., 2017). HT1080 cells have a more varied cell cycle response to XPO1 inhibition and undergo significant cell death. In addition, DNA damage associates with S-phase entry and progression defects (Burke et al., 2017). The difference in DNA damage formation and cell cycle progression defects between normal cells, RPE1, and cancer cells, HT1080, suggests that both nucleolar stress and cell cycle progression are necessary for DNA damage formation. In support of this, low concentration RNA polymerase I inhibitors that minimize cell cycle effects but potently block transcription inhibition prevent selinexor induced DNA damage formation (Figures 3.8 and 3.11). It is probable that DNA damage formation is dependent on both nucleolar function and cell cycle progression given that G1-phase arrest also prevents DNA damage formation (Figure 3.10). p53, an important regulator of the cell cycle and

nucleolar stress response, is the most frequently lost tumor suppressor proteins. We show that loss of function of p53 in HT1080 leads to an enhanced DNA damage response to selinexor. In addition, there is an increased nucleolar transcription rate and redistribution of nucleolar proteins (Figure 3.10 B and A, respectively). Loss of p53 may enhance the effects of selinexor in tumors through these and other mechanisms, an important finding as selinexor and other SINE molecules progress toward clinical applications. Cell cycle progression effects and increased DNA damage response via nucleolar stress may also be affected by oncogenic stress through oncogenes such as RAS; HT1080 express oncogenic N-RAS (Paterson et al., 1987). Intriguingly, non-small cell lung tumors that express oncogenic K-RAS are sensitized to selinexor treatment (Kim et al., 2016). Loss of cell cycle control through either activation of oncogenes and/or loss of tumor suppressor proteins may lead to enhanced nucleolar disruption and DNA damage response, leading to increased sensitivity to XPO1 inhibitors in tumor cells.

The data presented here reveal an interesting premise for the anti-cancer mechanisms of XPO1 inhibition. Given the differences in selinexor response between normal and cancer cell lines, it is crucial to understand the mechanisms of response of selinexor and other SINE molecules. This study presents that XPO1 inhibition causes both nucleolar stress and DNA damage, responses that can be important for therapeutic response (Hosoya and Miyagawa, 2014; Quin et al., 2014). Developing an integrated understanding of the complex effects of XPO1 inhibition on different cellular processes will be important for this promising new target in anti-cancer therapeutics.

Chapter 4 : Discussion and Future Directions

4.1: Summary

The data presented in this thesis represent a novel anti-cancer mechanism for XPO1 inhibition. Selective inhibitors of nuclear export, namely selinexor, cause DNA double strand breaks in cancer cells. While DNA damage can occur throughout interphase, the timing of DNA damage within the cell cycle correlates with cell fate. There is an increase in cell death when DNA damage occurs in G1-phase compared to formation in S/G2-phase where progression through mitosis occurs more often (Figure 2.17). In addition, DNA damage forms in distinct clusters that are proximal to and within nucleoli. As discussed in chapter 3, selinexor induced DNA damage overlaps with many proteins that are involved in ribosome biogenesis. Concomitant to DNA damage formation, nucleolar reorganization and dysfunction are observed; consistent with previously published studies (Bai et al., 2013; Tabe et al., 2015). We find that DNA damage formation is dependent both on active RNA polymerase I transcription and cell cycle progression. In addition, overexpression of the transcription factor, UBF, and loss of p53 lead to increased transcription of rRNA as well as enhanced selinexor induced DNA damage response. Together, these data represent a novel mechanism of response to inhibition of XPO1 in cancer.

4.2: The correlation between DNA damage and cell death

The formation of DNA double strand breaks in cells is often associated with cell death. Mammalian cells often enter programmed cell death following DNA damage events that are to great to be repaired (Blank and Shiloh, 2007; Rich et al., 2000; Roos and Kaina, 2006). In

addition, many cytotoxic therapeutics have been successful in the clinic due to their ability to cause large DNA damage events and force cells into death pathways (Bentle et al., 2006; Michod and Widmann, 2007). In these studies, we present that DNA damage formation occurs after XPO1 inhibition in cancer cells. In the fibrosarcoma derived cell line, HT1080, about 35-40% of cells have DNA damage at 8 hours after selinexor treatment (Figure 2.1). When HT1080 cells expressing the DNA damage reporter, mCherry BP1-2, are longitudinally tracked during live cell microscopy, we report that about 50% of all cells in the population acquire damage at some point within the first 72 hours of selinexor treatment (Figure 2.13). While the timing of DNA damage within the cell cycle correlates with cell fate (Figure 2.13), we restricted that analysis to exclude those cells that do not form DNA damage at any point during treatment. Interestingly, it appears that DNA damage formation following selinexor treatment does not enhance the rate at which cells die (Figure 4.1). However, significant synergy is observed when selinexor is combined with

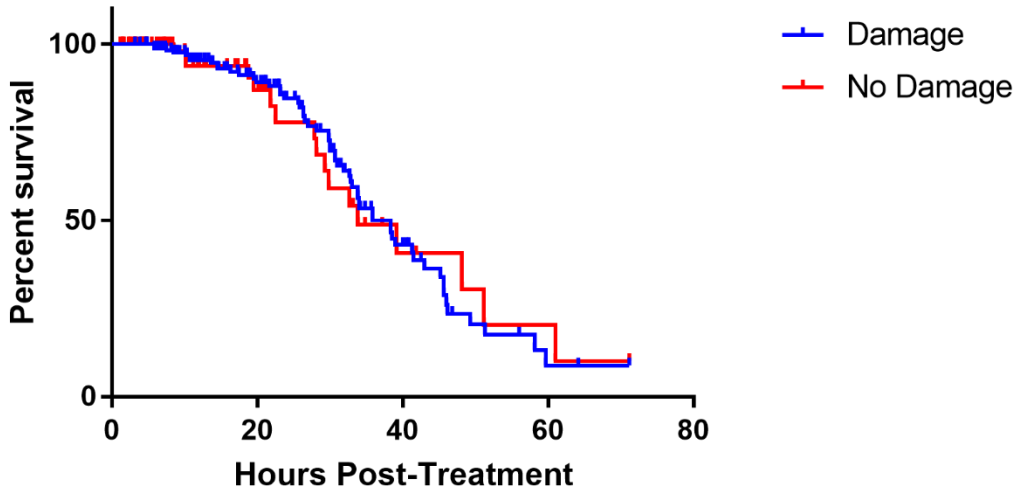

Figure 4.1. Survival of HT1080 cells after selinexor treatment. HT1080 cells that express mAG-hGem(1/110) and mCherry-BP1-2 were treated with 1μM selinexor and imaged every 10 minutes for 72 hours (see Figure 2.13). Cells were separated into those that form DNA damage foci and those that do not. A Kaplan-Meier survival curve shows that there is no difference in death kinetics between those cells that form damage and those that do not.

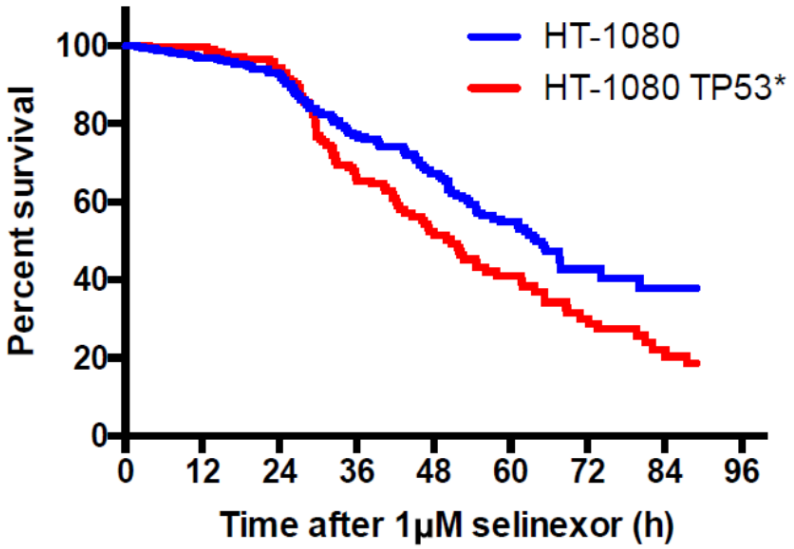

Figure 4.2. Loss of p53 in HT1080 leads to increased death after XPO1 inhibition. HT1080 parental and HT1080 TP53* cells expressing the FUCCI cell cycle reporter system were longitudinally tracked over 96 hours after 1μM selinexor. Cell death events were reported and a Kaplan-Meier survival curve was produced. A significant increase in the amount of death was observed in the TP53* cells. Adapted from (Marcus et al. 2018, in review).

genotoxic therapeutics (Figures 2.14 and 2.16), and selinexor treatment has been shown to increase the DNA damage response of cells treated with other damaging agents (Gravina et al., 2017). These synergistic effects may be due to downregulation of DNA damage response proteins following XPO1 inhibition, such as Chk1, Rad51 and BRCA1 (Ranganathan et al., 2016; Tabe et al., 2015). In contrast, we observe increased DNA damage formation frequency and increased DNA damage foci-cluster per cell after overexpression of UBF and loss of function of p53 (TP53*) (Figures 3.7 and 3.12). Longitudinal tracking of HT1080 parental and TP53* cells shows that increased death is observed when p53 expression is lost (Figure 4.2). While it remains to be seen if DNA damage contributes to an increase in death following XPO1 inhibition when p53 expression is lost, the two processes appear to be linked. Although survival

after selinexor in cells overexpressing UBF is not known, the increase in DNA damage formation may prove a key insight in expected survival among may other factors contributing to overall XPO1 inhibitor response. The importance of DNA damage formation in cancer cells to overall response after XPO1 inhibition remains an open question.

4.3: The formation of DNA damage at nucleoli may give insight to where in the genome break sites are occurring

In these studies, we have shown that DNA damage formation occurs in distinct foci that are composed of multiple double strand break sites (Figures 2.1 and 2.7). In addition, it was observed that DNA damage occurs proximal to or within nucleoli, and overlaps with proteins involved with ribosome biogenesis (Figure 3.5). Live cell microscopy of cells expressing the DNA damage reporter mCherry BP1-2 and the RNA polymerase I transcription factor EGFP-UBF suggest that DNA damage to some frequency occurs near where UBF is bound (Figure 3.6A,B). However, the exact site of the double strand breaks is not known at this point. Nucleoli are highly dynamic structures that are the center for multiple processes including ribosome biogenesis (Boisvert et al., 2007) and organization of select regions of chromatin including centromeres, telomeres and other heterochromatic regions (Funabiki et al., 1993; Németh et al., 2010; Padeken and Heun, 2014). In addition, XPO1 is known have some function at these various genomic regions. As discussed in Chapters 1 and 3, XPO1 binds the chaperone protein NMD3 to translocate the assembled ribosome subunit out of the nucleus (Ho et al., 2000). XPO1 was originally described for its role in attachment of the microtubles during mitosis in *S. pombe* (Funabiki et al., 1993). Inhibition of XPO1 by leptomycin B has been shown to cause mitotic

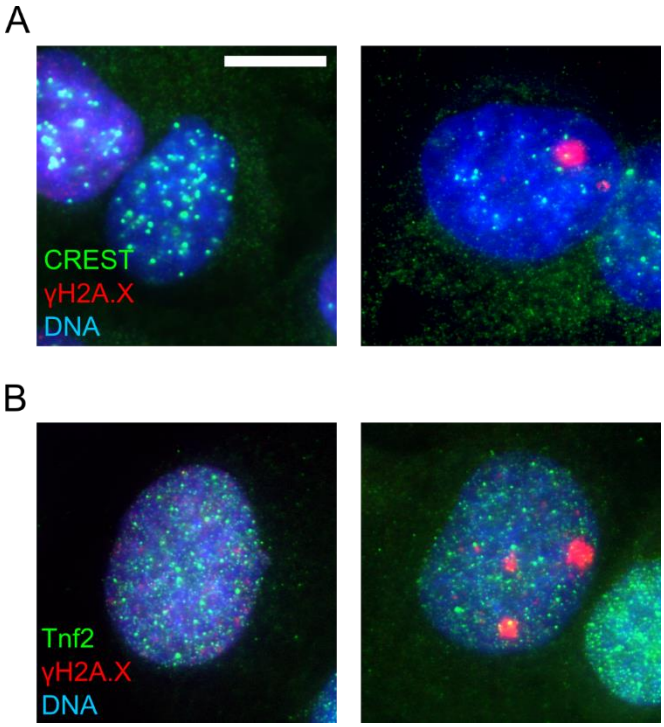

Figure 4.3. Other nucleolar associated bodies may associate with DNA damage after XPO1 inhibition. HT1080 cells were treated for 8 hours with 1μM selinexor and then coimmunostained with γH2A.X and either (A) CREST, a marker for centromeres, or (B) Tnf2, a component of the telomere cap. Overlap of DNA damage and these regions is observed to a limited extent suggesting it is possible that selinexor induced DNA damage may occur at these regions.

defects (Knauer et al., 2006) which could lead to DNA damage (Guerrero et al., 2010). XPO1 has also been shown to bind components of the telomere cap, including TPP1 (Chen et al., 2007).

In order to follow up on the potential of DNA damage in these regions, we treated HT1080 cells for 8 hours with 1μM selinexor and costained γH2A.X with CREST, a component of the centromere, or Tnf2, a telomere associated protein (Figure 4.3). There does appear to be overlap of DNA damage with CREST, suggesting that the centromere may be a site of DNA damage after XPO1 inhibition (Figure 4.3A). While overlap of Tnf2 is observed in some γH2A.X foci, it is absent in others (Figure 4.3B). Similar to the observations made with ribosome biogenesis proteins, the lack of colocalization may be a product of temporal changes as

the nucleoli respond to the stresses of XPO1 inhibition. Further investigation and expansion of experimental techniques may be required to determine the location of DNA damage.

Given the data presented in Chapter 3 regarding the disruption of nucleolar function and transcription, it is plausible that DNA damage is caused by feedback into areas with active rDNAtranscription. This idea is strengthened by evidence that acute inhibition of RNA polymerase I prevents DNA damage independent of cell cycle effects (Figures 3.8 and 3.11, respectively). Taking into account the S-phase progression defects observed with XPO1 inhibition (Figure 2.10 and (Marcus et al., 2015)), DNA damage formation may be interlinked with multiple processes. Previous studies have described fragile sites prone to DNA damage during replication. rDNA gene arrays are one such area where active transcription conflicts with replication forks and DNA damage occurs (reviewed in (Lin and Pasero, 2012)). However, direct evidence of rDNA gene array damage has yet to be observed.

References

Aggarwal, A., and Agrawal, D.K. (2014). Importins and exportins regulating allergic immune responses. Mediators Inflamm. *2014*, 476357.

Ahfeldt, T., Schinzel, R.T., Lee, Y.-K., Hendrickson, D., Kaplan, A., Lum, D.H., Camahort, R., Xia, F., Shay, J., Rhee, E.P., et al. (2012). Programming human pluripotent stem cells into white and brown adipocytes. Nat. Cell Biol. *14*, 209–219.

Aloisi, A., Di Gregorio, S., Stagno, F., Guglielmo, P., Mannino, F., Sormani, M.P., Bruzzi, P., Gambacorti-Passerini, C., Saglio, G., Venuta, S., et al. (2006). BCR-ABL nuclear entrapment kills human CML cells: ex vivo study on 35 patients with the combination of imatinib mesylate and leptomycin B. Blood *107*, 1591–1598.

Azmi, A.S., Aboukameel, A., Bao, B., Sarkar, F.H., Philip, P.A., Kauffman, M., Shacham, S., and Mohammad, R.M. (2013). Selective inhibitors of nuclear export block pancreatic cancer cell proliferation and reduce tumor growth in mice. Gastroenterology *144*, 447–456.

Bai, B., Moore, H.M., and Laiho, M. (2013). CRM1 and its ribosome export adaptor NMD3 localize to the nucleolus and affect rRNA synthesis. Nucl. Austin Tex *4*, 315–325.

Bauer, R.A. (2015). Covalent inhibitors in drug discovery: from accidental discoveries to avoided liabilities and designed therapies. Drug Discov. Today *20*, 1061–1073.

Bentle, M.S., Bey, E.A., Dong, Y., Reinicke, K.E., and Boothman, D.A. (2006). New tricks for old drugs: the anticarcinogenic potential of DNA repair inhibitors. J. Mol. Histol. *37*, 203–218.

Blank, M., and Shiloh, Y. (2007). Programs for cell death: apoptosis is only one way to go. Cell Cycle Georget. Tex *6*, 686–695.

Boeynaems, S., Bogaert, E., Van Damme, P., and Van Den Bosch, L. (2016). Inside out: the role of nucleocytoplasmic transport in ALS and FTLD. Acta Neuropathol. (Berl.) *132*, 159–173.

Bogerd, H.P., Fridell, R.A., Benson, R.E., Hua, J., and Cullen, B.R. (1996). Protein sequence requirements for function of the human T-cell leukemia virus type 1 Rex nuclear export signal delineated by a novel in vivo randomization-selection assay. Mol. Cell. Biol. *16*, 4207–4214.

Boisvert, F.-M., van Koningsbruggen, S., Navascués, J., and Lamond, A.I. (2007). The multifunctional nucleolus. Nat. Rev. Mol. Cell Biol. *8*, 574–585.

Burke, R.T., and Orth, J.D. (2016). Through the Looking Glass: Time-lapse Microscopy and Longitudinal Tracking of Single Cells to Study Anti-cancer Therapeutics. J. Vis. Exp. JoVE.

Burke, R.T., Loriaux, M.M., Currie, K.S., Mitchell, S.A., Maciejewski, P., Clarke, A.S., DiPaolo, J.A., Druker, B.J., Spurgeon, S.E., and Lannutti, B.J. (2013). A potential therapeutic strategy for chronic lymphocytic leukemia by combining Idelalisib and GS-9973, a novel spleen tyrosine kinase (Syk) inhibitor. Oncotarget *5*, 908–915.

Burke, R.T., Marcus, J.M., and Orth, J.D. (2017). Inhibition of exportin-1 function results in rapid cell cycle-associated DNA damage in cancer cells. Oncotarget *8*, 39460–39475.

Chen, L.-Y., Liu, D., and Songyang, Z. (2007). Telomere maintenance through spatial control of telomeric proteins. Mol. Cell. Biol. *27*, 5898–5909.

Chen, Y., Camacho, S.C., Silvers, T.R., Razak, A.R.A., Gabrail, N.Y., Gerecitano, J.F., Kalir, E., Pereira, E., Evans, B.R., Ramus, S.J., et al. (2016). Inhibition of the Nuclear Export Receptor XPO1 as a Therapeutic Target for Platinum-Resistant Ovarian Cancer. Clin. Cancer Res. Off. J. Am. Assoc. Cancer Res.

Chittajallu, D.R., Florian, S., Kohler, R.H., Iwamoto, Y., Orth, J.D., Weissleder, R., Danuser, G., and Mitchison, T.J. (2015). In vivo cell-cycle profiling in xenograft tumors by quantitative intravital microscopy. Nat. Methods *12*, 577–585.

Chou, T.-C., and Martin, N. (2005). CompuSyn for Drug Combinations: PC Software and User's Guide: A Computer Program for Quantitation of Synergism and Antagonism in Drug Combinations, and the Determination of IC50 and ED50 and LD50 Values (Paramus, NJ: ComboSyn Inc).

Chou, T.-C., and Talalay, P. (1983). Analysis of combined drug effects: a new look at a very old problem. Trends Pharmacol. Sci. *4*, 450–454.

Chou, T.-C., and Talalay, P. (1984). Quantitative analysis of dose-effect relationships: the combined effects of multiple drugs or enzyme inhibitors. Adv. Enzyme Regul. *22*, 27–55.

Clewell, R.A., Sun, B., Adeleye, Y., Carmichael, P., Efremenko, A., McMullen, P.D., Pendse, S., Trask, O.J., White, A., and Andersen, M.E. (2014). Profiling dose-dependent activation of p53-mediated signaling pathways by chemicals with distinct mechanisms of DNA damage. Toxicol. Sci. Off. J. Soc. Toxicol. *142*, 56–73.

Colis, L., Peltonen, K., Sirajuddin, P., Liu, H., Sanders, S., Ernst, G., Barrow, J.C., and Laiho, M. (2014). DNA intercalator BMH-21 inhibits RNA polymerase I independent of DNA damage response. Oncotarget *5*, 4361–4369.

Conforti, F., Zhang, X., Rao, G., De Pas, T., Yonemori, Y., Rodriguez, J.A., McCutcheon, J.N., Rahhal, R., Alberobello, A.T., Wang, Y., et al. (2017). Therapeutic Effects of XPO1 Inhibition in Thymic Epithelial Tumors. Cancer Res. *77*, 5614–5627.

Corno, C., Stucchi, S., De Cesare, M., Carenini, N., Stamatakos, S., Ciusani, E., Minoli, L., Scanziani, E., Argueta, C., Landesman, Y., et al. (2017). FoxO-1 contributes to the efficacy of the combination of the XPO1 inhibitor selinexor and cisplatin in ovarian carcinoma preclinical models. Biochem. Pharmacol. *147*, 93–103.

Crochiere, M.L., Baloglu, E., Klebanov, B., Donovan, S., del Alamo, D., Lee, M., Kauffman, M., Shacham, S., and Landesman, Y. (2015). A method for quantification of exportin-1 (XPO1) occupancy by Selective Inhibitor of Nuclear Export (SINE) compounds. Oncotarget *7*, 1863–1877.

Dimitrova, N., Chen, Y.-C.M., Spector, D.L., and de Lange, T. (2008). 53BP1 promotes non-homologous end joining of telomeres by increasing chromatin mobility. Nature *456*, 524–528.

Dobbelstein, M., and Sørensen, C.S. (2015). Exploiting replicative stress to treat cancer. Nat. Rev. Drug Discov. *14*, 405–423.

Domínguez, D., Montserrat-Sentís, B., Virgós-Soler, A., Guaita, S., Grueso, J., Porta, M., Puig, I., Baulida, J., Francí, C., and García de Herreros, A. (2003). Phosphorylation Regulates the Subcellular Location and Activity of the Snail Transcriptional Repressor. Mol. Cell. Biol. *23*, 5078–5089.

Drosten, M., Sum, E.Y.M., Lechuga, C.G., Simón-Carrasco, L., Jacob, H.K.C., García-Medina, R., Huang, S., Beijersbergen, R.L., Bernards, R., and Barbacid, M. (2014). Loss of p53 induces cell proliferation via Ras-independent activation of the Raf/Mek/Erk signaling pathway. Proc. Natl. Acad. Sci. *111*, 15155–15160.

Etchin, J., Berezovskaya, A., Conway, A.S., Galinsky, I.A., Stone, R.M., Baloglu, E., Senapedis, W., Landesman, Y., Kauffman, M., Shacham, S., et al. (2016). KPT-8602, a second-generation inhibitor of XPO1-mediated nuclear export, is well tolerated and highly active against AML blasts and leukemia-initiating cells. Leukemia.

Flach, J., Bakker, S.T., Mohrin, M., Conroy, P.C., Pietras, E.M., Reynaud, D., Alvarez, S., Diolaiti, M.E., Ugarte, F., Forsberg, E.C., et al. (2014). Replication stress is a potent driver of functional decline in ageing haematopoietic stem cells. Nature *512*, 198–202.

Franek, M., Kovaříková, A., Bártová, E., and Kozubek, S. (2016). Nucleolar Reorganization Upon Site-Specific Double-Strand Break Induction. J. Histochem. Cytochem. Off. J. Histochem. Soc. *64*, 669–686.

Freibaum, B.D., Lu, Y., Lopez-Gonzalez, R., Kim, N.C., Almeida, S., Lee, K.-H., Badders, N., Valentine, M., Miller, B.L., Wong, P.C., et al. (2015). GGGGCC repeat expansion in C9orf72 compromises nucleocytoplasmic transport. Nature *525*, 129–133.

Funabiki, H., Hagan, I., Uzawa, S., and Yanagida, M. (1993). Cell cycle-dependent specific positioning and clustering of centromeres and telomeres in fission yeast. J. Cell Biol. *121*, 961–976.

Gomez, D., Wenner, T., Brassart, B., Douarre, C., O'Donohue, M.-F., El Khoury, V., Shin-Ya, K., Morjani, H., Trentesaux, C., and Riou, J.-F. (2006). Telomestatin-induced telomere uncapping is modulated by POT1 through G-overhang extension in HT1080 human tumor cells. J. Biol. Chem. *281*, 38721–38729.

Govoni, M., Farabegoli, F., Pession, A., and Novello, F. (1994). Inhibition of Topoisomerase II Activity and Its Effect on Nucleolar Structure and Function. Exp. Cell Res. *211*, 36–41.

Gravina, G., Senapedis, W., McCauley, D., Baloglu, E., Shacham, S., and Festuccia, C. (2014). Nucleo-cytoplasmic transport as a therapeutic target of cancer. J. Hematol. Oncol.J Hematol Oncol *7*, 85.

Gravina, G.L., Mancini, A., Sanita, P., Vitale, F., Marampon, F., Ventura, L., Landesman, Y., McCauley, D., Kauffman, M., Shacham, S., et al. (2015). KPT-330, a potent and selective exportin-1 (XPO-1) inhibitor, shows antitumor effects modulating the expression of cyclin D1 and survivin [corrected] in prostate cancer models. BMC Cancer *15*, 941.

Gravina, G.L., Mancini, A., Colapietro, A., Marampon, F., Sferra, R., Pompili, S., Biordi, L.A., Iorio, R., Flati, V., Argueta, C., et al. (2017). Pharmacological treatment with inhibitors of nuclear export enhances the antitumor activity of docetaxel in human prostate cancer. Oncotarget *8*, 111225–111245.

Guerrero, A.A., Gamero, M.C., Trachana, V., Fütterer, A., Pacios-Bras, C., Díaz-Concha, N.P., Cigudosa, J.C., Martínez-A, C., and van Wely, K.H.M. (2010). Centromere-localized breaks indicate the generation of DNA damage by the mitotic spindle. Proc. Natl. Acad. Sci. U. S. A. *107*, 4159–4164.

Gyori, B.M., Venkatachalam, G., Thiagarajan, P.S., Hsu, D., and Clement, M.-V. (2014). OpenComet: an automated tool for comet assay image analysis. Redox Biol. *2*, 457–465.

Haines, J.D., Herbin, O., de la Hera, B., Vidaurre, O.G., Moy, G.A., Sun, Q., Fung, H.Y.J., Albrecht, S., Alexandropoulos, K., McCauley, D., et al. (2015). Nuclear export inhibitors avert progression in preclinical models of inflammatory demyelination. Nat. Neurosci. *18*, 511–520.

Hamamoto, T., Seto, H., and Beppu, T. (1983). Leptomycins A and B, new antifungal antibiotics. II. Structure elucidation. J. Antibiot. (Tokyo) *36*, 646–650.

Hannan, R.D., Stefanovsky, V., Taylor, L., Moss, T., and Rothblum, L.I. (1996). Overexpression of the transcription factor UBF1 is sufficient to increase ribosomal DNA transcription in neonatal cardiomyocytes: implications for cardiac hypertrophy. Proc. Natl. Acad. Sci. U. S. A. *93*, 8750–8755.

Helmrich, A., Ballarino, M., and Tora, L. (2011). Collisions between replication and transcription complexes cause common fragile site instability at the longest human genes. Mol. Cell *44*, 966–977.

Hijaz, M., Chhina, J., Mert, I., Taylor, M., Dar, S., Al-Wahab, Z., Ali-Fehmi, R., Buekers, T., Munkarah, A.R., and Rattan, R. (2016). Preclinical evaluation of olaparib and metformin combination in BRCA1 wildtype ovarian cancer. Gynecol. Oncol. *142*, 323–331.

Ho, J.H., Kallstrom, G., and Johnson, A.W. (2000). Nmd3p is a Crm1p-dependent adapter protein for nuclear export of the large ribosomal subunit. J. Cell Biol. *151*, 1057–1066.

Hosoya, N., and Miyagawa, K. (2014). Targeting DNA damage response in cancer therapy. Cancer Sci. *105*, 370–388.

Huang, R., Wu, T., Xu, L., Liu, A., Ji, Y., and Hu, G. (2002). Upstream binding factor up-regulated in hepatocellular carcinoma is related to the survival and cisplatin-sensitivity of cancer cells. FASEB J. Off. Publ. Fed. Am. Soc. Exp. Biol. *16*, 293–301.

Huang, W., Yue, L., Qiu, W., Wang, L.-W., Zhou, X., and Sun, Y. (2009). Prognostic value of CRM1 in pancreas cancer. Clin. Investig. Med. Médecine Clin. Exp. *32*, E315.

Kashyap, T., Argueta, C., Aboukameel, A., Unger, T.J., Klebanov, B., Mohammad, R.M., Muqbil, I., Azmi, A.S., Drolen, C., Senapedis, W., et al. (2016). Selinexor, a Selective Inhibitor of Nuclear Export (SINE) compound, acts through NF-κB deactivation and combines with proteasome inhibitors to synergistically induce tumor cell death. Oncotarget.

Kim, J., McMillan, E., Kim, H.S., Venkateswaran, N., Makkar, G., Rodriguez-Canales, J., Villalobos, P., Neggers, J.E., Mendiratta, S., Wei, S., et al. (2016). XPO1-dependent nuclear export is a druggable vulnerability in KRAS-mutant lung cancer. Nature *538*, 114–117.

Kim, J.-S., Krasieva, T.B., Kurumizaka, H., Chen, D.J., Taylor, A.M.R., and Yokomori, K. (2005). Independent and sequential recruitment of NHEJ and HR factors to DNA damage sites in mammalian cells. J. Cell Biol. *170*, 341–347.

Kim, S.H., Kaminker, P., and Campisi, J. (1999). TIN2, a new regulator of telomere length in human cells. Nat. Genet. *23*, 405–412.

Knauer, S.K., Bier, C., Habtemichael, N., and Stauber, R.H. (2006). The Survivin-Crm1 interaction is essential for chromosomal passenger complex localization and function. EMBO Rep. *7*, 1259–1265.

Kruhlak, M., Crouch, E.E., Orlov, M., Montaño, C., Gorski, S.A., Nussenzweig, A., Misteli, T., Phair, R.D., and Casellas, R. (2007). The ATM repair pathway inhibits RNA polymerase I transcription in response to chromosome breaks. Nature *447*, 730–734.

Kudo, N., Khochbin, S., Nishi, K., Kitano, K., Yanagida, M., Yoshida, M., and Horinouchi, S. (1997). Molecular cloning and cell cycle-dependent expression of mammalian CRM1, a protein involved in nuclear export of proteins. J. Biol. Chem. *272*, 29742–29751.

Kuo, L.J., and Yang, L.-X. (2008). Gamma-H2AX - a novel biomarker for DNA double-strand breaks. Vivo Athens Greece *22*, 305–309.

Lapalombella, R., Sun, Q., Williams, K., Tangeman, L., Jha, S., Zhong, Y., Goettl, V., Mahoney, E., Berglund, C., Gupta, S., et al. (2012). Selective inhibitors of nuclear export show that CRM1/XPO1 is a target in chronic lymphocytic leukemia. Blood *120*, 4621–4634.

Lee, J.J., Kong, M., Ayers, G.D., and Lotan, R. (2007). Interaction index and different methods for determining drug interaction in combination therapy. J. Biopharm. Stat. *17*, 461–480.

Li, T., Kon, N., Jiang, L., Tan, M., Ludwig, T., Zhao, Y., Baer, R., and Gu, W. (2012). Tumor suppression in the absence of p53-mediated cell cycle arrest, apoptosis, and senescence. Cell *149*, 1269–1283.

Lin, Y.-L., and Pasero, P. (2012). Interference Between DNA Replication and Transcription as a Cause of Genomic Instability. Curr. Genomics *13*, 65–73.

Ma, H., and Pederson, T. (2013). The nucleolus stress response is coupled to an ATR-Chk1–mediated G2 arrest. Mol. Biol. Cell *24*, 1334–1342.

Marcus, J.M., Burke, R.T., DeSisto, J.A., Landesman, Y., and Orth, J.D. (2015). Longitudinal tracking of single live cancer cells to understand cell cycle effects of the nuclear export inhibitor, selinexor. Sci. Rep. *5*, 14391.

Marijon, H., Gery, S., Elloul, S., Friedlander, S.Y., Unger, T.J., Carlson, R., Shacham, S., Kauffman, M., and Koeffler, H.P. (2015). Selinexor, a selective inhibitor of nuclear export (SINE) compound, shows enhanced antitumor activity in combination with PARP inhibitor, olaparib, in models of triple-negative breast cancer (Philidelphia, PA).

Mazouzi, A., Velimezi, G., and Loizou, J.I. (2014). DNA replication stress: Causes, resolution and disease. Exp. Cell Res. *329*, 85–93.

Michod, D., and Widmann, C. (2007). DNA-damage sensitizers: potential new therapeutical tools to improve chemotherapy. Crit. Rev. Oncol. Hematol. *63*, 160–171.

Moore, H.M., Bai, B., Boisvert, F.-M., Latonen, L., Rantanen, V., Simpson, J.C., Pepperkok, R., Lamond, A.I., and Laiho, M. (2011). Quantitative Proteomics and Dynamic Imaging of the Nucleolus Reveal Distinct Responses to UV and Ionizing Radiation. Mol. Cell. Proteomics MCP *10*.

Mosammaparast, N., and Pemberton, L.F. (2004). Karyopherins: from nuclear-transport mediators to nuclear-function regulators. Trends Cell Biol. *14*, 547–556.

Nair, J.S., Musi, E., and Schwartz, G.K. (2017). Selinexor (KPT-330) Induces Tumor Suppression through Nuclear Sequestration of IκB and Downregulation of Survivin. Clin. Cancer Res. Off. J. Am. Assoc. Cancer Res. *23*, 4301–4311.

Nakayama, R., Zhang, Y.-X., Czaplinski, J.T., Anatone, A.J., Sicinska, E.T., Fletcher, J.A., Demetri, G.D., and Wagner, A.J. (2016). Preclinical activity of selinexor, an inhibitor of XPO1, in sarcoma. Oncotarget *7*, 16581–16592.

Neggers, J.E., Vercruysse, T., Jacquemyn, M., Vanstreels, E., Baloglu, E., Shacham, S., Crochiere, M., Landesman, Y., and Daelemans, D. (2015). Identifying drug-target selectivity of small-molecule CRM1/XPO1 inhibitors by CRISPR/Cas9 genome editing. Chem. Biol. *22*, 107–116.

Neggers, J.E., Vanstreels, E., Baloglu, E., Shacham, S., Landesman, Y., and Daelemans, D. (2016). Heterozygous mutation of cysteine528 in XPO1 is sufficient for resistance to selective inhibitors of nuclear export. Oncotarget.

Németh, A., Conesa, A., Santoyo-Lopez, J., Medina, I., Montaner, D., Péterfia, B., Solovei, I., Cremer, T., Dopazo, J., and Längst, G. (2010). Initial Genomics of the Human Nucleolus. PLoS Genet. *6*.

Newlands, E.S., Rustin, G.J., and Brampton, M.H. (1996). Phase I trial of elactocin. Br. J. Cancer *74*, 648–649.

Noske, A., Weichert, W., Niesporek, S., Röske, A., Buckendahl, A.-C., Koch, I., Sehouli, J., Dietel, M., and Denkert, C. (2008). Expression of the nuclear export protein chromosomal region maintenance/exportin 1/Xpo1 is a prognostic factor in human ovarian cancer. Cancer *112*, 1733–1743.

Orth, J.D., Loewer, A., Lahav, G., and Mitchison, T.J. (2012). Prolonged mitotic arrest triggers partial activation of apoptosis, resulting in DNA damage and p53 induction. Mol. Biol. Cell *23*, 567–576.

Padeken, J., and Heun, P. (2014). Nucleolus and nuclear periphery: velcro for heterochromatin. Curr. Opin. Cell Biol. *28*, 54–60.

Panov, K.I., Friedrich, J.K., Russell, J., and Zomerdijk, J.C.B.M. (2006). UBF activates RNA polymerase I transcription by stimulating promoter escape. EMBO J. *25*, 3310–3322.

Paterson, H., Reeves, B., Brown, R., Hall, A., Furth, M., Bos, J., Jones, P., and Marshall, C. (1987). Activated N-ras controls the transformed phenotype of HT1080 human fibrosarcoma cells. Cell *51*, 803–812.

Penman, S., Vesco, C., and Penman, M. (1968). Localization and kinetics of formation of nuclear heterodisperse RNA, cytoplasmic heterodisperse RNA and polyribosome-associated messenger RNA in HeLa cells. J. Mol. Biol. *34*, 49–69.

Perry, R.P. (1962). The Cellular Sites of Synthesis of Ribosomal and 4s Rna. Proc. Natl. Acad. Sci. *48*, 2179–2186.

Quin, J.E., Devlin, J.R., Cameron, D., Hannan, K.M., Pearson, R.B., and Hannan, R.D. (2014). Targeting the nucleolus for cancer intervention. Biochim. Biophys. Acta BBA - Mol. Basis Dis. *1842*, 802–816.

Ranganathan, P., Kashyap, T., Yu, X., Meng, X., Lai, T.-H., McNeil, B., Bhatnagar, B., Shacham, S., Kauffman, M., Dorrance, A.M., et al. (2016). XPO1 Inhibition Using Selinexor Synergizes With Chemotherapy in Acute Myeloid Leukemia (AML) by Targeting DNA Repair and Restoring Topoisomerase IIα to the Nucleus. Clin. Cancer Res. Off. J. Am. Assoc. Cancer Res.

Rappold, I., Iwabuchi, K., Date, T., and Chen, J. (2001). Tumor suppressor p53 binding protein 1 (53BP1) is involved in DNA damage-signaling pathways. J. Cell Biol. *153*, 613–620.

Reynolds, R.C., Montgomery, P.O., and Hughes, B. (1964). Nucleolar “Caps” Produced by Actinomycin D. Cancer Res. *24*, 1269–1277.

Rich, T., Allen, R.L., and Wyllie, A.H. (2000). Defying death after DNA damage. Nature *407*, 777–783.

Roberts, B.J., Hamelehle, K.L., Sebolt, J.S., and Leopold, W.R. (1986). In vivo and in vitro anticancer activity of the structurally novel and highly potent antibiotic CI-940 and its hydroxy analog (PD 114,721). Cancer Chemother. Pharmacol. *16*, 95–101.

Roos, W.P., and Kaina, B. (2006). DNA damage-induced cell death by apoptosis. Trends Mol. Med. *12*, 440–450.

Roos, W.P., Thomas, A.D., and Kaina, B. (2016). DNA damage and the balance between survival and death in cancer biology. Nat. Rev. Cancer *16*, 20–33.

Rothkamm, K., Krüger, I., Thompson, L.H., and Löbrich, M. (2003). Pathways of DNA Double-Strand Break Repair during the Mammalian Cell Cycle. Mol. Cell. Biol. *23*, 5706–5715.

Sakaue-Sawano, A., Kurokawa, H., Morimura, T., Hanyu, A., Hama, H., Osawa, H., Kashiwagi, S., Fukami, K., Miyata, T., Miyoshi, H., et al. (2008). Visualizing spatiotemporal dynamics of multicellular cell-cycle progression. Cell *132*, 487–498.

Salas Fragomeni, R.A., Chung, H.W., Landesman, Y., Senapedis, W., Saint-Martin, J.-R., Tsao, H., Flaherty, K.T., Shacham, S., Kauffman, M., and Cusack, J.C. (2013). CRM1 and BRAF inhibition synergize and induce tumor regression in BRAF-mutant melanoma. Mol. Cancer Ther. *12*, 1171–1179.

Shen, A., Wang, Y., Zhao, Y., Zou, L., Sun, L., and Cheng, C. (2009). Expression of CRM1 in human gliomas and its significance in p27 expression and clinical prognosis. Neurosurgery *65*, 153–159; discussion 159-160.

Shibata, A., Conrad, S., Birraux, J., Geuting, V., Barton, O., Ismail, A., Kakarougkas, A., Meek, K., Taucher-Scholz, G., Löbrich, M., et al. (2011). Factors determining DNA double-strand break repair pathway choice in G2 phase. EMBO J. *30*, 1079–1092.

Slebos, R.J., and Taylor, J.A. (2001). A novel host cell reactivation assay to assess homologous recombination capacity in human cancer cell lines. Biochem. Biophys. Res. Commun. *281*, 212–219.

Sperka, T., Wang, J., and Rudolph, K.L. (2012). DNA damage checkpoints in stem cells, ageing and cancer. Nat. Rev. Mol. Cell Biol. *13*, 579–590.

Suram, A., Kaplunov, J., Patel, P.L., Ruan, H., Cerutti, A., Boccardi, V., Fumagalli, M., Di Micco, R., Mirani, N., Gurung, R.L., et al. (2012). Oncogene-induced telomere dysfunction enforces cellular senescence in human cancer precursor lesions. EMBO J. *31*, 2839–2851.

Tabe, Y., Kojima, K., Yamamoto, S., Sekihara, K., Matsushita, H., Davis, R.E., Wang, Z., Ma, W., Ishizawa, J., Kazuno, S., et al. (2015). Ribosomal Biogenesis and Translational Flux Inhibition by the Selective Inhibitor of Nuclear Export (SINE) XPO1 Antagonist KPT-185. PloS One *10*, e0137210.

Takai, H., Smogorzewska, A., and de Lange, T. (2003). DNA damage foci at dysfunctional telomeres. Curr. Biol. CB *13*, 1549–1556.

Taylor-Kashton, C., Lichtensztejn, D., Baloglu, E., Senapedis, W., Shacham, S., Kauffman, M.G., Kotb, R., and Mai, S. (2016). XPO1 Inhibition Preferentially Disrupts the 3D Nuclear Organization of Telomeres in Tumor Cells. J. Cell. Physiol. *231*, 2711–2719.

Thomas, F., and Kutay, U. (2003). Biogenesis and nuclear export of ribosomal subunits in higher eukaryotes depend on the CRM1 export pathway. J. Cell Sci. *116*, 2409–2419.

Turner, J.G., Dawson, J., and Sullivan, D.M. (2012). Nuclear export of proteins and drug resistance in cancer. Biochem. Pharmacol. *83*, 1021–1032.

Turner, J.G., Dawson, J.L., Grant, S., Shain, K.H., Dalton, W.S., Dai, Y., Meads, M., Baz, R., Kauffman, M., Shacham, S., et al. (2016). Treatment of acquired drug resistance in multiple myeloma by combination therapy with XPO1 and topoisomerase II inhibitors. J. Hematol. Oncol.J Hematol Oncol *9*, 73.

Tyler, P.M., Servos, M.M., de Vries, R.C., Klebanov, B., Kashyap, T., Sacham, S., Landesman, Y., Dougan, M., and Dougan, S.K. (2017). Clinical Dosing Regimen of Selinexor Maintains Normal Immune Homeostasis and T-cell Effector Function in Mice: Implications for Combination with Immunotherapy. Mol. Cancer Ther. *16*, 428–439.

van der Watt, P.J., Maske, C.P., Hendricks, D.T., Parker, M.I., Denny, L., Govender, D., Birrer, M.J., and Leaner, V.D. (2009). The Karyopherin proteins, Crm1 and Karyopherin beta1, are overexpressed in cervical cancer and are critical for cancer cell survival and proliferation. Int. J. Cancer *124*, 1829–1840.

Xu, H., and Krystal, G.W. (2010). Actinomycin D Decreases Mcl-1 Expression and Acts Synergistically with ABT-737 against Small Cell Lung Cancer Cell Lines. Clin. Cancer Res. *16*, 4392–4400.

Xu, D., Grishin, N.V., and Chook, Y.M. (2012). NESdb: a database of NES-containing CRM1 cargoes. Mol. Biol. Cell *23*, 3673–3676.

Xu, K., Chen, Z., Cui, Y., Qin, C., He, Y., and Song, X. (2015). Combined olaparib and oxaliplatin inhibits tumor proliferation and induces G2/M arrest and γ-H2AX foci formation in colorectal cancer. OncoTargets Ther. *8*, 3047–3054.

Yang, J., Bill, M.A., Young, G.S., La Perle, K., Landesman, Y., Shacham, S., Kauffman, M., Senapedis, W., Kashyap, T., Saint-Martin, J.-R., et al. (2014). Novel small molecule XPO1/CRM1 inhibitors induce nuclear accumulation of TP53, phosphorylated MAPK and apoptosis in human melanoma cells. PloS One *9*, e102983.

Yao, Y., Dong, Y., Lin, F., Zhao, H., Shen, Z., Chen, P., Sun, Y.-J., Tang, L.-N., and Zheng, S.-E. (2009). The expression of CRM1 is associated with prognosis in human osteosarcoma. Oncol. Rep. *21*, 229–235.

Yoshimura, M., Ishizawa, J., Ruvolo, V., Dilip, A., Quintás-Cardama, A., McDonnell, T.J., Neelapu, S.S., Kwak, L.W., Shacham, S., Kauffman, M., et al. (2014). Induction of p53-

mediated transcription and apoptosis by exportin-1 (XPO1) inhibition in mantle cell lymphoma. Cancer Sci. *105*, 795–801.

Zerfaoui, M., Errami, Y., Naura, A.S., Suzuki, Y., Kim, H., Ju, J., Liu, T., Hans, C.P., Kim, J.G., Abd Elmageed, Z.Y., et al. (2010). Poly(ADP-ribose) polymerase-1 is a determining factor in Crm1-mediated nuclear export and retention of p65 NF-kappa B upon TLR4 stimulation. J. Immunol. Baltim. Md 1950 *185*, 1894–1902.

Zhang, Y., and Xiong, Y. (2001). A p53 amino-terminal nuclear export signal inhibited by DNA damage-induced phosphorylation. Science *292*, 1910–1915.

Zheng, Y., Gery, S., Sun, H., Shacham, S., Kauffman, M., and Koeffler, H.P. (2014). KPT-330 inhibitor of XPO1-mediated nuclear export has anti-proliferative activity in hepatocellular carcinoma. Cancer Chemother. Pharmacol. *74*, 487–495.